USGS
science for a changing world

Argon Thermochronology of Mineral Deposits—A Review of Analytical Methods, Formulations, and Selected Applications

U.S. Geological Survey Bulletin 2194

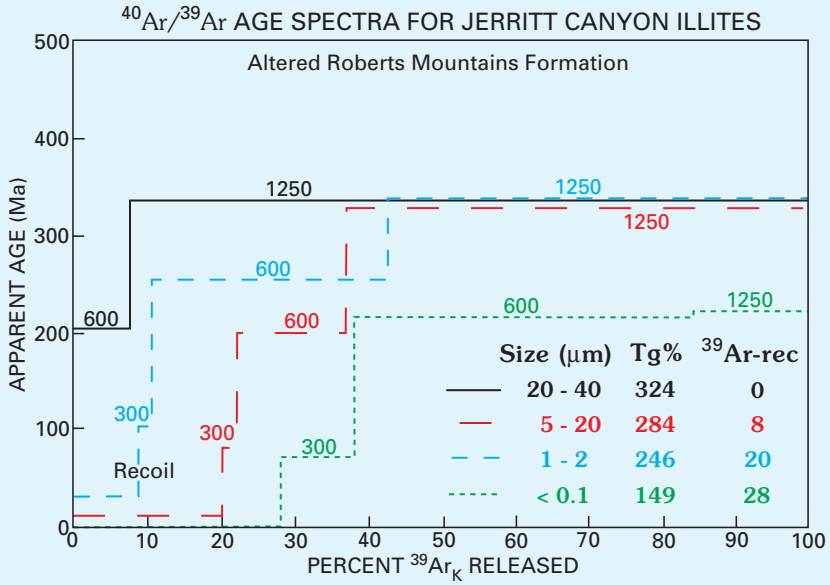

U.S. Department of the Interior
U.S. Geological Survey

Argon Thermochronology of Mineral Deposits—A Review of Analytical Methods, Formulations, and Selected Applications

By Lawrence W. Snee

U.S. Geological Survey Bulletin 2194

U.S. Department of the Interior
U.S. Geological Survey

U.S. Department of the Interior
Gale A. Norton, Secretary

U.S. Geological Survey
Charles G. Groat, Director

Version 1.0, 2002

This publication is only available online at:
http://pubs.usgs.gov/bul/b2194/

Manuscript approved for publication August 23, 2002
Published in the Central Region, Denver, Colorado
Graphics by L.W. Snee
Photocomposition by Norma J. Maes
Edited by L.M. Carter

Contents

Figures

Tables

Argon Thermochronology of Mineral Deposits—A Review of Analytical Methods, Formulations, and Selected Applications

By Lawrence W. Snee

Abstract

$^{40}Ar/^{39}Ar$ geochronology is an experimentally robust and versatile method for constraining time and temperature in geologic processes. The argon method is the most broadly applied in mineral-deposit studies. Standard analytical methods and formulations exist, making the fundamentals of the method well defined. A variety of graphical representations exist for evaluating argon data. A broad range of minerals found in mineral deposits, alteration zones, and host rocks commonly is analyzed to provide age, temporal duration, and thermal conditions for mineralization events and processes. All are discussed in this report. The usefulness of and evolution of the applicability of the method are demonstrated in studies of the Panasqueira, Portugal, tin-tungsten deposit; the Cornubian batholith and associated mineral deposits, southwest England; the Red Mountain intrusive system and associated Urad-Henderson molybdenum deposits; and the Eastern Goldfields Province, Western Australia.

Introduction

The $^{40}Ar/^{39}Ar$ isotopic dating technique has evolved over the past 10 years into the most commonly applied geochronologic method used in mineral-deposit research. The method has gained this popularity as a result of its natural versatility and experimental robustness. Because potassium-bearing minerals commonly form during processes associated with mineralization, either by direct precipitation from mineralizing fluids or as a result of alteration, an argon geochronometer (meaning, a datable mineral) is often present, and that mineral can be used in determining the age of the mineralization event. Perhaps more importantly, because argon geochronology is a precise analytical method, it is commonly possible to resolve the age of thermal events that were closely spaced in time. This capability is especially applicable for defining duration and timing of events in complex ore deposits.

Before 1988, even though high-precision argon geochronology was routinely employed in geologic framework studies, it had not been shown to be a valuable tool for unraveling the fundamental questions of economic geology. To test the applicability of high-precision $^{40}Ar/^{39}Ar$ geochronology in economic geology, Snee and others (1988) used the detailed paragenetic framework defined by Kelly and Rye (1979) for the Panasqueira, Portugal, tin-tungsten deposit to provide the geologic backdrop to move the method into applications that were more fundamental. From this deposit, carefully characterized muscovites were used to address mineral-deposit questions that reached beyond simply attempting to determine the apparent age of this world-class deposit. In fact, this study not only resolved the age of the deposit to less than $\pm$0.30 percent absolute, but also defined the duration of hydrothermal activity. The study also showed that thermal activity was episodic as well as spatially and temporally complex. The detailed geologic understanding of the Panasqueira deposit provided the physical framework for the definition of empirical constraints on diffusion of argon from muscovite (of structural state $2M_1$). Thus from the study on the Panasqueira tin-tungsten deposit, Snee and others (1988) showed that high-precision $^{40}Ar/^{39}Ar$ geochronology is truly a *thermochronologic* method that experimentally connects time and temperature and makes its use in mineral-deposit studies valuable.

Since 1988, many exciting new applications of high-precision $^{40}Ar/^{39}Ar$ thermochronology in mineral-deposit research have been employed. Relatively simplistic studies to determine the age of deposits are now routinely producing precision of less than 0.2 percent; these precise dates commonly provide critical data for constraining genetic models and exploration strategies (Losada-Calderon and others, 1994; Ford and Snee, 1996; Marsh and others, 1997; Lamb and Cox, 1998; Haeberlin and others, 1999). The applicability of the method also is expanding as argon systematics of other datable minerals, such as alunite, jarosite, hollandite, illite, and adularia, are being unraveled. (See, for example, Love and others, 1988; Brooks and Snee, 1996; Vasconcelos and others, 1994; Lippolt and Hautmann, 1995; Folger and others, 1996; Hall and others, 1997.) Many imaginative studies (Goldfarb and others, 1991, 1993; Kontak and others, 1994; Powell and others, 1995; Kent and McCuaig, 1997; Leach and others, 1998; Reynolds and others, 1998) have been published on complex thermochronologic details of mineral deposits; these studies are pressing the method across new frontiers. Laser-probe studies (Dong and others, 1997; Onstott and others, 1997; Clark and others, 1998) also are pushing the technique in new directions by opening the possibility of analyzing alteration assemblages in place without the need for mineral separation. And now the method is being combined not only with basic geologic framework details but also with other high-precision geochronologic, isotopic, and paleomagnetic methods to both certify the argon data and build a more complex and complete geochronologic framework for these deposits. (See, for example, Kontak and others, 1990; Perkins and others, 1990; Geissman and others, 1992; Perkins and others, 1992; Chesley and others, 1993; Zweng and others, 1993; Keppie and others, 1993; Giuliani and others, 1994; Kent and McDougall, 1995; Miller and others, 1994, 1995; Ribeiro-Althoff and others, 1997; Hofstra and others, 1999.)

Part of this review was prepared to accompany lectures at a short course on the use of geochronology in mineral-deposit

research given at the University of Western Australia in January 2001. The purpose of this expanded version of the original course notes is to publish procedures and assumptions used in the U.S. Geological Survey (USGS) Denver, Colo., argon laboratory and to provide a more comprehensive understanding of the analytical fundamentals and applications of the $^{40}Ar/^{39}Ar$ geochronologic technique. To that end, I do the following herein:

- Summarize the basic principles underlying the method, including the general formulations for calculating apparent age and analytical errors
- Give an assessment of argon standards used in our laboratory
- Discuss closure temperature as a concept, and review closure-temperature ranges for typical minerals
- Describe processes of argon loss and thermal resetting of minerals
- Describe the phenomenon of ^{39}Ar recoil
- List minerals that are useful in geochronologic studies of mineral deposits

Upon this analytical foundation I build a strategy for dating mineral deposits and I review some mineral-deposit studies that have been done in the Denver USGS argon geochronology laboratory.

Acknowledgments

This report is based on more than 15 years of laboratory studies conducted in the U.S. Geological Survey argon geochronology laboratory, Denver, Colo. More than 100 guest investigators have used this laboratory, resulting in more than 300 reports and abstracts. Each guest brought his or her unique manner of looking at geology and geochronology to our laboratory and to each experiment. The results of these studies form the foundation for this report. Equally important are the individuals who have built and maintained our laboratory and who have prepared rocks and minerals for analysis. These individuals include John Chesley, Ross Yeoman, Dan Miggins, Shahid Mirza Baig, Gary Davidson, Amy Bern, Libby Prueher, Steve Harlan, Cayce Lilleseve, and Brian Penn. Without their efforts, sometimes over 24-hour long periods, the laboratory would not have functioned. I also express gratitude to the U.S. Geological Survey TRIGA reactor crew, especially Tim Debey, Paul Helfer, Rick Perryman, and Darryl Liles for their expert maintenance and operation of the USGS research reactor. They provided virtually all the neutrons that activated our samples. Some of the results described in this report have been derived from published results from other laboratories. The dedication of these researchers has led to the robust nature of the $^{40}Ar/^{39}Ar$ geochronologic method. Lorna Carter has turned my feeble attempt at writing into reasonable English. Special thanks are extended to Professor David Groves of the Centre for Global Metallogeny, University of Western Australia (UWA), and the University administration for granting me a Gledden Visiting Senior Fellowship in early 2001. This fellowship provided me the opportunity to refresh my mind and to develop a first draft of this report to accompany course notes for a series of lectures at UWA. Subsequent studies with David Groves, Neal McNaughton, and Noreen Vielreicher, supported by funding from the Australian Research Council and the Australian Mineral Industries Research Association, are revealing the power of the argon method in addressing problems of Archean gold deposits.

Basis of the $^{40}Ar/^{39}Ar$ Technique

Formulations of the Method

The $^{40}Ar/^{39}Ar$ dating technique is a variant of the conventional K-Ar method and is based on the formation of ^{39}Ar during irradiation of potassium-bearing samples in a nuclear reactor. To obtain a date by this technique, a sample of unknown age and a standard of known age are irradiated together to produce ^{39}Ar from ^{39}K by fast-neutron bombardment. Wänke and Konig (1959), who irradiated meteorite samples weighing approximately 5 g (grams), described the earliest application of the technique. They used a counting technique to measure the activities of products formed from three reactions, $^{39}K(n,p)^{39}Ar$, $^{40}Ca(n, \alpha)^{37}Ar$, and $^{40}Ar(n, \lambda)^{41}Ar$. (The reaction expressed as $^{39}K(n,p)^{39}Ar$, for example, signifies that a fast neutron is incorporated within the ^{39}K atom with the resultant ejection of a proton causing the formation of ^{39}Ar.) Soon afterwards Sigurgeirsson (1962), Merrihue (1965), Merrihue and Turner (1966), and Mitchell (1968) established the foundation for mass spectrometric determination. (The historical development of the $^{40}Ar/^{39}Ar$ method is fascinating and can be read in these papers or in summaries in Faure (1986), Snee (1982b), and McDougall and Harrison (1999).)

In the early experiments, the importance of the $^{40}Ar/^{39}Ar$ technique lay in three aspects. First and most important, no direct chemical analysis of potassium is required, unlike the conventional K-Ar method, in which both ^{40}K and ^{40}Ar must be measured separately and quantitatively. In a conventional K-Ar analysis, argon (a gas) in one aliquot is measured by isotope-dilution, gas-source mass spectrometry. Potassium (a solid) in a separate aliquot is determined by some other analytical method such as flame photometry, X-ray fluorescence, or isotope-dilution, solid-source mass spectrometry. This poses the danger that, because of sample inhomogeneity, different potassium and (or) argon contents may exist in each aliquot. By contrast, in the $^{40}Ar/^{39}Ar$ technique, because only the relative isotopic abundances or ratios of argon are measured during a single procedure, sample-inhomogeneity problems are circumvented, thus improving the accuracy. Similarly, greater precision results because of the use of gas-source mass spectrometry, an extremely precise analytical technique. The second advantage of the $^{40}Ar/^{39}Ar$ technique, which was recognized in the early experiments, is the ability to analyze precisely very small (milligram-size) samples. This was particularly valuable in early applications for dating meteorites and later for lunar samples. Perhaps the greatest advantage of the technique, later described by Merrihue and Turner (1966), is the ability to release argon from samples by step-wise (incremental) heating instead of one-step total fusion.

The result is a series of dates from a single sample that potentially reveals information about the distribution of argon within the sample. The combination of these advantages increases both the accuracy and precision of the $^{40}Ar/^{39}Ar$ method over the conventional K-Ar technique. However, the $^{40}Ar/^{39}Ar$ technique will suffer if proper corrections are not made for interfering radiation-induced isotopes; fortunately, these corrections are well known, routinely made, and discussed herein.

For the purposes of this review, I consider it important to outline in some detail the formulations underlying the $^{40}Ar/^{39}Ar$ dating technique. Modern analytical details and formulations of the $^{40}Ar/^{39}Ar$ dating technique are similar to those comprehensively described by Dalrymple and others (1981) in U.S. Geological Survey Professional Paper 1176, "Irradiation of samples for $^{40}Ar/^{39}Ar$ dating using the Geological Survey TRIGA reactor." In the following discussion some additional experimental considerations that have been revealed since 1981 are included to provide the accurate foundation of current analytical procedures.

The determination of a sample's age is based on the production of ^{39}Ar from ^{39}K, and the age is directly proportional to the $^{40}Ar/^{39}Ar$ ratio of the sample. As derived by Grasty and Mitchell (1966) and modified by Mitchell (1968), the production of ^{39}Ar can be calculated from the relationship,

$$^{39}Ar_K = {}^{39}K\Delta T \int \phi(\varepsilon)\sigma(\varepsilon)d\varepsilon \ , \qquad (1)$$

where:
subscript K refers to potassium-derived ^{39}Ar;
ΔT is the length of irradiation;
$\phi(\varepsilon)$ is the neutron flux density at energy ε;
$\sigma(\varepsilon)$ is the capture cross section of ^{39}K for neutrons having energy ε; and integration is performed over the entire energy spectrum of neutrons.

The formulation of the age equation results from dividing this equation into the K-Ar age equation,

$$^{40}Ar_R = {}^{40}K\ (\lambda_\varepsilon/\lambda)(e^{(\lambda_\varepsilon+\lambda_{\beta^-})t}-1), \qquad (2)$$

where:
$^{40}Ar_R$ is radiogenic argon derived from the natural decay of potassium;
λ_ε is the decay constant for the decay of ^{40}K to ^{40}Ar;
λ_{β^-} is the decay constant for decay of ^{40}K to ^{40}Ca;
λ is the total decay constant for the decay of ^{40}K to ^{40}Ca and ^{40}Ar; and
t is the time since decay began following the closure of the system to loss of daughter products.

The resultant rearranged expression is

$$(e^{\lambda t}-1)/(^{40}Ar_R/^{39}Ar_K) = (\lambda/\lambda_\varepsilon)(^{39}K/^{40}K)\Delta T \int \phi(\varepsilon)\sigma(\varepsilon)d\varepsilon. \qquad (3)$$

The integrated quantity in this equation is very difficult, if not impossible, to evaluate directly; but in any particular irradiation, if a "monitor" (standard of known age) is irradiated adjacent to the sample of unknown age, the resulting relationship is

$$1 = [(e^{\lambda t}{}_m-1)/(^{40}Ar_R/^{39}Ar_K)_m]/[(e^{\lambda t}{}_u-1)/(^{40}Ar_R/^{39}Ar_K)_u], \qquad (4)$$

where subscripts m and u refer to "monitor" and "unknown," respectively. Rearranging this equation and using the conventions $J = (e^{\lambda t}{}_m-1)/(^{40}Ar_R/^{39}Ar_K)_m$ (Grasty and Mitchell, 1966) and $F = {}^{40}Ar_R/^{39}Ar_K$ (Dalrymple and Lanphere, 1971) results in

$$t_u = (1/\lambda)\ln(JF+1), \qquad (5)$$

which is the standard $^{40}Ar/^{39}Ar$ age equation. J is commonly referred to as the fluence parameter and F is the ratio of radiogenic ^{40}Ar to potassium-derived nucleogenic ^{39}Ar. The universally used decay constants are those recommended by Steiger and Jäger (1977), that is, $\lambda_\varepsilon = 0.581\times10^{-10}$/yr, $\lambda_{\beta^-} = 4.962\times10^{-10}$/yr, and $\lambda = \lambda_\varepsilon + \lambda_{\beta^-} = 5.543\times10^{-10}$/yr.

Dating material by this method would be a simple matter of measuring the $^{40}Ar/^{39}Ar$ ratios of the sample and standard after irradiation if not for the fact that numerous other argon isotope-producing reactions occur during irradiation, and nonradiogenic (atmospheric or extraneous) argon is always present. Several investigators (Stoenner and others, 1965; Mitchell, 1968; Brereton, 1970; Turner, 1971a; Dalrymple and others, 1981; Roddick, 1983) have reported details of these interfering reactions, and standard methods are now employed to make quantitative corrections for the interferences. Of these reactions those with the potentially most serious deleterious effects are $^{41}K(n,d)^{40}Ar$, $^{40}K(n,p)^{40}Ar$, $^{40}Ca(n,n\alpha)^{36}Ar$, $^{42}Ca(n,\alpha)^{39}Ar$, and $^{35}Cl(n,\alpha)^{36}Cl$, with subsequent β^- decay to ^{36}Ar. (The ^{35}Cl interference can become serious if irradiated samples are not analyzed within 6 months after irradiation.) Several additional reactions produce minor to trivial quantities of interfering argon isotopes, including $^{43}Ca(n,n\alpha)^{39}Ar$, $^{40}K(n,d)^{39}Ar$, $^{40}K(n,nd)^{38}Ar$, $^{41}K(n,\alpha)^{38}Cl$ with subsequent β^- decay to ^{38}Ar, $^{39}K(n,nd)^{37}Ar$, $^{42}Ca(n,n\alpha)^{38}Ar$, $^{43}Ca(n,\alpha)^{40}Ar$, and $^{44}Ca(n,n\alpha)^{40}Ar$. Fortunately two nuclear reactions, $^{40}Ca(n,\alpha)^{37}Ar$ and $^{37}Cl(n,\gamma)^{38}Cl$, with subsequent β^- decay to ^{38}Ar, produce isotopes of argon that are used to determine extent of interferences of argon isotopes produced from calcium and chlorine. An additional correction must be made for the decay of ^{37}Ar because it is radioactive; ^{37}Ar decays by electron capture with a half life of 35.1 ± 0.1 days to ^{37}Cl (Stoenner and others, 1965). ^{39}Ar is also radioactive and decays by β^- emission to ^{39}K; because its half life is 269 ± 3 years, corrections for this decay in most experiments are virtually unnecessary—although we always make this correction as well. In addition, pure crystalline salts of CaF_2 and K_2SO_4 are commonly irradiated with samples to directly measure the argon-isotope production ratios from these interfering reactions. Our laboratory includes CaF_2 and K_2SO_4 with each group of samples irradiated and has found some variation in production ratios from irradiation to irradiation. Although the variation is generally minor, in some cases, such as dating of young whole-rock basalt samples, significant inaccuracies may result in the calculation of apparent age if careful corrections are not made. Table 1 shows the averages with standard deviations and ranges for the six production ratios for CaF_2 and K_2SO_4 irradiated in the Denver argon geochronology laboratory from 1987 until the present (2002). Table 2 is a compilation of all the production ratios for the majority of 75 irradiations (DD1 through DD75) that were used to calculate the averages in table 1. From table 1, the large variation of 1.560×10^{-2} to 4.970×10^{-3} in the $(^{40}Ar/^{39}Ar)_K$ ratio is important. For young potassium-rich samples this variation could result in great inaccuracy if the proper ratio is not applied to the correction.

Table 1. Averages with standard deviations and ranges for production ratios determined for irradiations in the Geological Survey TRIGA reactor (GSTR) by the Denver argon geochronology laboratory from year 1987 to year 2002.

Production ratio	Average	Std. deviation	High	Low	Number
$(^{37}Ar/^{39}Ar)_K$	1.645×10^{-4}	$\pm0.729\times10^{-4}$	3.38×10^{-4}	5.5×10^{-5}	52
$(^{38}Ar/^{39}Ar)_K$	1.312×10^{-2}	$\pm0.009\times10^{-2}$	1.343×10^{-2}	1.300×10^{-2}	55
$(^{40}Ar/^{39}Ar)_K$	9.219×10^{-3}	$\pm2.039\times10^{-3}$	1.560×10^{-2}	4.970×10^{-3}	55
$(^{39}Ar/^{37}Ar)_{Ca}$	6.984×10^{-4}	$\pm0.811\times10^{-4}$	9.900×10^{-4}	5.050×10^{-4}	49
$(^{36}Ar/^{37}Ar)_{Ca}$	2.683×10^{-4}	$\pm0.078\times10^{-4}$	2.90×10^{-4}	2.35×10^{-4}	53
$(^{38}Ar/^{37}Ar)_{Ca}$	4.4×10^{-5}	$\pm1.9\times10^{-5}$	1.16×10^{-4}	1.8×10^{-5}	50

Along with necessary corrections for interfering nuclear reactions, corrections must be made for naturally occurring isotopes of argon (^{40}Ar, ^{38}Ar, and ^{36}Ar) that exist throughout nature and are incorporated in varying amounts in standards and unknowns. These incorporated argon isotopes are commonly referred to as atmospheric or extraneous argon and may have their origin from the minor amounts of argon that are present before a mineral closes to argon diffusion or from true atmospheric argon incorporated within the mineral structure during its life or released from the extraction system while an experiment is conducted. Fortunately, the present-day argon atmospheric ratios of $^{40}Ar/^{36}Ar$ and $^{38}Ar/^{36}Ar$ are well known and easy to measure in most laboratories; accepted values are 295.5 for $(^{40}Ar/^{36}Ar)_{At}$ and 1,581 for $(^{40}Ar/^{38}Ar)_{At}$.

Taking into account the preceding discussion on interfering isotopes of argon, in order to determine the actual F (that is, $^{40}Ar_R/^{39}Ar_K$ ratio) of a sample or standard, the isotopic abundances of five argon isotopes (^{40}Ar, ^{39}Ar, ^{38}Ar, ^{37}Ar, and ^{36}Ar) are measured by mass spectrometry. Then, the corrections for all irradiation-produced interfering isotopes of argon are made. Next, the correction for atmospheric argon is made using the measured atmospheric argon ratio as determined from measuring atmospheric argon on the same mass spectrometer. This measured ratio also will be used to correct the argon abundances for mass discrimination that takes place in all mass spectrometers. F in its simplest form is calculated from the following expression.

$$F = {}^{40}Ar_R/{}^{39}Ar_K =$$

$$\{(^{40}Ar/^{39}Ar) - 295.5[(^{36}Ar/^{39}Ar) - (^{36}Ar/^{37}Ar)_{Ca}(^{37}Ar/^{39}Ar)] - (^{40}Ar/^{39}Ar)_K\}/$$

$$\{1 - (^{39}Ar/^{37}Ar)_{Ca}(^{37}Ar/^{39}Ar)\}. \quad (6)$$

In this form, no correction is made for Cl-derived argon isotopes and other relatively minor interference corrections are ignored. In the argon geochronology laboratory at the USGS, Denver, we correct for all minor K-, Ca-, and Ar-derived interfering argon isotopes as well as Cl-derived argon isotopes. The resultant formulation for F is complex as follows:

$$F = \{A - [C_3C_4((E-C_5B)/(1- C_4 C_5))]-C_1[G-C_{10}C_6(D-C_7((E-C_5B)/(1-C_4C_5))-C_8(B-(C_4(E-C_5B)/(1-C_4C_5)))- C_1(G-(C_2(E-C_5B)/(1-C_4C_5)))-C_2(E-C_5B)/(1-C_4C_5))/(1-C_9 C_{10}C_6)]\}/\{B-[C_4(E-C_5B)/(1-C_4C_5)]\}, \quad (7)$$

where $F={}^{40}Ar_R/{}^{39}Ar_K$,
$A={}^{40}Ar$,
$B={}^{39}Ar$,
$D={}^{38}Ar$,
$E={}^{37}Ar$,
$G={}^{36}Ar$,
$C_1=(^{40}Ar/^{36}Ar)_{At}$,
$C_2=(^{36}Ar/^{37}Ar)_{Ca}$,
$C_3=(^{40}Ar/^{39}Ar)_K$,
$C_4=(^{39}Ar/^{37}Ar)_{Ca}$,
$C^5=(^{37}Ar/^{39}Ar)_K$,
$C_6=(^{36}Ar/^{38}Ar)_{Cl}$,
$C_7=(^{38}Ar/^{37}Ar)_{Ca}$,
$C_8=(^{38}Ar/^{39}Ar)_K$,
$C_9=(^{38}Ar/^{36}Ar)_{At}$,
$C_{10}=Cl_D$, with subscript D = corrected for decay.

Standards

Many standards are used for $^{40}Ar/^{39}Ar$ geochronology. Reviews of some of the more commonly used are presented in Roddick (1983), McDougall and Harrison (1999), and Dalrymple and others (1993). At the USGS Denver argon geochronology laboratory, we use two standards. Our primary standard is a hornblende, MMhb-1, from the McClure Mountain Complex in southern Colorado with percent K = 1.555, $^{40}Ar_R=1.624\times10^{-9}$ mol/g, and K-Ar age=520.4 ± 1.7 Ma (Alexander and others,

1978; Dalrymple and others, 1981; Samson and Alexander, 1987). Hornblende MMhb-1 is used worldwide as an interlaboratory $^{40}Ar/^{39}Ar$ standard and is particularly appropriate for use as a standard with samples of Mesozoic and older age.

Our secondary standard is a sanidine from the Fish Canyon Tuff, FCT, also from southern Colorado. Steven and others (1967) determined a conventional K-Ar age for this sanidine of 28.5 ± 0.8 Ma. We have calibrated sanidine FCT against hornblende MMhb-1 in our laboratory with a resultant $^{40}Ar/^{39}Ar$ age of 27.84 ± 0.04 Ma. FCT is particularly useful as a standard for samples with Cenozoic and Mesozoic age.

A great deal of disagreement exists as to the actual age of hornblende MMhb-1 (Dalrymple and others, 1993; Renne and others, 1994; McDougall and Harrison, 1999); the published international mean age is 520.4±1.7 Ma; the Denver argon geochronology laboratory has used this value until recently. The disagreement results because the range in apparent ages determined in 18 laboratories is nearly 15 m.y., a difference in age of nearly 3 percent, and all ages are used to calculate the mean. Thus, the accuracy of this age is in question. Because the precision of the method is now commonly in the 0.2 percent range, and because the method is applied to problems requiring greater accuracy, such as resolution of the age of time units on the geologic age scale, a more accurate age is necessary. In view of this, Renne and others (1994, 1998a, 1998b) have evaluated both the accuracy of isotopic dating methods and the intercalibration of geochronologic methods. In a comprehensive review of argon geochronology standards, Renne and others (1998b) compared the commonly used standards, recalibrated two of these commonly used standards, and assessed the quality of each standard. From their careful work, among other conclusions, they recommended that the best age for MMhb-1 hornblende, as calibrated against the newly determined age of 98.79±0.96 Ma for their primary standard GA-1550 biotite, is 523.1±2.6 Ma, excluding the error in decay constant, and 523.1±4.6 Ma including decay constant errors. A slightly higher age of 525.1, with identical errors, is calculated if the primary standard used for calibration is GHC-305 biotite. Because Renne and others (1998b) considered the K-Ar data for GHC-305 to be less accurate than those for GA-1550, we have adopted an age of 523.1 Ma for MMhb-1 hornblende as well as their best age of 28.02±0.16 Ma for FCT sanidine. For most experiments on Phanerozoic samples, this 0.4-percent difference is relatively unimportant. However, for time-scale studies or analyses of Archean-age rocks, this difference can be important and must be recognized.

The issue of standard-age inaccuracy becomes increasingly problematic for comparison of Proterozoic and older argon ages to dates determined by other isotopic systems, especially the U-Pb system (Renne and others, 1998a). Inaccuracies of only 1 percent at 2,500 Ma translate to 25 m.y., and serious discordance between isotopic systems may result simply because of standard-age inaccuracy and not actual geologic age difference. A case in point is in the giant Western Australia gold belt where the viability of the argon system applied to Archean problems has been questioned because of discordances between argon dates determined by Kent and McDougall (1996) and reasonable ages based on geology and other isotopic dating (Witt and others, 1996). The discordance and apparent inconsistency likely result from inaccuracies in the assumed age of the argon irradiation standard (James Dunlap, Australian National University, written commun., 2001).

Because the supply of the original MMhb-1 hornblende standard is nearly depleted, recently USGS argon geochronologists recollected at the McClure Mountain Complex locality in south-central Colorado from which the original MMhb-1 standard was taken, and have begun to process a new hornblende standard, MMhb-2 (Kunk and others, 1994). We are in the process of carefully calibrating the age of this new hornblende standard using (1) a high-precision pipetting method calibrated at the National Institute of Standards and Technology to precisely (within 0.1 percent) and accurately (within 0.25 percent, excluding the decay constant error) determine the argon content, and (2) an isotope-dilution thermal ionization mass spectrometry method at the National Institute of Standards and Technology to precisely (within 0.1 percent) and accurately (within 0.25 percent) determine the potassium content. The potassium analyses have been completed with percent K = 1.5500±0.0011 (1σ, six determinations) for hornblende MMhb-2. The potassium content of MMhb-1 was also redetermined by this method and is 1.55713±0.00072 (1σ, three determinations). Once the argon content has been accurately determined, the standard will be released for worldwide use and the accuracy of the $^{40}Ar/^{39}Ar$ method will be comparable to its precision.

This calibration is by so-called "first principles" (Lanphere and Dalrymple, 2000) and when completed will provide an analytically accurate measurement. However, others (Roddick, 1983; Renne and others, 1998b; McDougall and Harrison, 1999) have argued that MMhb-1 (and presumably MMhb-2) hornblende is an inhomogeneous material at the single-grain level and thus not adequate for modern, high-precision, small sample-size analyses. It is also of an age (≈520 Ma) and potassium content that its usefulness for monitoring very young samples is marginal. Other laboratory standards are being proposed for the international $^{40}Ar/^{39}Ar$ dating standard. Clearly, considering the high precision and robust nature of the $^{40}Ar/^{39}Ar$ method in contrast to its lower accuracy, it is time for the argon community to evaluate potential standards and to accurately determine the age of the accepted standard(s). Renne and others (1994, 1998a, 1998b) have begun this process, and others, such as Roddick (1987) and Baksi and others (1996), are contributing to the better characterization of $^{40}Ar/^{39}Ar$ standards.

Thermal Release Experiments and Age Spectra

The $^{40}Ar/^{39}Ar$ method was first used in "total-fusion" experiments in which an irradiated sample was completely melted and all isotopes of argon were measured in a single analysis to calculate a date for the sample (for example, Turner, 1970a,b). This total-fusion date is roughly analogous to a conventional K-Ar date for the sample, except that neither isotopic concentration measurement nor direct measurement of potassium content is

Table 2. Production ratios determined for irradiations in GSTR done by the Denver argon geochronology laboratory and used in argon data reductions from year 1987 to year 2002.

[– indicates not determined]

Package	$(^{37}Ar/^{39}Ar)_K$	$(^{38}Ar/^{39}Ar)_K$	$(^{40}Ar/^{39}Ar)_K$	$(^{39}Ar/^{37}Ar)_K$	$(^{36}Ar/^{37}Ar)_K$	$(^{38}Ar/^{37}Ar)_K$	Comments
Pre-DD8□	.002200	.01300	.006270	.000673	.000264	.000032	From Dalrymple and others, 1981
DD8□	.00019	.01300	.007520				30 hrs irradiation
DD9□	.000448	.01300	.012600		.000255	.000069	100 "
DD10□	.000201	.01320	.012900	.000749	.000275	.000049	30 "
DD11□	.000208	.01310	.012100		.000263	.000051	30 "
DD12□	.000182	.01300	.009070	.000699	.000266	.000028	30 "
DD13□	.000139	.01300	.008760	.000708	.000269	.000029	30 "
DD14□	.000111	.01310	.008780	.000655	.000269	.000035	30 "
DD15□	.000158	.01320	.009120				96 "
DD16□	.000234	.01300	.011350	.000666	.000264	.000037	30 "
DD18□	.000146	.01305	.015600	.000746	.000251	.000030	30 "
DD19□	.000164	.01301	.009500	.000682	.000271	.000031	30 "
DD23□	.000174	.01304	.004970	.000675	.000261	.000037	20 "
DD24□	.000174	.01302	.008840	.000825	.000261	.000059	40 "
DD25□	.000128	.0130 6	.011800	.000990	.000264	.000032	30 "
DD26□	.000235	.01310	.010110	.000648	.000270	.000037	25 "
DD27□	.000110	.01313	.007700	.000641	.000263	.000064	60 "
DD28□	.000083	.01306	.008780	.000768	.000261	.000030	30 "
DD30□	.000082	.01306	.009184	.000636	.000270	.000032	35 "
DD31□	.000082	.01306	.009184	.000636	.000270	.000032	30 "
DD32□				.000656	.000256	.000037	20 "
DD33□	.000110	.01307	.009760	.000681	.000270	.000027	30 "
DD34□	.000080	.01310	.007135	.000675	.000265	.000035	123 "
DD35□	.000176	.01312	.006660	.000779	.000266	.000067	33 "
DD36□	.000110	.01307	.009760	.000681	.000270	.000027	21 "
DD37□	.000149	.01313	.008990	.000694	.000280	.000037	30 "
DD38□	.000149	.01313	.008990	.000681	.000270	.000030	25 "
DD41□	.000260	.01310	.015200	.000841	.000235	.000030	30 "
DD42□	.000099	.01318	.007500	.000630	.000290	.000021	30 "

required. Very soon after the first uses of the $^{40}Ar/^{39}Ar$ method, it was realized that a sample could be progressively degassed in increasing temperature increments (Merrihue and Turner, 1966). A date can be calculated for each increment of gas evolved and the dates can be plotted sequentially and weighted by percent of total released argon to form an age spectrum. The age spectrum is an interpretive tool, the character of which can be evaluated within a theoretical framework to interpret the apparent distribution of potassium and argon within the sample. Turner (1968) showed that the dates for the temperature increments of some meteorites were identical within analytical precision, and that when plotted on an age-spectrum diagram, which shows the

Table 2—Continued. Production ratios determined for irradiations in GSTR done by the Denver argon geochronology laboratory and used in argon data reductions from year 1987 to year 2002.

[– indicates not determined]

Package	$(^{37}Ar/^{39}Ar)_K$	$(^{38}Ar/^{39}Ar)_K$	$(^{40}Ar/^{39}Ar)_K$	$(^{39}Ar/^{37}Ar)_K$	$(^{36}Ar/^{37}Ar)_K$	$(^{38}Ar/^{37}Ar)_K$	Comments
DD43□	.000055	.01313	.007950	.000680	.000280	.000056	30 hrs irradiation
DD44□	.000092	.01315	.008050		.000268	.000051	16 "
DD45□	.000150	.01308	.007950	.000635	.000266	.000045	30 "
DD46□	.000150	.01309	.008000	.000674	.000269	.000044	60 "
DD47□	.000100	.01308	.008034	.000609	.000271	.000039	20 "
DD49□	.000110	.01306	.007800	.000595	.000270	.000024	30 "
DD50□	.000127	.01308	.006200	.000505	.000271	.000018	30 "
DD51□	.000134	.01316	.008400	.000670	.000272	.000053	52.25 "
DD52□	.000175	.01317	.009750				8 "
DD53□	.000175	.01309	.007920	.000685	.000268	.000044	28.5 "
DD54□				.000685	.000275	.000044	40 "
DD55□				.000670	.000271	.000080	30 "
DD56□	.000145	.01310	.010400	.000786	.000271	.000035	20 "
DD57□	.000300	.01304	.009350	.000720	.000270	.000047	30 "
DD59□	.000129	.01321	.006850	.000665	.000270	.000058	30 "
DD60□	.000225	.01311	.007400	.000685	.000270	.000045	25 "
DD61□	.000175	.01311	.010400	.000634	.000270	.000046	15 "
DD62□	.000115	.01321	.007100	.000635	.000266		60 "
DD63□	.000225	.01337	.012000		.000274		25 "
DD64□	.000175	.01318	.009050	.000692	.000274		20 "
DD65□	.000338	.01322	.011530	.000915	.000273	.000083	20 "
DD66□	.000320	.01322	.009315	.000648	.000275	.000086	20 "
DD67□	.000120	.01326	.009480	.000698	.000272	.000039	30 "
DD68□	.000100	.01326	.008500				30 "
DD70□	.000140	.01312	.009150	.000675	.000274	.000045	30 "
DD71□		.01318	.006000	.000818	.000271	.000050	20 "
DD72□		.01307	.008950	.000779	.000268	.000027	15 "
DD73□		.01325	.010500				18 "
DD74□	.000192	.01343	.010100	.000687	.000267	.000116	129 hrs
DD75□	.000207	.01323	.009050	.000736	.000269	.000035	30 "

date of each temperature increment as a function of percent ^{39}Ar released during the experiment, the spectra formed "plateaus" (fig. 1). (Until geologic significance is placed upon the analytical number, I prefer to use "date," "apparent age," or "numerical age" to refer to the analytical number determined by solving the "age" equation using isotopic data produced for a sample in the laboratory. In contrast, I use "age" or a specific type of "age," such as "emplacement age," "cooling age," or "age of metamorphism," to refer to a date that has been constrained by geologic data and is interpreted to have geologic meaning.)

Ideally a sample dated by the $^{40}Ar/^{39}Ar$ age-spectrum technique will yield concordant dates for all temperature steps. If a

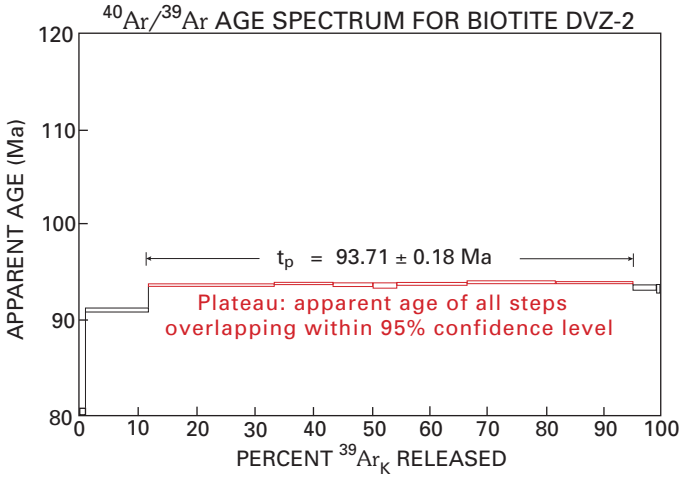

Figure 1. A typical $^{40}Ar/^{39}Ar$ age spectrum. Vertical axis plots apparent age; horizontal axis is cumulative percent ^{39}Ar released, from 0 to 100 percent. Lowest extraction temperature step is plotted at left; each progressively higher temperature step is plotted successively to right to form spectrum of apparent dates obtained from the sample during the heating experiment. Length of corresponding segment represents percentage of ^{39}Ar released during each heating step. Vertical thickness of bar shows 2σ error envelope above and below age of that individual step. This age spectrum is for a biotite from the Domenigoni pluton in the Peninsular Ranges batholith south of Riverside, Calif.; plateau date is 93.71±0.18 (1σ) Ma.

sample's age spectrum is 100 percent concordant, that is, all temperature steps yield identical dates within two standard deviations (2σ) of the weighted mean date for all temperature steps, then clearly the best date for the sample is a weighted mean of the dates of all temperature steps. The geologic significance of the resultant date must then be evaluated using geologic or other independent constraints.

For a sample to exhibit 100 percent concordancy in apparent ages across all temperature steps is unusual. Most dated samples display some discordancy on the age spectrum because of a physical or chemical disturbance, such as the presence of ^{40}Ar that was not derived from the in-place decay of ^{40}K, or the loss of some ^{40}Ar after the original closure of the sample to ^{40}Ar diffusion. However, even if an age spectrum shows some degree of discordancy, the interpreted dates usually hold geologic significance. Some commonly used terms for interpreted dates derived from an age spectrum are *total-gas date* (or age), *integrated date* (or age), *plateau date* (or age), and *preferred date* (or age). The *total-gas date* from a thermal release experiment is the average of the dates of all temperature steps for the sample weighted according to percentage of released ^{39}Ar in each step; the total-gas date is comparable to a conventional K-Ar date but is more precise and more accurate for the reasons previously stated. An *integrated date* is virtually identical to the total-gas date but is preferred by some others. The *plateau date* is the weight-averaged date for that part of the age spectrum composed of contiguous gas fractions that together represent more than 50 percent of the total ^{39}Ar released from the sample and for which no difference in apparent age can be detected between any two fractions at the 95 percent confidence level (Fleck and others, 1977). The term plateau has been used by others (for example, Lanphere and Dalrymple, 1971; Dalrymple and Lanphere, 1974; Harrison, 1983; see also McDougall and Harrison, 1999) to refer to a "high-temperature segment" of an age spectrum throughout which the dates of the plateau-defining steps are concordant at the 95 percent confidence level. In some cases, by this usage, a single step may define a plateau. Finally, some age spectra show near concordancy, and weight-average dates of the near-concordant parts of the spectrum may have some geologic meaning. I refer to these dates as *preferred dates* that consist either of an apparent plateau comprising less than 50 percent of the total released ^{39}Ar or of fractions of gas whose dates overlap within three standard deviations (3σ) of the weighted mean.

Error Analysis

In order to determine the actual $^{40}Ar_R/^{39}Ar_K$ ratio (F) of a sample or standard, we measure the isotopic abundances of five argon isotopes (^{40}Ar, ^{39}Ar, ^{38}Ar, ^{37}Ar, and ^{36}Ar) by mass spectrometry. Each of these laboratory measurements has an associated error estimated as the standard deviation of analytical precision. These analytical errors, along with those resulting from the measurement of reactor-induced interfering argon isotopes and atmospheric argon isotopes, are propagated in our error calculation for F. In the Denver argon geochronology laboratory, we also independently estimate an error for each measured F by using a pooled coefficient of variation for numerous measurements of multiple splits of an extracted gas fraction from a single sample; this pooled coefficient of variation is 0.11 percent, at 1σ. Both error estimates are calculated, and the larger estimate is used for any analysis to ensure a conservative error. For an error estimate on any calculated date, the error in the J-value is included in the estimate. Errors in J are analytical errors calculated at 1σ from the calculation of the J-value associated with monitors (standards) adjacent to each unknown. Our error equation is modified from that published by Dalrymple and others (1981) in which we derive our error formula by differentiation of our equation for F; this equation includes errors in chlorine-derived argon isotopes and other minor interferences. Roddick (1987, 1988) and Scaillet (2000) presented an alternative approach to error analysis that avoids the need to make simplifying assumptions. Roddick developed a more rigorous numerical error propagation that takes into account the direct effect of the analytical error of each measurement on F.

To evaluate an age spectrum, we compare the errors associated with the F-values of adjacent fractions of gas at the 95 percent confidence level (2σ) using the critical value test (McIntyre, 1963; Dalrymple and Lanphere, 1969). The Critical Value, C.V. equals $1.96\ [(\sigma_1)^2/n_1 + (\sigma_2)^2/n_2]^{1/2}$, where σ_1 and σ_2 are the standard deviations of the analytical measurements (in this case, the F-values) and n_1 and n_2 are the number of measurements. If two adjacent fractions are analytically identical in F-value, the difference in their F-values must be less than the calculated critical value. If a plateau is defined for a sample, the apparent age of the plateau segment is the weighted mean of the apparent ages of the steps on the plateau, and the error in the plateau date is the standard deviation (1σ) of the apparent ages included in the plateau-date calculation.

Ultimately apparent ages of several samples are compared. To decide whether an absolute difference exists between two apparent ages, we again employ the critical value test. If the difference between two apparent ages is less than their critical value, an age difference has not been established. This does not mean that there is no age difference, but only that if one exists, it cannot be resolved by our method. In contrast, if the difference between two apparent ages is greater than the critical value, an apparent age difference has been detected. Apparent ages of populations also are compared in this way. After a population is defined on some criterion (for example, all belong to the population of a single vein set), all dates determined for that population are averaged and a weighted mean apparent age with associated standard deviation can be calculated.

$^{39}Ar/^{37}Ar$ (Apparent K/Ca) Diagrams

During irradiation ^{39}Ar is produced from ^{39}K and ^{37}Ar is produced from ^{40}Ca. After correction for interfering argon isotopes, $^{39}Ar/^{37}Ar$ ratios provide valuable information on the relative distribution of K with respect to Ca in a sample. An $^{39}Ar/^{37}Ar$ diagram is complementary to the sample's age spectrum diagram and displays the relative $^{39}Ar/^{37}Ar$ ratio for each temperature step of the sample plotted against percent ^{39}Ar released. The $^{39}Ar/^{37}Ar$ ratio is directly proportional to the K/Ca ratio corresponding to each temperature step of the analysis. The proportionality constant is controlled by the ratio of fast to thermal neutrons during irradiation and thus not only is reactor dependent but also can change from irradiation to irradiation in a single reactor. For the Geological Survey TRIGA reactor (GSTR), Dalrymple and others (1981) determined the relationship to be

$$K/Ca = (0.49 \pm 0.09)\ {}^{39}Ar_K/{}^{37}Ar_{Ca} \qquad (8)$$

The constant of proportionality was calculated using data from 19 samples for which K/Ca was measured by independent chemical means. The Denver argon geochronology laboratory has not repeated this experiment, but based on more than 70 irradiations since 1986, using hornblende MMhb-1 as our standard, we have observed that its $^{39}Ar_K/^{37}Ar_{Ca}$ always lies between 0.40 and 0.41. The reported K/Ca of this hornblende is 0.208 (Samson and Alexander, 1987), which is within error of the K/Ca calculated using the preceding equation with our measured $^{39}Ar_K/^{37}Ar_{Ca}$ values of 0.40 to 0.41. So for samples irradiated in GSTR, a semiquantitative K/Ca can be calculated for a sample, using this equation. This, however, is not a universal equation, because the fast-to-thermal neutron ratios of other reactors are not the same as that of GSTR.

An $^{39}Ar_K/^{37}Ar_{Ca}$ diagram for a sample can prove to be quite useful in the interpretation of complex age spectra. From our experience, for example, standard amphibole will exhibit a constant $^{39}Ar_K/^{37}Ar_{Ca}$ ratio throughout the temperature range of release of structurally controlled argon (fig. 2).

In contrast, it is common for argon that is released at lower extraction temperatures—and less commonly at higher extraction temperatures—to have strikingly different $^{39}Ar_K/^{37}Ar_{Ca}$ as well as different apparent ages.

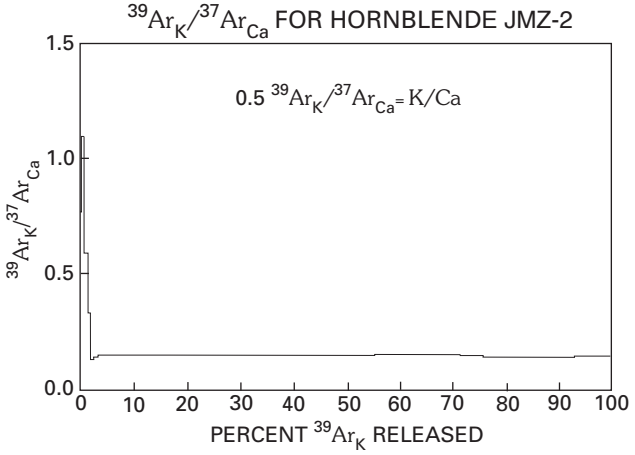

Figure 2. A typical $^{39}Ar_K/^{37}Ar_{Ca}$ relation. Analogous to an age-spectrum diagram, vertical axis plots $^{39}Ar_K/^{37}Ar_{Ca}$; horizontal axis is cumulative percent ^{39}Ar released from 0 to 100 percent. Each segment of the line corresponds to $^{39}Ar_K/^{37}Ar_{Ca}$ for a temperature step. For the TRIGA reactor, K/Ca is approximately $0.5(^{39}Ar_K/^{37}Ar_{Ca})$. This plot is for a hornblende from the Peninsular Ranges batholith; its age spectrum defines a plateau that is ≈90 percent concordant with a plateau date of 101.9±0.2 Ma and a constant K/Ca throughout the plateau.

We have interpreted these different ratios to reflect contributions of argon from a variety of sources, such as fluid inclusions, intergrown minerals such as pyroxene, plagioclase, biotite, or actinolite, or the influence of system blank. In studies of white micas, Roeske and others (1995), Christiansen and Snee (1994), and Till and Snee (1995) used K/Ca ratios with isochron diagrams and back-scattered element images to define the phases reflected in complex argon release spectra. Thus, an $^{39}Ar_K/^{37}Ar_{Ca}$ diagram is an effective graphical tool for elucidating argon systematics within a sample (fig. 3).

Correlation Diagrams

Two correlation diagrams are used to interpret $^{40}Ar/^{39}Ar$ data, and in most cases either or both are used to confirm age-spectrum results or to try to derive useful information from complex age spectra. These diagrams are particularly useful for determining and illustrating the age of the sample and the composition of the trapped (the nonradiogenic) component(s) of the sample. The isochron diagram (fig. 4*A*) (Merrihue and Turner, 1966) is a plot of $^{40}Ar/^{36}Ar$ versus $^{39}Ar/^{36}Ar$ after reactor-induced interferences have been deleted. The inverse correlation diagram (fig. 4*B*) is a plot of $^{36}Ar/^{40}Ar$ versus $^{39}Ar/^{40}Ar$ with reactor-induced interferences removed (Turner, 1971b). Although some have argued that one has more utility than the other (Roddick and others, 1980; McDougall, 1985; Phillips and Onstott, 1986), the "two types of diagrams***yield the same information provided the correct mathematics are used for estimating correlation coefficients and for the least squares fit" (Dalrymple and others, 1988, p. 589). Choice of one over the other simply comes down to personal preference. Excellent discussions of the constructions, formulations, and error analysis of

these diagrams are presented in the reports just listed as well as York (1969), Roddick (1978), and Wendt and Carl (1991).

We use correlation diagrams to evaluate the nature of the trapped nonradiogenic argon component and to help unravel complex argon age spectra. Heizler and Harrison (1988) and Till and Snee (1995; fig. 5) showed how this approach can be useful. Both studies demonstrated that multiple trapped components of nonradiogenic argon can be revealed by careful isochron analyses and some pure luck. In both studies, age spectra that did not provide unambiguous age information were interpretable with associated isochron analysis.

Argon Loss

In contrast to the simple argon release displayed in a plateau spectrum, Turner (1968) showed that some age spectra exhibited a distinct increase in dates across an age spectrum from low-temperature to high-temperature extraction steps (fig. 6). Turner showed theoretically that an age spectrum will exhibit a step-up in dates if argon is lost from a sample in a geologic environment by thermally activated volume diffusion.

The age spectrum will exhibit a plateau if the sample had never been disturbed after formation or if the sample had been completely reset by a younger thermal event (end-member curves 1.0 and 0). Depending on the amount of thermal disturbance, that is, the percentage of argon lost, the date of the younger, low-temperature fractions will be equal to, or older than, the age of the thermal disturbance that affected the sample, whereas the date of the older, high-temperature fractions will be equal to, or younger than, the original age of closure. This step-up in dates exhibited by an age spectrum and apparently resulting from argon loss due to geologic activity has been experimentally reproduced by Harrison (1981) from hornblende (fig. 7) and has been observed by numerous investigators from hornblende, muscovite, and potassium feldspar.

The reliability of hornblende, muscovite, and potassium feldspar to record geologically induced thermally activated argon loss as exhibited in an age spectrum produced by experimental degassing in the laboratory has been called into question by Lee and others (1991). They contended that hydrous minerals, in particular, but potassium feldspar as well, undergo changes, including dehydration, melting, and phase conversions, during heating under vacuum. These heating-induced changes prevent release of argon by thermally activated volume diffusion from the mineral. Thus, according to Lee and others (1991), experimental reproduction of the geologic phenomenon of argon loss is impossible.

Although the mechanism responsible for the development of apparent argon-loss age spectra from some hornblendes, potassium feldspars, and muscovites may not be completely understood, there is no question that this pattern is exhibited by many, if not most, of these minerals after they undergo partial argon loss due to reheating in the geologic environment. Besides thermally activated volume diffusion, several other possible mechanisms can explain apparent argon-loss spectra. For example, two or more phases of different isotopic ages may

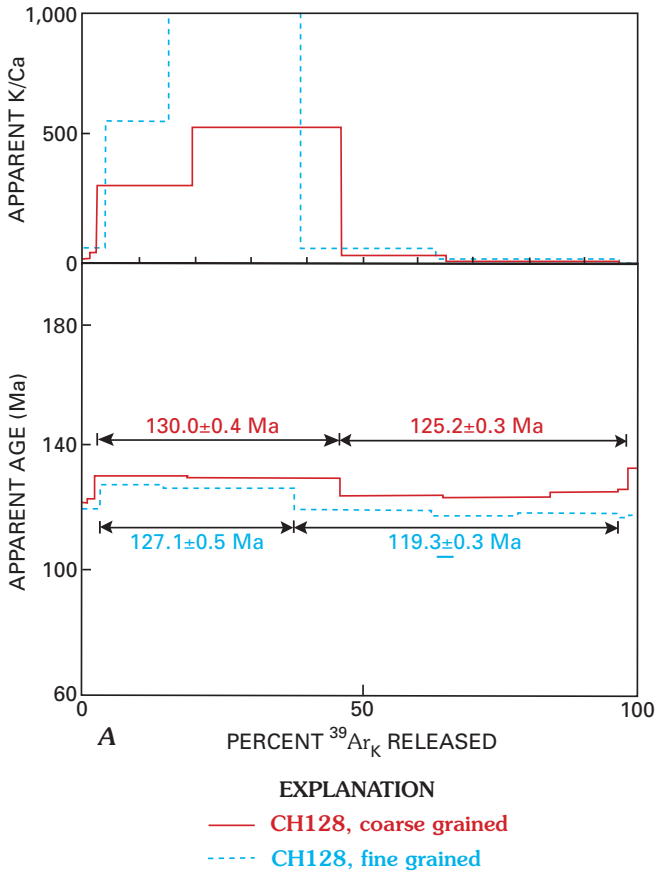

Figure 3 (above and following page). Diagrams of age and K/Ca spectra, and back-scattered electron image of Alaskan white mica sample. *A*, Age spectra for fine-grained and coarse-grained fraction of white mica from Cosmos Hills, Alaska (Christiansen and Snee, 1994) show a bimodal age distribution that is mirrored by the K/Ca diagram; grain sizes show different apparent ages. K/Ca indicates that high-K white mica (phengite in this case) controls argon in high-age part of hump; low-K white mica (paragonite) controls argon in low-age part of spectrum. *B*, Back-scattered electron image confirms complex intergrowth; ph, phengite; pg, paragonite; ms, muscovite; cld, chloritoid.

coexist in one rock. If two different phases of similar character, such as the white micas, phengite and muscovite, coexist in a mineral separate, and if each phase degasses in vacuum over different temperature ranges, then the resultant age spectrum will represent a mixture of the age spectra for both samples and will resemble an argon-loss spectrum (Till and Snee, 1995). Similarly, a single-phase mineral separate that has several grain sizes or structural types that degas over different temperature ranges under vacuum can produce the same result (Cosca and others, 1992). In both of these examples, the apparent argon-loss spectrum can be interpreted as if it had resulted from thermally activated volume diffusion. That is, the apparent age of the younger, lower temperature fractions is approximately the age of, or older than, the age of thermal resetting. Therefore, apparent argon-loss spectra give us considerable potential for understanding the thermal histories of complex geologic environments. However, we must use caution when interpreting apparent argon-loss spectra because other, nongeologic factors, such as extraction-system blanks and sample impurity, can affect the character of an age spectrum.

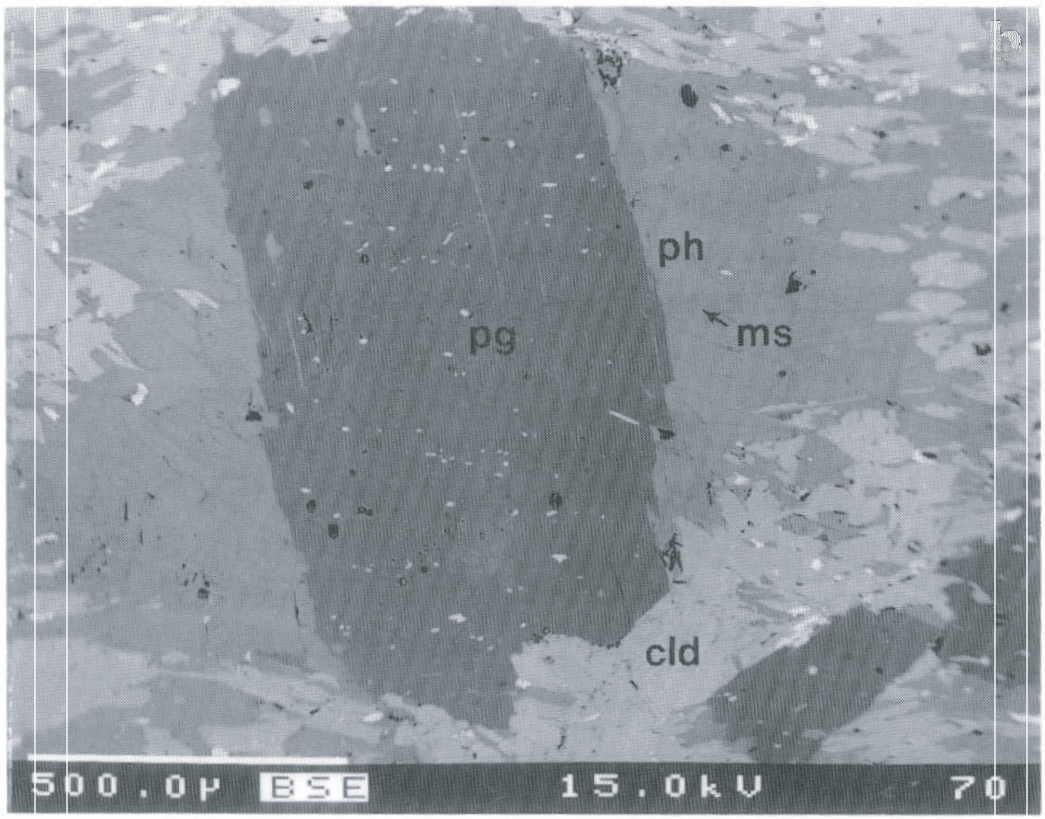

B

Extraneous Argon

Dalrymple and Lanphere (1969) defined extraneous ^{40}Ar as consisting of two types—excess ^{40}Ar and inherited ^{40}Ar. Excess ^{40}Ar results from other than in-place radioactive decay; inherited ^{40}Ar is incorporated in a system from mineral grains that retain an older reservoir of argon. The mechanism for the incorporation of excess ^{40}Ar into a rock or mineral is unknown, but several possible explanations exist. If a rock or mineral crystallizes in an environment that contains argon with an $^{40}Ar/^{36}Ar$ composition greater than 295.5 (the present-day atmospheric argon composition) and if this enriched argon is incorporated into the rock or mineral, the initial $^{40}Ar/^{36}Ar$ ratio of the mineral will have "excess ^{40}Ar" relative to present day. Similarly, hydrothermal fluids are known to carry argon that commonly has an isotopic composition greater than 295.5, perhaps due to fluid interaction with rocks containing radiogenic argon. For fluids that derive argon from very old, potassium-rich rocks, incorporated $^{40}Ar/^{36}Ar$ ratios could conceivably be much greater than 100,000. If these fluids alter or become incorporated in a rock or mineral, excess ^{40}Ar can be added to that rock or mineral.

Several studies (such as Lanphere and Dalrymple, 1971, 1976; Kaneoka, 1974) have documented that large quantities of excess ^{40}Ar in a sample will produce a saddle-shaped $^{40}Ar/^{39}Ar$ age spectrum that exhibits anomalously old dates for lower temperature and higher temperature extraction steps (fig. 8). Small quantities of excess ^{40}Ar commonly only affect the lower temperature extraction steps, resulting in an L-shaped spectrum. ^{40}Ar-enriched argon derived from the lower temperature parts of the release spectrum commonly is associated with low-retention sites, such as fluid inclusions, defects, and alteration; higher relative K/Ca is common for these steps. ^{40}Ar-enriched argon derived from the higher temperature parts of the spectrum is likely associated with low-potassium, high-retention mineral phases, such as pyroxene; lower relative K/Ca is common for these higher temperature steps.

^{39}Argon Recoil

^{39}Ar recoil occurs as a direct result of the production of ^{39}Ar from the $^{39}K(n,p)\ ^{39}Ar$ nuclear reaction. When a fast neutron collides with a ^{39}K nucleus, a proton is ejected to form an ^{39}Ar nucleus. The ejected proton causes "recoil" of the ^{39}Ar atom.

To interpret an $^{40}Ar/^{39}Ar$ age spectrum as representing the natural behavior of argon released from a sample requires that none of the features of the spectrum be produced by the experimental method itself. The recoil of ^{39}Ar from a sample during irradiation is a function of the experimental method and violates this assumption. The result of the loss of ^{39}Ar from a sample is the anomalous increase in the $^{40}Ar/^{39}Ar$ of the material and an increase in the apparent age (fig. 9).

The mean energy of the recoil in most research reactors ranges between 100 and 200 keV (Turner and Cadogan, 1974). Using the work of Davies and others (1963), Turner and Cadogan (1974) reasoned that if an outer layer of material were affected by recoil, its mean depth of depletion would be 0.082 µm. In simpler terms, if the ^{39}Ar atom is in a weakly held location, it could

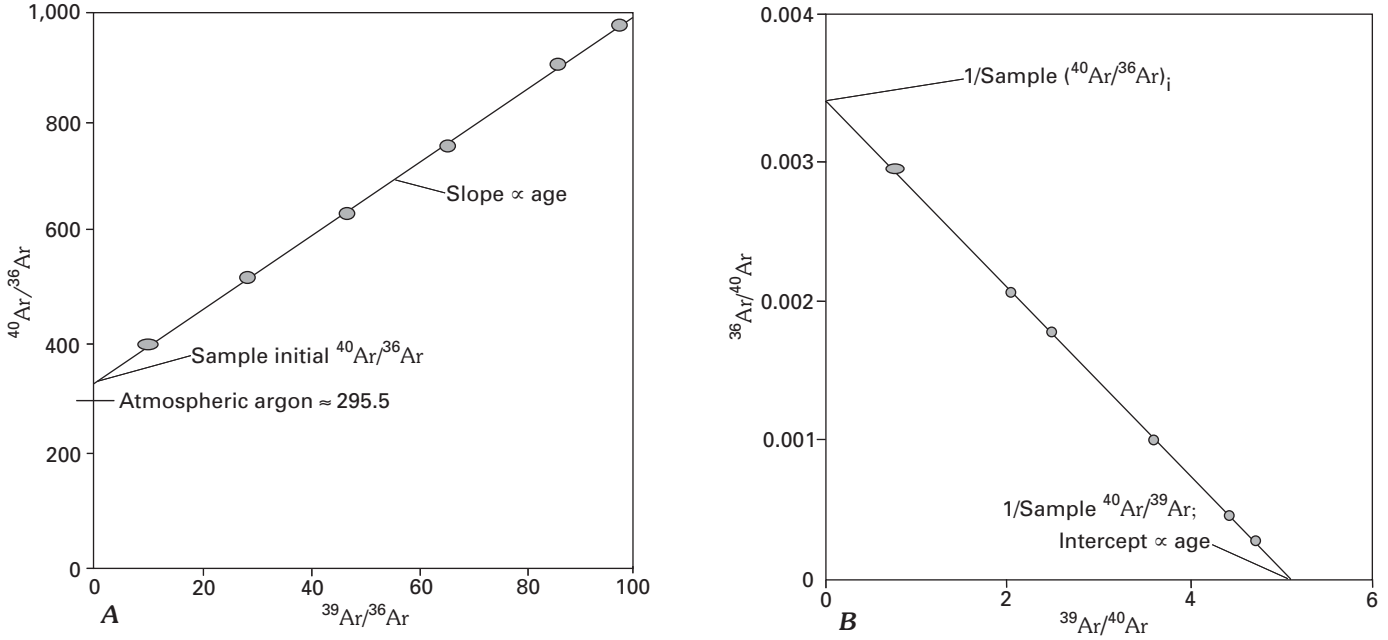

Figure 4. Hypothetical isochron (A) and hypothetical inverse correlation (B) diagrams. Slope of line in the isochron diagram is directly proportional to age, and intercept is initial $^{40}Ar/^{36}Ar$. Generally accepted $^{40}Ar/^{36}Ar$ atmospheric ratio is 295.5. Intercepts of line in inverse correlation diagram are $1/(^{40}Ar/^{36}Ar)_i$ (where i=initial; vertical axis) and 1/F (horizontal axis).

be completely ejected from the ^{39}K site perhaps ending up in an adjacent site or being completely ejected from the material. Huneke (1976), Huneke and Smith (1976), and Onstott and others (1995) showed that ^{39}Ar recoil could affect age spectra of samples in which potassium is principally located in fine-grained phases adjacent to potassium-poor minerals, such as in fine-grained basalts. We have shown (Folger and others, 1996) that ^{39}Ar recoil has a significant effect on illite/white mica grains that are less than 10 μm. In this study, for grain sizes less than 0.1 μm, we documented that as much as 28 percent of the ^{39}Ar was recoiled completely out of the sample; the amount of recoiled ^{39}Ar was indirectly proportional to grain size decreasing essentially to zero from samples with grain sizes exceeding 10 μm.

Closure Temperature and Diffusion

The apparent age calculated for a mineral from its accumulated radioactive decay products is the time when the chemical system of that mineral became closed to diffusion of that particular radioactive decay product. Many early studies (Jäger, 1962, 1965, 1967; Jäger and others, 1967; Hart, 1964; Aldrich and others, 1965; Armstrong and others, 1966; Hanson and Gast, 1967; Hanson and others, 1975; Berger, 1975; Berger and York, 1981, among others) showed that isotopic dates for minerals in the Rb-Sr and K-Ar systems gave discordances that were best explained as cooling ages that were younger than age of formation or ages that had been thermally reset. These studies also showed that different minerals exhibited characteristic retentivity to diffusion of daughter products, reflecting different isotopic closure temperatures for each mineral. Closure to diffusion is controlled chiefly by temperature but also by cooling rate (Carslaw and Jaeger, 1959; Dodson, 1973), chemical compositional variation (for example, Till and Snee, 1995), and structural state variation or strain history (Cosca and others, 1992). Closure to diffusion takes place over a temperature range; each mineral has its characteristic closure-temperature range. The apparent age is a measure of when the mineral cooled through the closure-temperature range. The closure-temperature range is higher and narrower for fast cooling, and conversely, is lower and broader if cooling was slow. For the $^{40}Ar/^{39}Ar$ system, closure temperatures of the most commonly used geochronometers are reasonably well known; and $^{40}Ar/^{39}Ar$ isotopic dates provide a thermochronology that connects time and temperature.

The argon geochronometers that have the best documented closure temperatures are hornblende, biotite, muscovite, and potassium feldspar. Commonly accepted closure temperatures that span a range from rapid (1,000 °C/m.y.) to slow cooling (5°C/m.y.) are 580°–480 °C for hornblende (Harrison, 1981), 325°–270 °C for muscovite (Snee and others, 1988; $2M_1$ structural state), 340°–280 °C for biotite (McDougall and Harrison, 1999; Snee, 1982b); and a wide range of ≥300 °C to ≤150 °C for microcline and orthoclase feldspars (McDougall and Harrison, 1999). (Each of these is discussed in more detail in the following sections.) When different minerals with different argon-closure temperatures are used in combination for some geologic terranes, cooling curves (such as shown in fig. 10) can be derived.

Again, as with the applicability of the concept of volume diffusion to $^{40}Ar/^{39}Ar$ studies, argument exists within the argon community on the validity of the closure-temperature concept. Villa (1997) argued that field observations going back to the original work defining the closure concept (Jäger, 1967), when viewed in the context of newer work, can be interpreted entirely as a function of isotopic inheritance. Our work and that of many others have shown that mixed argon reservoirs arising from intergrowth of phases can simulate the behavior predicted for

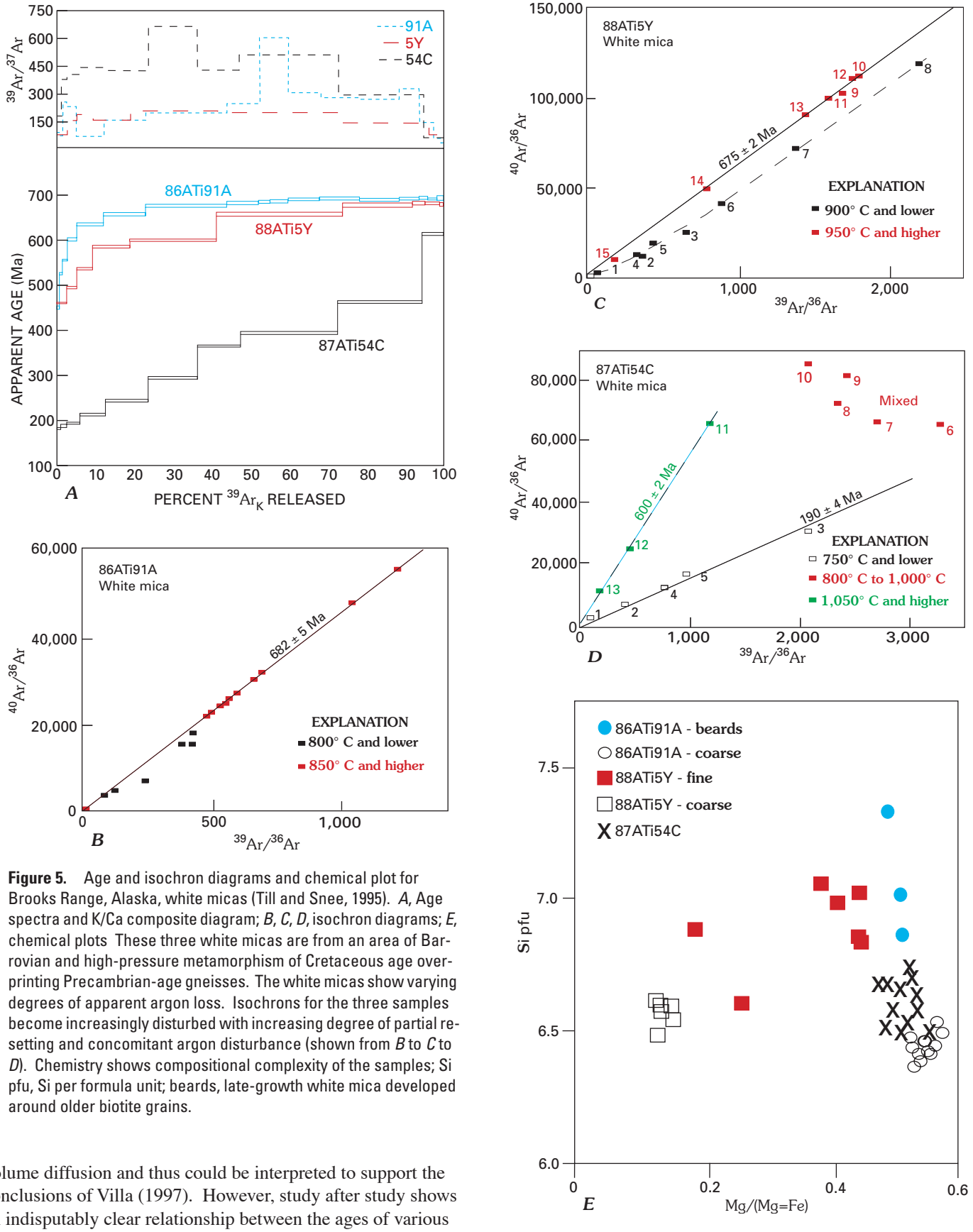

Figure 5. Age and isochron diagrams and chemical plot for Brooks Range, Alaska, white micas (Till and Snee, 1995). *A*, Age spectra and K/Ca composite diagram; *B*, *C*, *D*, isochron diagrams; *E*, chemical plots These three white micas are from an area of Barrovian and high-pressure metamorphism of Cretaceous age overprinting Precambrian-age gneisses. The white micas show varying degrees of apparent argon loss. Isochrons for the three samples become increasingly disturbed with increasing degree of partial resetting and concomitant argon disturbance (shown from *B* to *C* to *D*). Chemistry shows compositional complexity of the samples; Si pfu, Si per formula unit; beards, late-growth white mica developed around older biotite grains.

volume diffusion and thus could be interpreted to support the conclusions of Villa (1997). However, study after study shows an indisputably clear relationship between the ages of various phases and geologic cooling after some thermal process. Furthermore, this relationship extends beyond the $^{40}Ar/^{39}Ar$ system into the U-Pb and Rb-Sr systems. The reality probably lies in between the extremes of the arguments, and ultimate resolution will require other approaches to resolve the conflict. In view of this, Dunlap (2000; see also York, 1984) assessed argon diffusion from the aspect of the natural environment by evaluating cooling rates over geologic time. Dunlap's

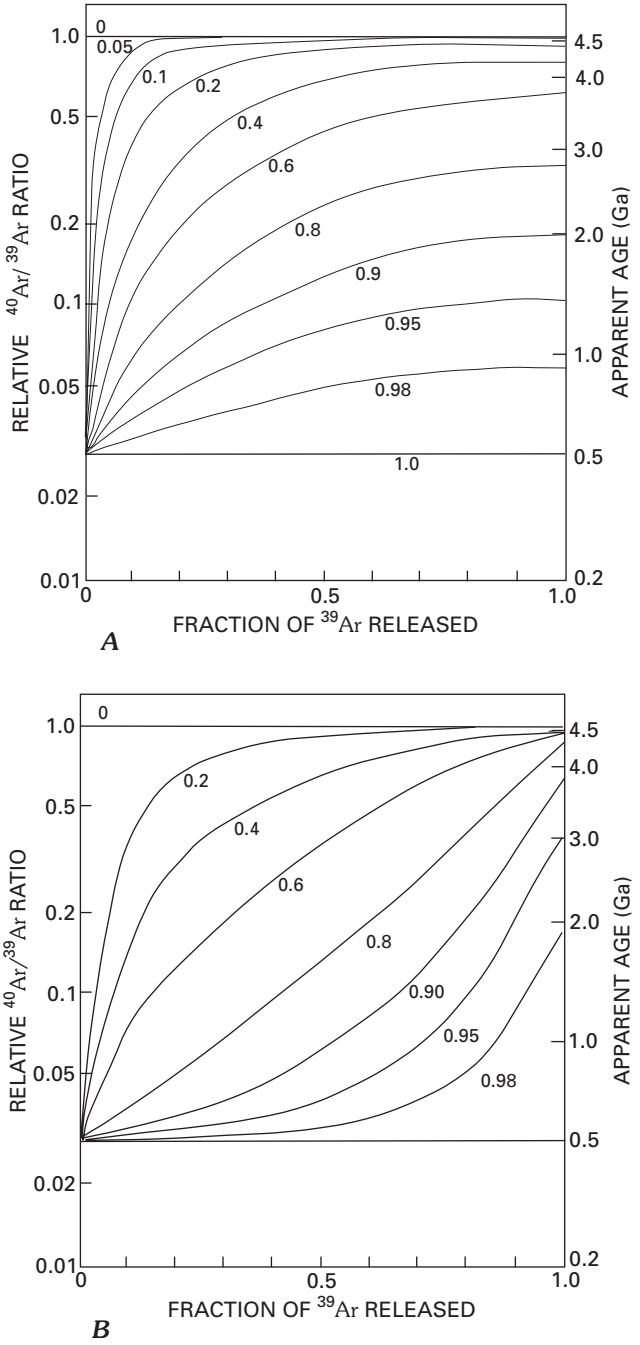

Figure 6. Examples of Turner's theoretical argon loss diagrams. Sample assumed to be 4.55-Ga meteorite affected from 0 percent to 100 percent (0 to 1.0) argon loss during a 500-Ma thermal event. Family of curves mimics degree of argon loss expected in argon age spectra. *A*, family of curves for sample of uniform-size spheres; *B*, family of curves for sample of lognormal distribution. Reproduced with permission of Grenville Turner (from Turner, 1968).

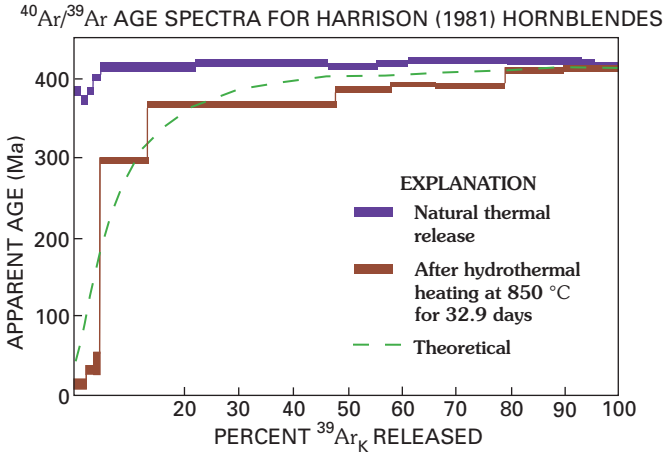

Figure 7. Hydrothermal heating of hornblende (modified from Harrison, 1981). Age spectrum diagram (blue) for undisturbed, natural hornblende shows a plateau formed by more than 95 percent of the released ^{39}Ar. Age spectrum (red) for the same hornblende that was hydrothermally treated at 850°C for 32.9 days, and subsequently irradiated and argon dated, shows stepping-up pattern with increased temperature of release that is typical of apparent argon loss. Dashed green curve represents 15 percent argon loss according to Turner's (1968) prediction. Reproduced with permission from Contributions to Mineralogy and Petrology, "Diffusion of ^{40}Ar in hornblende," by T. Mark Harrison, v. 78, p. 326, figure 1, 1981, © Springer Verlag. And with permission of the author, T. Mark Harrison.

conclusion is that ancient (Precambrian) orogens as a whole exhibit slower postorogenic cooling. When minerals like biotite are exposed in the crust to prolonged periods at elevated temperatures approaching or slightly lower than their closure-temperature range, the minerals have a tendency to lose argon. If this observation is correct, it lends support to the closure-temperature and diffusion concepts.

Some Minerals Useful for $^{40}Ar/^{39}Ar$ Geochronology

Amphiboles

Amphiboles are widespread in igneous and metamorphic rocks and contain as much as 2 percent potassium. Hornblende, primarily, but to some extent other amphiboles, has proved to be exceptionally retentive of radiogenic argon having a high closure temperature at or above 550°C (Harrison, 1981). In studies of emplacement, cooling, and uplift of plutonic rocks, hornblende forms the argon geochronologic proxy for a zircon crystallization date, assuming sufficient estimates for the cooling period after emplacement; and if the hornblende date is combined with zircon U-Pb dates, important high-temperature cooling constraints can result (for example, Premo and others, 1998). Hornblende in metamorphic rocks is also valuable for defining cooling history after metamorphism; moreover, in cases where hornblende is recovered from metamorphic rocks that formed at a temperature below the argon closure temperature for the hornblende in the rock, an $^{40}Ar/^{39}Ar$ date for that hornblende is one of the best estimates for the age of metamorphism. Hornblende also is present in a wide range of volcanic rocks and in skarns and provides a means for dating the volcanism and contact metamorphism. Amphibole has been used to date skarns (Berger and others, 1983; Chesley and others, 1993) and amphibole-facies associated mineralization (Napier and others, 1998), but its greatest utility in mineral-deposit geochronologic studies comes in the definition of premineralization cooling history of host rocks. Knowing the thermal history of the host is important in order to limit the possible interpretations of the ages of phases

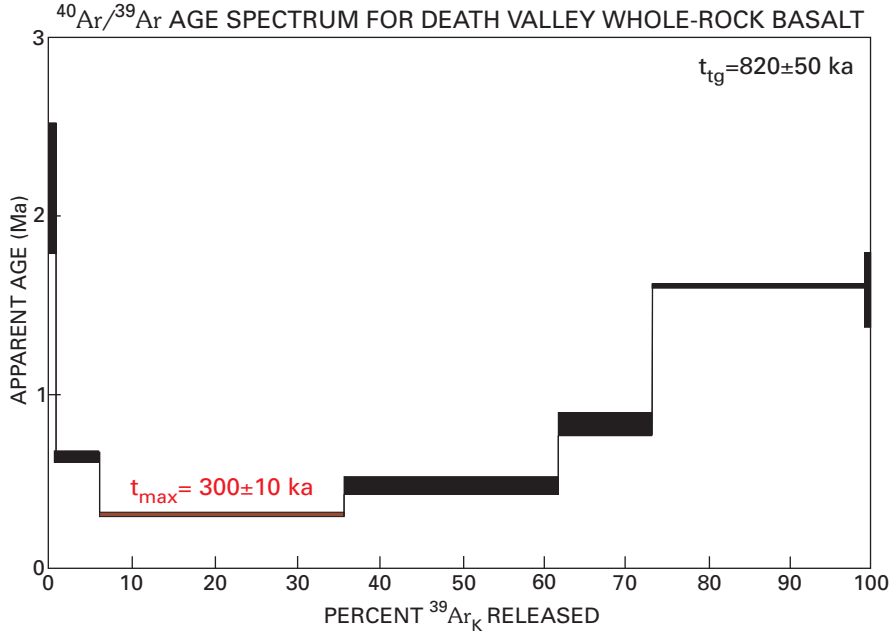

Figure 8. $^{40}Ar/^{39}Ar$ age spectrum for a sample with excess ^{40}Ar. Sample of whole-rock basalt from floor of Death Valley, Calif., displays anomalously old apparent ages for lower temperature and higher temperature steps. Low step in "saddle" is interpreted to be a maximum age estimate for the eruption of the basalt; t_{tg}= total-gas date; t_{max}= maximum estimated date for sample.

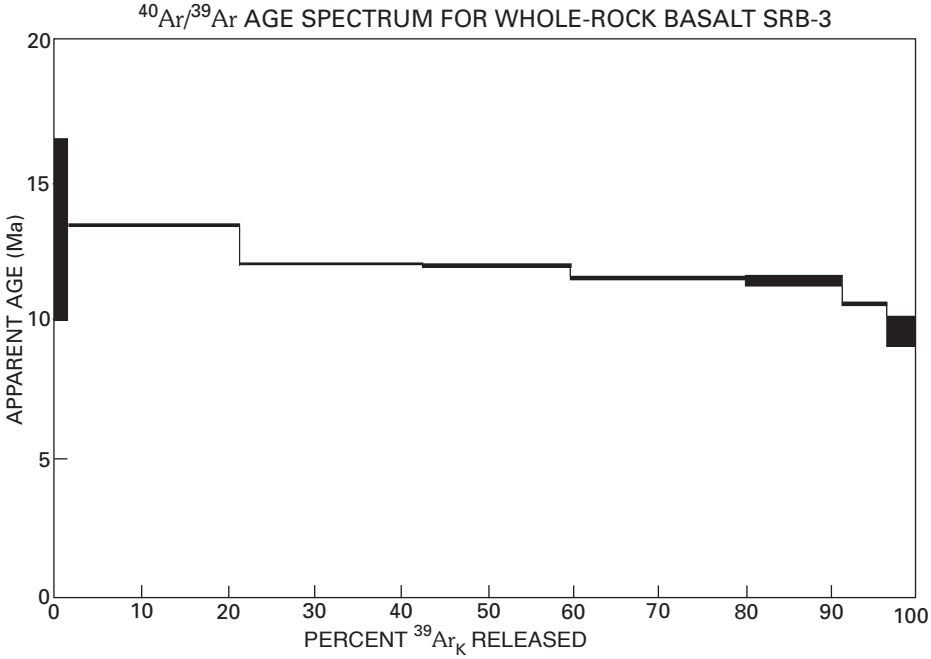

Figure 9. $^{40}Ar/^{39}Ar$ age spectrum for a sample exhibiting ^{39}Ar recoil. Characteristic stepping-downward in age spectrum results from the loss of ^{39}Ar by recoil out of sample during irradiation. Loss of ^{39}Ar increases the apparent $^{40}Ar/^{39}Ar$ ratio and age.

dated from the mineralized rocks. Lund and others (1986; this report, fig. 10) used amphibole dates from the host rocks of epithermal gold-bearing quartz veins in central Idaho to uniquely interpret the white mica dates as formation ages and not cooling ages. Other studies that have followed this approach include Snee and others (1995) and Goldfarb and others (1991, 1993, 1997).

Because most argon from hornblende apparently is released in the vacuum chamber during dehydration and decomposition as the hornblende is heated, much debate rages over the meaning of an age spectrum generated from step-wise heating experiments. Because the purpose of step-heating experiments in vacuum is to simulate volume diffusion resulting from heating in the geologic environment, this dehydration destroys that

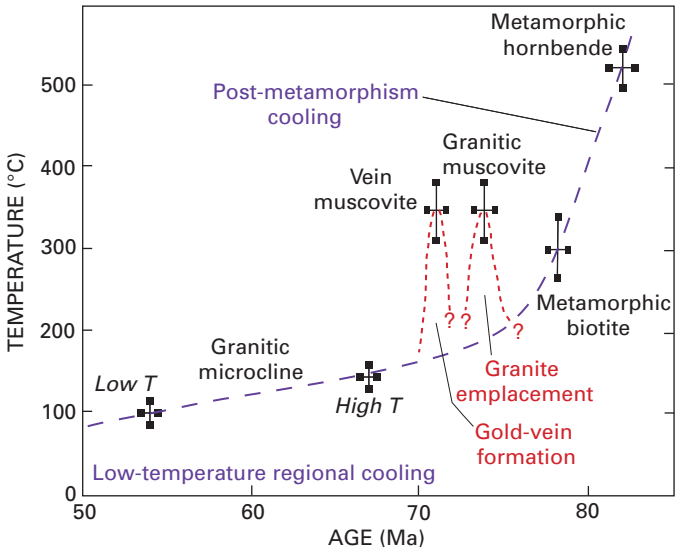

Figure 10. Example of a cooling curve for a mineralized area in Idaho (modified from Lund and others, 1986). Dashed line represents regional cooling after regional metamorphism; shape and trajectory of the curve are controlled by ages and closure-temperature estimates of dated minerals; bars represent approximate uncertainties in age and temperature. Dotted line represents emplacement of granitic rocks and subsequent gold-vein formation.

simulation. Nonetheless, numerous examples of apparent argon loss (that is, monotonic rise in apparent age with increasing extraction temperature) exist. From our extensive experience, many of these cases are directly a function of multiple generations of hornblende in a single sample or overgrowths of other amphiboles on an earlier formed hornblende (Snee and others, 1995; Baig, 1990; fig. 11). Whatever the case, valuable information is derived from step-heating experiments, and derived age spectra allow recognition of excess argon. Also, the lower temperature steps commonly remove argon that is derived from fluid inclusions and other mineral impurities and prevents this argon from diluting K-lattice-derived argon released from the true amphibole sites.

Some additional studies that explore the argon systematics of amphibole include Harrison (1981), Harrison and Fitz Gerald (1986), Onstott and Peacock (1987), Gaber and others (1988), Baldwin and others (1990), Kelley and Turner (1991), Wartho and others (1991), Lee and others (1991), Lee (1993), Rex and others (1993), Cosca and O'Nions (1994), Wartho (1995), and Dahl (1996a).

White Micas

Muscovite with as much as 10 percent potassium is common in metamorphic rocks, peraluminous plutonic rocks, pegmatites, and many mineral deposits. In metamorphic rocks, muscovite of structural polytype $2M_1$ (two-layered monoclinic, type 1) is the predominant species of white mica in Barrovian-type assemblages, whereas phengite (structural

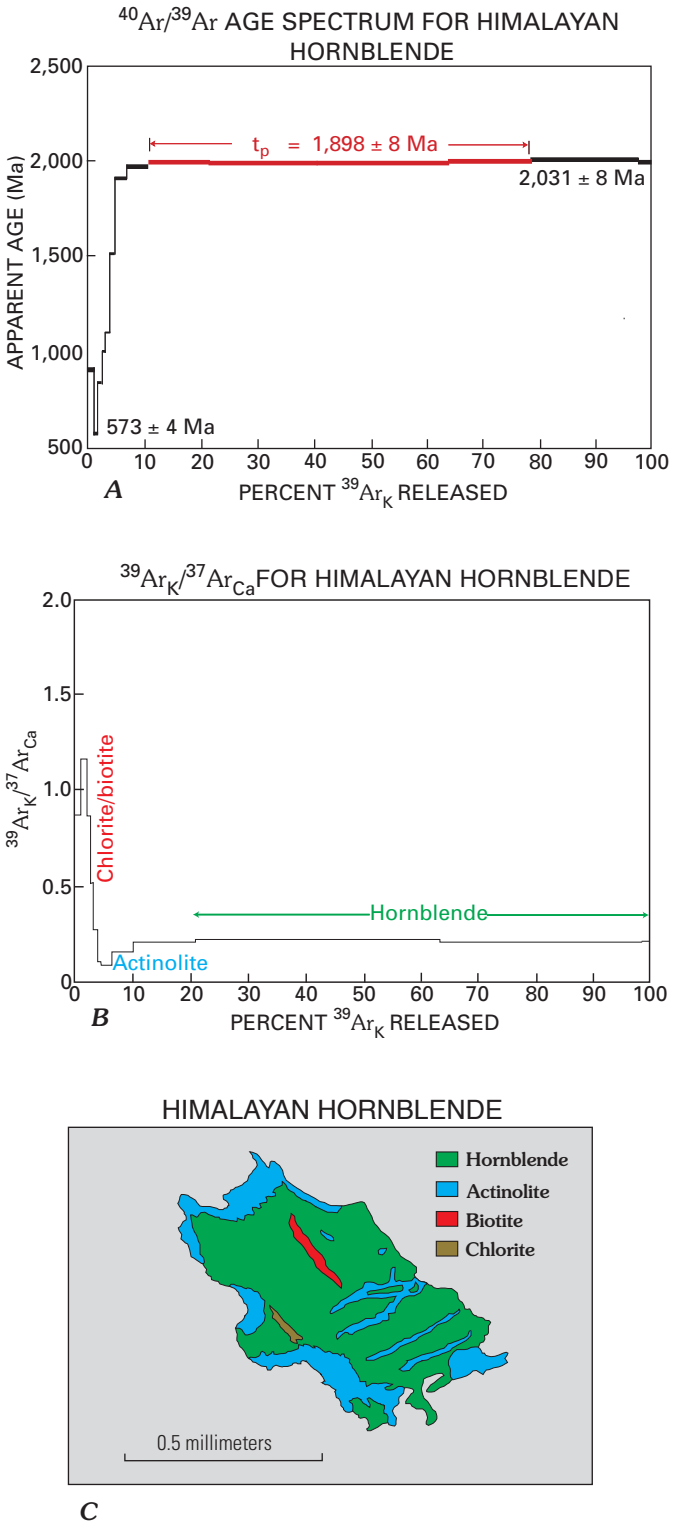

Figure 11. Complex argon systematics of a Precambrian amphibole from northern Pakistan. *A*, Age spectrum; *B*, K/Ca diagram. *C*, Drawing of a hornblende from thin section of sample that produced the age data, illustrating the complexities inherent in some amphiboles (Baig, 1990). K/Ca plot reflects influence on lower temperature steps of release pattern by presence of minor amounts of chlorite and biotite in the sample. Release of argon from actinolite affects low to intermediate temperature steps. Majority of age spectrum is controlled by argon from hornblende that retains its Precambrian age.

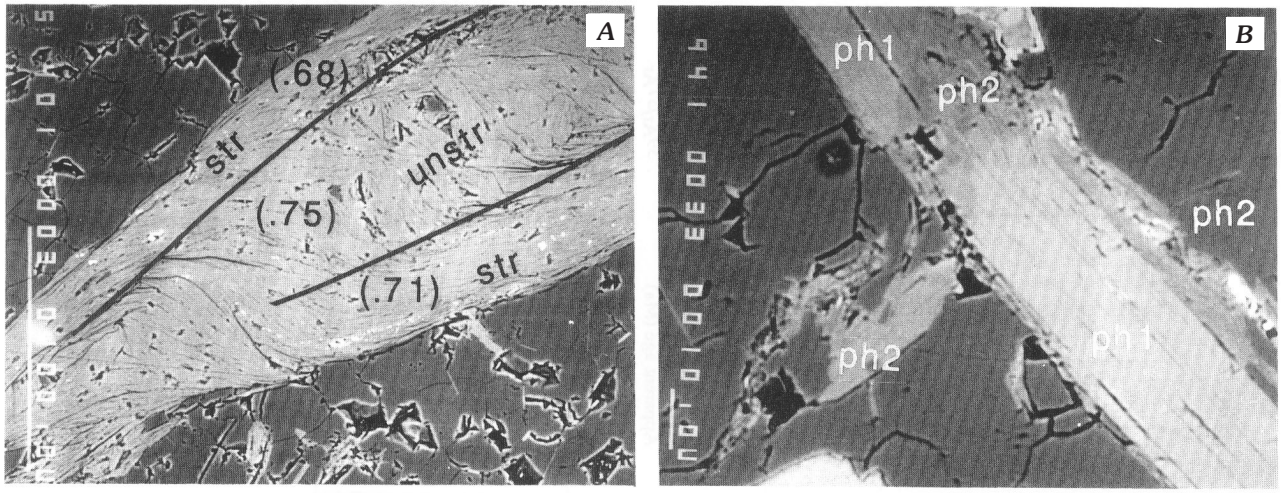

Figure 12. Back-scattered electron images of a white mica grain showing complexities of metamorphism that can affect argon systematics. *A*, Deformed white mica has strained and unstrained realms with slightly different chemistry. *B*, Two generations of phengite (ph1, ph2) with potentially different ages (Till and Snee, 1995). Mg/(Mg+Fe) values are indicated in parentheses; str, strained; unstr, unstrained.

polytype 3T; three-layered trigonal) is formed under high-pressure metamorphic conditions. Many geochronology studies have been done using white mica because of its high potassium content, geologic diversity, and argon retentivity. White micas can show complicated argon retention characteristics, but for well-behaved muscovites, numerous field studies (starting with the early work of Hanson and others, 1975, and Jäger, 1967) indicate that argon closure occurs at a temperature higher than that for biotite. An estimate for the closure-temperature range of muscovite, based on geologic information including fluid inclusion filling temperatures, is in the range of 270 °–325°C, covering slow to rapid cooling rates (Snee and others, 1988). Recently, Hames and Bowring (1994) and Kirschner and others (1996) have modeled $^{40}Ar/^{39}Ar$ age spectrum and laser-probe results to derive a closure-temperature estimate for muscovite of about 410 °C.

Many studies have shown that complicated argon age spectra are exhibited by some metamorphic white micas, especially in situations in which white micas of differing composition and age are intergrown (fig. 12; also figs. 3*A*, 3*B*, 5*A*–*E*; Scaillet, 1996; Hodges and others, 1994; Roeske and others, 1995; Till and Snee, 1995; Christiansen and Snee, 1994; Chopin and Maluski, 1980; Hammerschmidt and Frank, 1991; and Wijbrans and McDougall, 1986). Several suggestions have been made to account for these complexities. Scaillet and others (1992) showed that high-Si, Fe-rich phengite in the western Alps was completely reset under particular metamorphic conditions but that under these same conditions high-Si, Mg-rich phengite was not completely reset. In contrast, similar complexities in white mica argon systematics have also been ascribed to argon loss due to volume diffusion (Wijbrans and McDougall, 1986), thermal reequilibration of argon systematics in previously metamorphosed rocks (Wijbrans and McDougall, 1986; Hammerschmidt and Frank, 1991; Hames and Hodges, 1993; Reddy and others, 1996; Hames and Cheney, 1997), and the influence of deformational history on argon reequilibration (Chopin and Monie, 1984; Scaillet and others, 1990; Hammerschmidt and Frank, 1991). Similarly, complex age spectra in low-grade metamorphic rocks have been attributed to effects resulting from grain size or mica polytype (Cosca and others, 1992). An added complexity exists when paragonite and K-white mica are intergrown at the micrometer scale under blue-schist or greenschist facies conditions as demonstrated by Roeske and others (1995).

The closure temperature of phengite is unknown, although it must be higher than that for muscovite. Till and Snee (1995) showed that preexisting phengite of structural state 3T present in blue-schist facies rocks that underwent remetamorphism was not reset at temperatures as high as 525 °C but was completely reset at temperatures on the order of 580 °–620 °C. Other studies that have explored the complexity of argon systematics in white mica include Wijbrans and McDougall (1988), Wijbrans and others (1990), Hames and Cheney (1997), Ruffet and others (1995), Dahl (1996b), and Dalla Torre and others (1996). Clearly more must be done to understand white mica argon systematics.

Muscovite is a highly versatile mineral in $^{40}Ar/^{39}Ar$ studies of mineral deposits. Snee and others (1988) showed that carefully characterized muscovites could be used to define age and duration of mineralization in the long-lived Panasqueira (Portugal) tin-tungsten deposit. Chesley and others (1993) combined muscovite $^{40}Ar/^{39}Ar$ geochronology with other isotopic systems to define the age and duration of the Cornubian batholith (England) and the many associated mineral deposits. With the worldwide economic interest in gold deposits and the ubiquitous association of muscovite with orogenic gold mineralization, muscovite argon geochronology is a highly reliable means to define age constraints of these large systems. Goldfarb, Snee, and associates used muscovite geochronology of orogenic gold deposits constrained by the cooling history of host rocks to elucidate the mineralization history of gold deposits of Alaska (Goldfarb and others, 1991, 1993, 1997; Miller and others, 1994, 1995; Ford and Snee, 1996). Muscovite argon geochronology also has been used on early Paleozoic and Precambrian gold

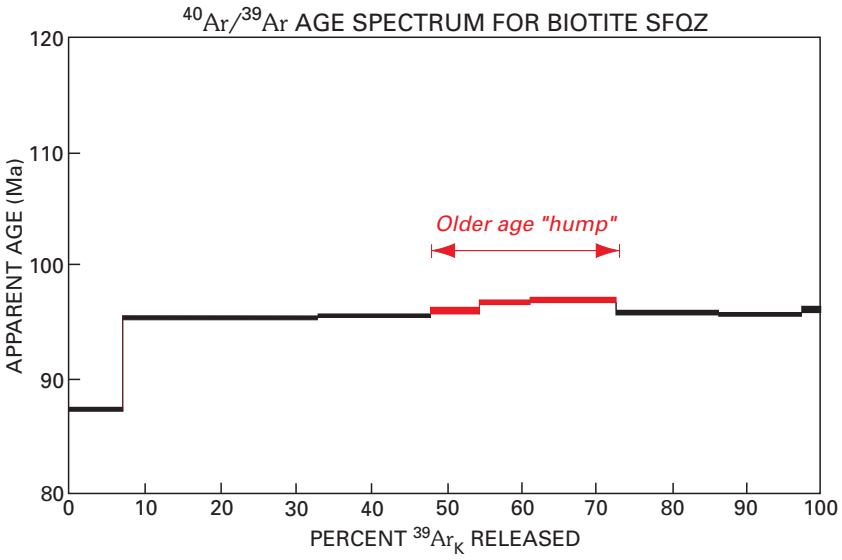

Figure 13. Typical age spectrum for a biotite sample that contains some chlorite. Typical form taken by a biotite age spectrum when chlorite is interlayered showing anomalously older apparent ages in middle temperature steps. Older apparent ages likely result from ^{39}Ar recoil from the chlorite and out of the sample or into the lower-T biotite sites.

deposits (Onstott and others, 1989; Fortes and others, 1997; Feng and others, 1992; Hanes and others, 1992; Kerrich, 1994; Kerrich and Cassidy, 1994; Kerrich and Kyser, 1994; Kent and McDougall, 1996; Perkins and Wyborn, 1998).

Brown Micas

The brown micas are the most commonly dated group of minerals by the conventional K-Ar method and remain a popular and important group used in modern $^{40}Ar/^{39}Ar$ studies, despite numerous problems with their argon systematics. Solid solution exists between the Mg-end member, phlogopite, and the Fe-end member, annite, with the term phlogopite generally reserved for Mg/Fe > 2, and biotite used for the others. Like the white micas, the brown micas are high in potassium and widespread in the geologic environment. As previously noted, argon retentivity of biotite has been shown by numerous field studies to be slightly less than that of muscovite; nonetheless, biotite is highly useful for understanding cooling in the 300 °C geologic realm. Harrison and others (1985) experimentally showed that for cooling rates ranging from 100 °C/Ma to 1°C/Ma, biotite argon closure temperature ranges from 345° to 280 °C. Harrison and others (1985) also showed argon diffusivity increases in brown micas with increasing Fe/Mg ratio, a result consistent with numerous empirical observations.

Despite biotite's popularity for geochronologic studies, the fact is that it is highly susceptible to alteration to chlorite. The presence of even minor amounts of chlorite seems to have serious deleterious effects on biotite's argon systematics. Disturbance to a biotite's age spectrum is generally manifested by a hump shape (convex upward) with anomalously high apparent ages for intermediate temperature steps of about 850° to 1,050°C (fig. 13). This temperature range of release corresponds to the majority of the temperature range of biotite argon release and thus strongly influences the biotite age spectrum.

Most experimental studies have shown that this effect is likely due to ^{39}Ar recoiled into surrounding biotite or completely out of the sample from intergrown fine-grained low-retentivity chlorite (Hess and others, 1987; Lo and Onstott, 1989; Hess and Lippolt, 1986). Lo and Onstott (1989) demonstrated that this kind of disturbance to a biotite age spectrum will result with as little as 1 percent chlorite present in a biotite lattice.

Despite this serious problem with biotite, valuable results can be obtained on carefully selected samples. In mineral deposit studies, biotite is less common than muscovite as a primary alteration phase. Its greater utility is in its use in definition of the thermal history of host rocks. Phlogopite generally seems to be more reliable than biotite. Some additional studies that show the usefulness of brown micas in both vacuum furnace and laser probe approaches include Snee (1982a), Gaber and others (1988), Ruffet and others (1991), Kelley and others (1997), Pickles and others (1997), Cheilletz and others (1993), and Phillips (1991).

Illite

Illite is structurally similar to the micas; most illites are di-octahedral like muscovite. Illite, however, differs chemically from muscovite in having more silicon and less potassium and having clay-size (<2μm) particles. The most common polymorph of illite has a disordered, unexpandable, one-layered monoclinic cell (1M), but other polytypes, including 3T and $2M_1$, also are known. Illite commonly is interlayered with smectite, which is an expandable Ca, Na-clay. Illites and illite/smectites are common in sedimentary rocks and are formed by diagenetic and low-grade metamorphic processes. As temperature of process increases, grain size increases (perhaps by a process such as Ostwald ripening; Eberl and others, 1990), expandability decreases, and the ratio of 2M to 1M polytype increases. Illite also forms in the hydrothermal environment, and the common term "sericitization" is used for the process of alteration of feldspar to illite, illite/smectite, and (or) white mica (muscovite and paragonite). For some low-temperature hydrothermal mineral deposits, illite may be the only datable argon geochronometer available (Halliday, 1978; Ilchik, 1995; Folger and others, 1996; Phinisey and others, 1996; Hofstra and others, 1999).

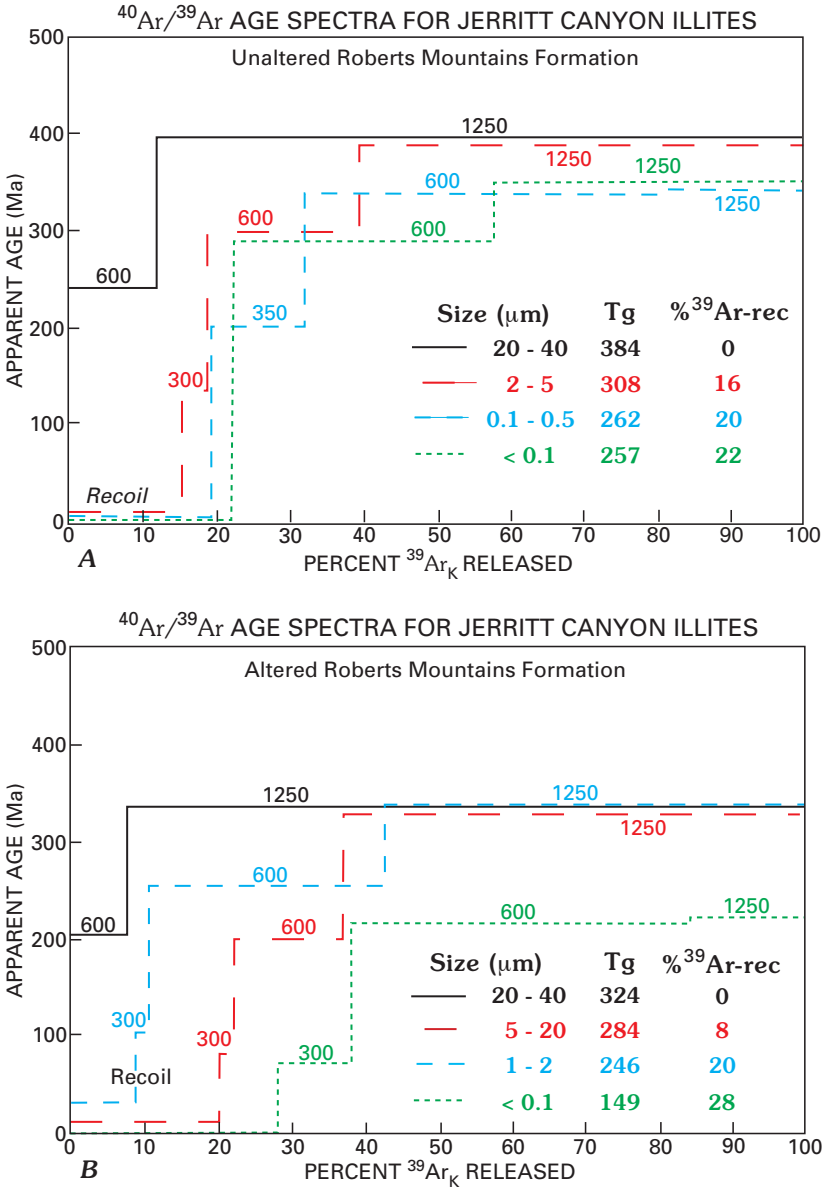

Figure 14. Age spectra for size fractions of illite from Jerritt Canyon, Nev. *A*, One sample of unaltered Roberts Mountains Formation sedimentary rock metamorphosed to low grade. Size fractions less than 5 μm show as much as 22 percent ^{39}Ar recoil. *B*, One sample of altered Roberts Mountains Formation sedimentary rock metamorphosed to low grade and subsequently altered. Size fractions less than 5 μm show as much as 28 percent ^{39}Ar recoil (% ^{39}Ar-rec in figure). In both cases, the recoiled argon was captured in vacuum-evacuated vials. Apparent argon-loss spectra result from mixing of argon reservoirs of different ages (Folger and others, 1996). True age of gold mineralization is approximately 40 Ma. Mineralization event was not hot enough to completely reset illite. Size (μm), grain-size range of analyzed illite fraction; Tg, total-gas age of analyzed fraction; % ^{39}Ar-rec, percent ^{39}Ar recoiled from sample and captured in break-seal volume. Heating temperature of each fraction is indicated above or below corresponding bar.

Illite, in its broadest definition, has been used in both K-Ar and $^{40}Ar/^{39}Ar$ geochronology with mixed to poor success. The reasons for this are clear from the preceding paragraph—illite has a wide range of compositions, structural types, grain sizes, and modes of formation. Very fine grained illite is affected by ^{39}Ar recoil as high as 30–80 percent in $^{40}Ar/^{39}Ar$ geochronology (Foland and others, 1984; Hess and Lippolt, 1986; Folger and others, 1996; Kapusta and others, 1997). Conventional K-Ar analysis has been used to avoid the problems from recoil, but this approach suffers from being unable to evaluate argon systematics (Halliday, 1978). Because illite and illite/smectite are formed within a growth continuum that extends into muscovite and phengite (Hunziker and others, 1986), equally troublesome is the potential for the incorporation of inherited argon from older grains that may serve as the cores for growth of larger grains.

A vacuum encapsulation approach has been developed and routinely is used to capture recoiled ^{39}Ar (Foland and others, 1992; Smith, Evensen, and York, 1993; Folger and others, 1996; fig. 14). This process results in total-gas dates that are identical to conventional K-Ar dates, and it allows evaluation of the sample's argon systematics. This approach has great promise for studies on uncomplicated illite. However, with respect to mineral-deposit geochronologic studies, Folger and others (1996) showed conclusively that in low-temperature Carlin-type deposits, illite that formed during mineralization can use older illite or white mica grains as crystallization nuclei. If the mineralization process did not degas these nuclei, inherited argon will be incorporated in the sample. In the case of Carlin-type deposits, if this risk is not recognized, erroneous interpretations may result (Arehart and others, 1993; Morris and Tooker, 1996; Wilson and Parry, 1995, 1996, 1997; Mako, 1997). Recent studies using laser degassing of illite grains (Dong and others, 1995, 1997; Kapusta and others, 1997; Onstott and others, 1997) are promising a valuable new approach for exclusively releasing argon for pure young-growth illite.

Alkali Feldspar

This diverse group has extensive applicability in $^{40}Ar/^{39}Ar$ thermochronologic studies. Potassium feldspar has high

potassium content, widespread abundance in nature, anhydrous crystal character, and well-documented argon retention characteristics. Potassium feldspar remains stable during heating to high temperature in the extraction system, so it lends itself to being used in volume diffusion modeling. These models are then used to develop comprehensive thermal models of the natural environment. Because the thermal character of the geologic environment has a profound effect on both the alkali feldspar species and the argon systematics of the species in that environment, for purposes of this discussion, I will subdivide alkali feldspars into three species: low-temperature potassium feldspar, sanidine, and adularia.

Low-Temperature Potassium Feldspar

Low-temperature potassium feldspar is the premier example of a mineral that had been deemed virtually useless for conventional K-Ar dating but has become one of the most widely applied minerals in $^{40}Ar/^{39}Ar$ thermochronology. In K-Ar studies it was recognized early that orthoclase and microcline potassium feldspar dates were commonly much younger than those of any other dated coexisting minerals, leading to the conclusion that potassium feldspar easily lost radiogenic argon in the natural environment. Largely through the work of Harrison and his associates, and others, such as Foland (1994), the argon systematics of low-temperature potassium feldspar have been comprehensively unraveled. (See, among others, Harrison and McDougall, 1982; Harrison, 1990; Foster and others, 1990; Harrison and others, 1991; Fitz Gerald and Harrison, 1993; Lovera, 1992; Lovera and others, 1989, 1991, 1993, 1996; Harrison and Be, 1983.) As this work is well described in McDougall and Harrison (1999), I will not attempt to duplicate that description. However, based on their work, low-temperature potassium feldspar normally exhibits argon release behavior that can be best modeled assuming a multi-diffusion domain approach. This method results in the derivation of a range of argon diffusion temperatures from carefully analyzed potassium feldspar. These data, in turn, provide comprehensive understanding of the thermal conditions of the geologic environment. Commonly the model temperatures range from as high as 350 °C to as low as 150 °C or lower, a range that is exceedingly valuable for understanding low-temperature crustal activity such as cooling and uplift. However, low-temperature potassium feldspar also is a valuable mineral for dating rapidly cooled magmatic systems (Geissman and others, 1992).

Sanidine and Anorthoclase

Sanidine, the high-temperature potassium feldspar common in intermediate to felsic-composition volcanic rocks, and anorthoclase, the alkali feldspar more common in sodium-rich volcanic rocks, are additional minerals that met with mixed success in conventional K-Ar studies. Because in many cases sanidine did not release all of its argon when heated in the extraction system, anomalously young K-Ar apparent ages routinely resulted. With the move from K-Ar dating to $^{40}Ar/^{39}Ar$ geochronology, sanidine has risen in favor because it is no longer necessary to extract all argon from the mineral to derive meaningful age information. In fact it is our experience that of the common material dated from volcanic rocks, including sanidine, biotite, hornblende, and whole rocks, sanidine is the most reliable and the least likely to produce disturbed argon age spectra. When more than one phase from a particular sample is analyzed, sanidine is the likeliest to produce the best analytical precision and the greatest accuracy. Because of the high precision and accuracy of sanidine argon dates, sanidine is very valuable in defining detailed extrusive history of volcanic fields (Brooks and others, 1995; Scott and others, 1995; Snee and Rowley, 2000; Rowley and others, 2001; E.A. duBray and others, unpub. data, 2002) and the mineralization history of volcanic complexes (Yambrick and Snee, 1989; Rowley and others, 1992, 2001; Setterfield and others, 1992; Shubat and Snee, 1992; Henry and others, 1997; Snee and Rowley, 2000).

Adularia

Adularia is a low-temperature form of potassium feldspar that is regarded as a distinct variety because of its morphology and restricted paragenesis. Adularia has a high potassium content, ranging up to 17 percent K_2O. It can form in epithermal mineral deposits and under low-temperature fluid-flow conditions, such as are present in marine saline basins. Adularia has proved effective in dating mineralization history (Halliday and Mitchell, 1976; Groff and others, 1997; Love and others, 1998, among others) and in some cases has been used to date fluid flow and potassium metasomatism along fault surfaces. Brooks and Snee (1996) used sanidine with adularia rims to date volcanic rocks in Nevada as well as the age of fluid flow along low-angle detachment fault surfaces that displaced them. In their study, Brooks and Snee (1996) used electron microprobe analysis of adularized sanidine to constrain interpretation of apparent argon-loss spectra, concluding that detachment faulting occurred as long as 11 m.y. after volcanism (fig. 15).

Because adularia in all occurrences commonly has a tendency to precipitate on older potassium feldspar, it is essential to carefully characterize the sample before analysis. Overgrowths of adularia on sanidine are not obvious under the microscope but can be resolved using elemental mapping in the electron microprobe or SEM.

Plagioclase

Plagioclase is a common mineral in volcanic rocks and is used to date basaltic rocks, which normally lack better argon geochronometers. Plagioclase has potassium contents ranging from 0.1 to more than 1 percent and has been shown to yield reasonable dates, especially when thermal-release spectra, isochrons, and K/Ca diagrams jointly are used to evaluate the distribution of argon in the sample. In some cases, especially for young, low-potassium plagioclase, excess argon may mask the low level of radiogenic argon, resulting in anomalously old apparent ages. Age-spectrum analysis generally will reveal the presence of the excess argon.

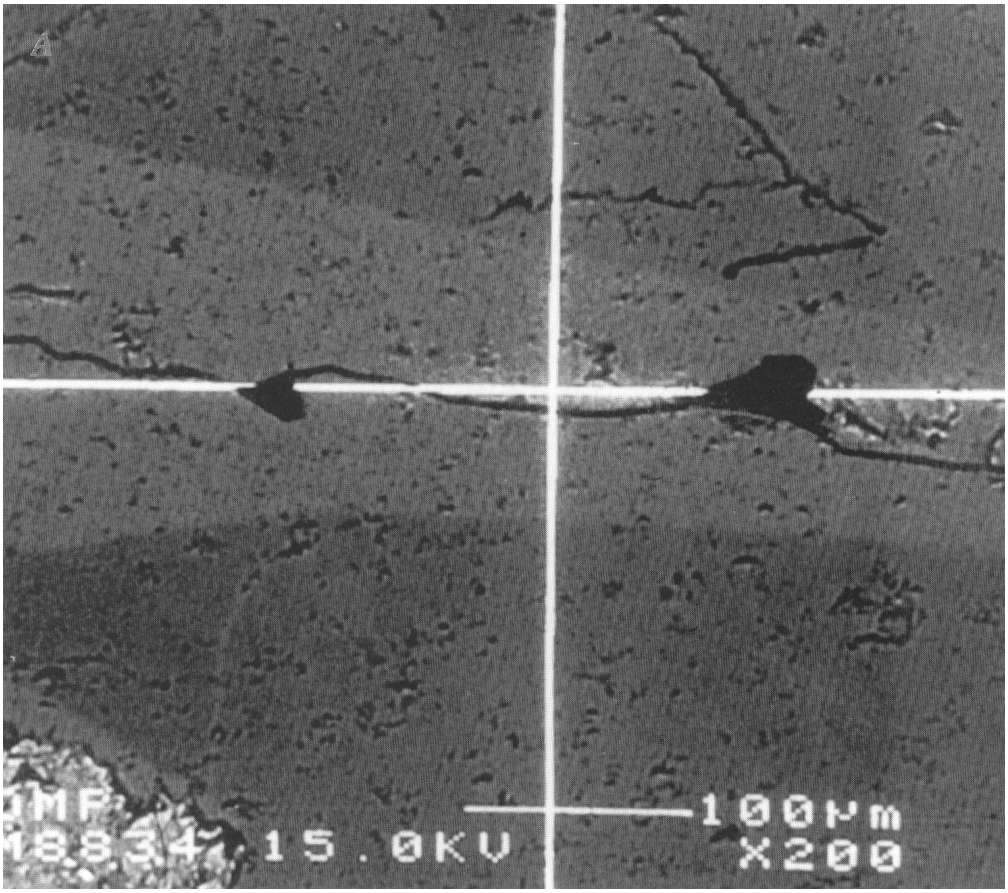

Figure 15. Back-scattered electron image of adularia formed along cracks in sanidine. Sanidine has 12.4 weight percent K_2O and 3.0 weight percent Na_2O; adularia along fracture has 16.7 weight percent K_2O and 0.1 weight percent Na_2O (Brooks and Snee, 1996).

Whole Rocks

Volcanic rocks, low-grade metamorphic rocks, and volcanic glasses commonly can be used for K-Ar and $^{40}Ar/^{39}Ar$ geochronology, especially in cases in which a pure potassium-bearing phase of reasonable grain size is difficult to obtain. As noted, one of the strengths of the $^{40}Ar/^{39}Ar$ thermal-release method is the means to evaluate the distribution of argon within a single phase and to use that information to assess the geologic conditions when the argon was incorporated into the phase. An analysis of a multi-component sample, such as a whole rock, complicates this assessment. However, useful information on argon distribution and, in many cases, accurate age information can be derived from carefully selected samples. Numerous successful studies have been done on whole-rock basalt. However, Baker and others (1996) have recommended caution in interpretation even of apparently well behaved samples. Confidence in the results can be increased when independent geologic constraints are employed (Miggins and others, 2002). Low-grade metamorphic rocks, such as slates and phyllites, produce variable results (Reynolds and Muecke, 1978; Wintsch and others, 1996); however, considering the implications from the prior discussion on illite, many obstacles must be overcome to produce meaningful results. Volcanic glass, in general, normally does not produce usable $^{40}Ar/^{39}Ar$ dates because of the deleterious effects from radiogenic ^{40}Ar loss, recoiled ^{39}Ar, and excess ^{40}Ar. However, tektite, a melt glass produced from meteorite impact, does produce precise and accurate $^{40}Ar/^{39}Ar$ ages, as shown by Izett and others (1992), Dalrymple and others (1993), and Swisher and others (1992).

Alunite and Jarosite

Alunite and jarosite are common minerals in the epithermal environment, forming from the reaction with host rocks of hydrothermal sulfuric acid derived from the oxidation of sulfides. Alunite is hydrated potassium aluminum sulfate; jarosite is hydrated potassium iron sulfate. The habit of both is massive, and granular to dense; they are commonly mixed with quartz, kaolin, and iron oxide minerals. Both, but especially alunite, have been used in conventional K-Ar studies (for example, Ashley and Silberman, 1976). Recent attempts at $^{40}Ar/^{39}Ar$ dating using both vacuum furnace and laser-probe approaches have produced some success (Vasconcelos and others, 1994; Love and others, 1998). I expect much more work in the future on alunite and jarosite because, in many epithermal deposits, no other suitable potassium-bearing phase exists to provide potential geochronologic constraints. Recently in the Denver argon geochronology laboratory, we analyzed an alunite from a Precambrian epithermal gold deposit in the Brazilian shield and confirmed its apparent age of 1,834 Ma (fig. 16; Juliani and

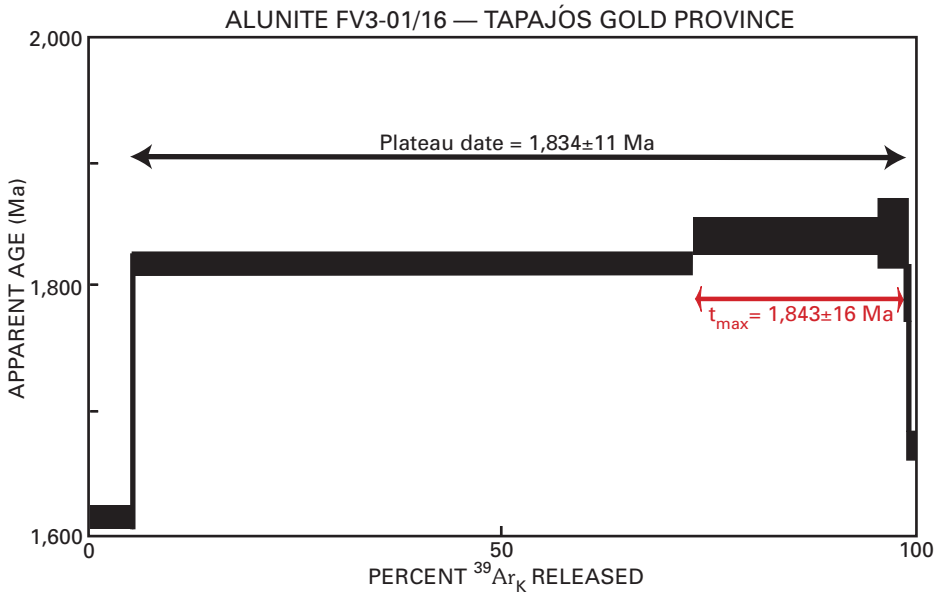

Figure 16. $^{40}Ar/^{39}Ar$ age spectrum for 1,834 Ma alunite from Brazil. Age spectrum for magmatic hydrothermal alunite associated with high-sulfidation mineralization from the Tapajós Gold Province, Brazil, yields a plateau with an apparent age of 1,834±11 Ma defined by 93.4 percent of the released ^{39}Ar. Although a plateau is exhibited, the gradual stepping-up in age may be a result of minor ^{40}Ar loss over geologic time. The apparent age of this alunite is consistent with other geochronology and geology for this deposit.

others, in press). Before this analysis, the oldest known alunite was 62 Ma (Bird and others, 1990). In a companion report to Juliani and others (in press), Landis and others (in press) evaluated noble gas systematics of a group of 10 alunites from the Brazilian gold deposit and derived an argon-closure temperature for alunite of 200° to 210 °C.

Manganese Oxides

Some manganese-oxide minerals, especially hollandite, cryptomelane, and others of the cryptomelane group, are gaining interest of argon geochronologists because they can contain 5 percent or more potassium. These minerals form in the supergene and hydrothermal environments. Thus, they have potential for direct dating of both weathering processes and mineral deposits. Recently, Vasconcelos and others (1992, 1994, 1995), Lippolt and Hautmann (1995), and Vasconcelos (1999) have published studies on the application of manganese oxides to argon geochronology. Of particular interest for mineral deposit research are the 1.8-Ga and 950-Ma ages (Lippolt and Hautmann, 1995) determined on hollandite from mineral deposits in Sweden and India. Not only are these dates consistent with the known age of the deposits, but also they clearly show the retentivity of the manganese-oxide structure. More work needs to be done to characterize these minerals, but they are promising for argon geochronological studies on mineral deposit and surficial processes.

Others

Among other materials that have been used for argon geochronology are lepidolite, fuchsite, evaporate minerals, feldspathoids, glauconite, and pyroxene. I have analyzed lepidolite, a lithium-mica from chemically evolved pegmatites in southern California, Colorado, and Maine, and fuchsite, a chronium-mica from mineral deposits in Pakistan and Alaska, and have obtained results that are consistent with geologic constraints. Others (for example, Smith, Schandl, and York, 1993) also have successfully dated fuchsites. Most $^{40}Ar/^{39}Ar$ attempts at dating evaporates, glauconite, and pyroxene have met with minimal success. Evaporates and glauconite have potential for success if technical pitfalls can be avoided—such as problems caused by fine grain size and by radiogenic argon loss; pyroxene, on the other hand, should be avoided, because it has a very low potassium content but generally very high amounts of excess argon.

Other materials that have been used for argon isotopic analysis or dating include sulfide minerals, magnetite, quartz, and fluid inclusions in quartz and muscovite. Of particular interest is work by Landis and Snee (1991) on the argon isotopic composition of irradiated amber. In 1988, Berner and Landis reported that gas bubbles in amber retained the compositional signature of the atmosphere at the time of formation. SEM elemental mapping of amber showed that some ambers contain quantities of potassium in the parts per million.

To test the hypothesis of Berner and Landis (1988), we (Landis and Snee, 1991) irradiated vacuum encapsulated amber ranging in age from Cretaceous through Recent, to convert a portion of the small amount of incorporated ^{39}K to ^{39}Ar. Because of the chemically inert nature of argon, ^{39}Ar proves to be an excellent tracer to evaluate diffusion processes. In the case of amber, we showed that ^{39}Ar did not diffuse out of the irradiated amber, and we calculated that over the length of geologic time represented by the amber samples, gases trapped within the amber structure would retain their original chemical compositional signature.

Standard Analytical Techniques

Many components of a study must be carefully planned and executed to ensure a successful result. Success is not only a function of the use of the best, most highly sensitive and precise analytical equipment but also one of the proper selection and preparation of samples. The most important aspect of a geochronologic study is selection of samples best suited to answer the question being posed. From the preceding discussion, that many complications can arise during the course of a study is obvious; and the smarter the investigators are in selecting appropriate samples, the greater the probability is of their being able to interpret the results.

The preparation of pure mineral separates is a critical aspect of any argon geochronologic study. Mineral separates for $^{40}Ar/^{39}Ar$ analysis are generally prepared by standard mineral separation techniques. Rock samples are crushed and sieved; for most samples the 80–120-mesh (180–125 μm) size fractions are used for mineral separation. Similar sizes are used for whole-rock samples, such as basalts. Initial mineral separations are done using heavy liquids, including methylene iodide, bromoform, lithium polytungstate, and sodium polytungstate in association with magnetic separation techniques. Whole-rock basalt samples may undergo removal of pyroxene, olivine, and plagioclase phenocrysts. After concentration, samples are normally hand-picked to near 100 percent purity. Before irradiation the samples are washed successively in acetone, ethanol, and deionized water in an ultrasonic cleaner.

Depending on age and potassium content, between 1 and 200 mg (milligrams) are loaded in aluminum capsules, which are stacked in silica-glass vials. Between every one to two samples and at the top and bottom of the glass vials, aluminum-encapsulated neutron fluence monitors (that is, the standards) are placed. We use hornblende standard MMhb-1 (K-Ar age = 520.4 Ma; Samson and Alexander, 1987; and recently modified to 523.1 Ma by Renne and others, 1998b) and sanidine standard FCT-3 ($^{40}Ar/^{39}Ar$ age = 27.84 Ma calibrated in the Denver argon geochronology laboratory against MMhb-1; and recently modified to 28.02 Ma by Renne and others, 1998b) as the fluence monitors, depending on the expected age of samples in the irradiation vial. In addition, CaF_2 and K_2SO_4 crystals are wrapped in aluminum capsules and included to monitor the production of interfering argon isotopes produced from Ca and K during irradiation. The vials are sealed under vacuum, and several vials are sealed in an aluminum irradiation canister. For some samples, which may be affected by ^{39}Ar recoil, a sample is packaged in an aluminum capsule and then individually sealed within a vacuum-evacuated, "breakseal," silica glass vial; after irradiation, these vials are attached directly to the extraction line, the seal is broken under vacuum, and any recoiled contents are analyzed.

Irradiations are done in the central thimble facility in the core of the U.S. Geological Survey TRIGA reactor (GSTR). Depending on age, samples are discontinuously irradiated for less than 1 hour to more than 100 hours; the younger the material, the shorter the irradiation, in order to minimize the effects from the production of interfering argon isotopes. Irradiation canisters are centered on the centerline of the reactor and rotated at 1 rpm throughout the period of irradiation to optimize neutron fluence distribution and to average out flux gradients.

For argon isotopic measurement in the Denver argon laboratory, samples are heated and analyzed in an internal resistance furnace system similar in design to that described by Staudacher and others (1978). (Many laboratories use laser-probe extraction (for example, Kelley and others, 1994) in place of, or in association with, resistance-furnace extraction methods. Our laboratory also is employing laser-probe extraction methods, but discussion of this methodology is beyond the scope of this report.) This system consists of a low-blank, double-vacuum resistance furnace, an ultra-high vacuum extraction line, and a rare-gas mass spectrometer (Mass Analyzer Products 215) equipped with a Nier-type source and Faraday and electron-multiplier detectors. Multiple samples are loaded into a Pyrex-glass sidearm located above the resistance furnace, which comprises a tantalum crucible with molybdenum liner surrounded by an outer can cooled with a water jacket. Within the outer can and around the crucible is a tungsten heating element that is shielded from the outer can by a heat shield. The volume containing the heating elements is evacuated to less than 1×10^{-7} torr. The crucible is on-line with the extraction line. A furnace controller provides power to the heating elements and can drive the system to the specified temperature in 2 minutes or less. The temperature of the crucible is monitored by a thermocouple whose feedback to the controller ensures that the set temperature during any heating step is maintained to within $\pm$2 °C. The gas released during each heating step is cleaned with Zr-Al and Zr-V-Fe getters (alloys with high efficiency for capturing contaminant gases). The extraction system includes three compartments, each separated from the others by valves. Gas is transferred between compartments by opening an intervening valve and freezing the gas with liquid nitrogen onto charcoal within a finger in the adjacent compartment. The liquid nitrogen is contained in a vessel exterior to the charcoal, and the freezing process is an efficient pump that transfers the gas in entirety between compartments. The furnace, sidearm, and first two compartments of the extraction line are evacuated and baked to 250 °C after each new addition of samples.

Samples commonly undergo incremental heating analysis, during which each sample is progressively heated for 20 minutes per heating step; argon from standards is released in a single 20-minute-long heating step. The gas from each step is transferred from the furnace to the getter section for 10 minutes, during which the furnace is turned off. After cleaning, the argon is expanded into the mass spectrometer and analyzed in static mode. Masses 40, 39, 38, 37, and 36 are analyzed and the data are collected and reduced on-line. Raw isotopic data are corrected for volume adjustments, mass discrimination, trap current settings, radioactive decay of ^{37}Ar and ^{39}Ar, and interfering argon isotopes. Measuring the $^{40}Ar/^{36}Ar$ ratio of atmospheric argon admitted to the system from an air pipette enables mass discrimination and atmospheric argon corrections.

Argon Thermochronology Applied to Mineral Deposits

$^{40}Ar/^{39}Ar$ geochronology has enormous potential for mineral deposit research. Not only can the method provide direct information on the age of a mineral deposit but also it can be used to unravel duration, number of episodes, and temperature of mineralization. The age-spectrum method provides information about the distribution of argon in the analyzed mineral whether the mineral formed before, during, or after an alteration/mineralization event. Even strongly altered wall-rock minerals can yield meaningful geochronology and provide constraints on the temperature of the mineralization event. Because the distribution of argon in the analyzed mineral is assessed by the age-spectrum method, conclusions can be drawn on the extent to which preexisting minerals were affected by the mineralization event.

General Strategy

Deriving the most information with least ambiguity requires more than simply directly dating minerals that were formed or reset by the mineralization process, although this is a critical part of the geochronologic procedure. It is equally important to define the premineralization cooling history of host rocks to provide constraints on the temperature of the host rocks during mineralization. Understanding the geologic and thermal constraints during and after mineralization and alteration is also critical. For dated minerals that may have formed during mineralization or alteration (for example, muscovite, alunite, adularia), we must know whether or not host rocks at the time of mineralization were cooler than the argon retention temperatures of the minerals, in order to be able to uniquely interpret their apparent ages. For ubiquitous minerals such as white mica, which may form during alteration activity, knowing the textural relationships and the temperature of mineralization will provide valuable constraints on whether or not preexisting white mica contributed inherited argon to alteration-associated white mica. It is also valuable to understand the complexity of the mineralization process, including the possibility of multiple events and prolonged activity, to avail ourselves of the full potential of the geochronologic method. Finally, knowing the postmineralization history is essential for understanding potential effects of those events on argon systematics.

Some Examples

Three published reports and one ongoing study are described here to illustrate the application of $^{40}Ar/^{39}Ar$ geochronology in studies of the age and origin of mineral deposits and in the unraveling of the tectonic history of orogenic belts.

Panasqueira, Portugal, Tin-Tungsten Deposit

Snee and others (1988) was the first study to use high-precision $^{40}Ar/^{39}Ar$ thermochronology on a well-characterized mineral deposit. The study defined the isotopic age and thermal history of the Panasqueira, Portugal, tin-tungsten deposit, which is spatially associated with Hercynian plutons, by obtaining 1σ analytical precisions between 0.7 percent (2.2 m.y. for single samples) and 0.3 percent (0.9 m.y. for populations) on muscovite associated with several stages of mineralization for this ≈300-Ma deposit.

The Panasqueira tin-tungsten deposit is located in north-central Portugal, near Fundão, along the south edge of the Iberian Hercynian plutonic and metamorphic belt (fig. 17). The ore deposit consists of a swarm of near-horizontal hydrothermal veins that crosscut a sequence of tightly folded pelitic schists. The quartz veins are spatially associated with a granite cupola (fig. 18) and contain economically significant amounts of wolframite, cassiterite, and chalcopyrite. An unusual mass of quartz, the silica cap, lies at the apex of the cupola.

Kelly and Rye (1979) worked out in detail the complex paragenesis of the tin-tungsten veins. They defined four stages of mineralization, which, from oldest to youngest, are the oxide-silicate, main sulfide, pyrrhotite alteration, and late carbonate stages. The economically important oxide-silicate stage (OSS) was subdivided into two substages, an earlier stage (I), represented by muscovite selvages that line the vein wall, and a later stage (II), consisting of intergrown coarse quartz, muscovite, wolframite, and arsenopyrite. Kelly and Rye (1979) originally thought that muscovite and quartz formed continuously during these two substages. The main sulfide stage (MSS) represents a period when sulfide deposition was dominant, but quartz and muscovite also formed. Pyrrhotite that formed during this stage was selectively replaced by marcasite and pyrite during the pyrrhotite alteration stage. Finally, carbonate minerals were widely deposited during the late carbonate stage.

To determine both the age of the Panasqueira deposit and its mineralization history, we selected well-characterized samples from the two muscovite-bearing stages, the oxide-silicate and the main sulfide stages. We chose samples from both substages of the OSS (I and II). One of our samples (fig. 19) represented both of these substages, and muscovite from each was carefully separated.

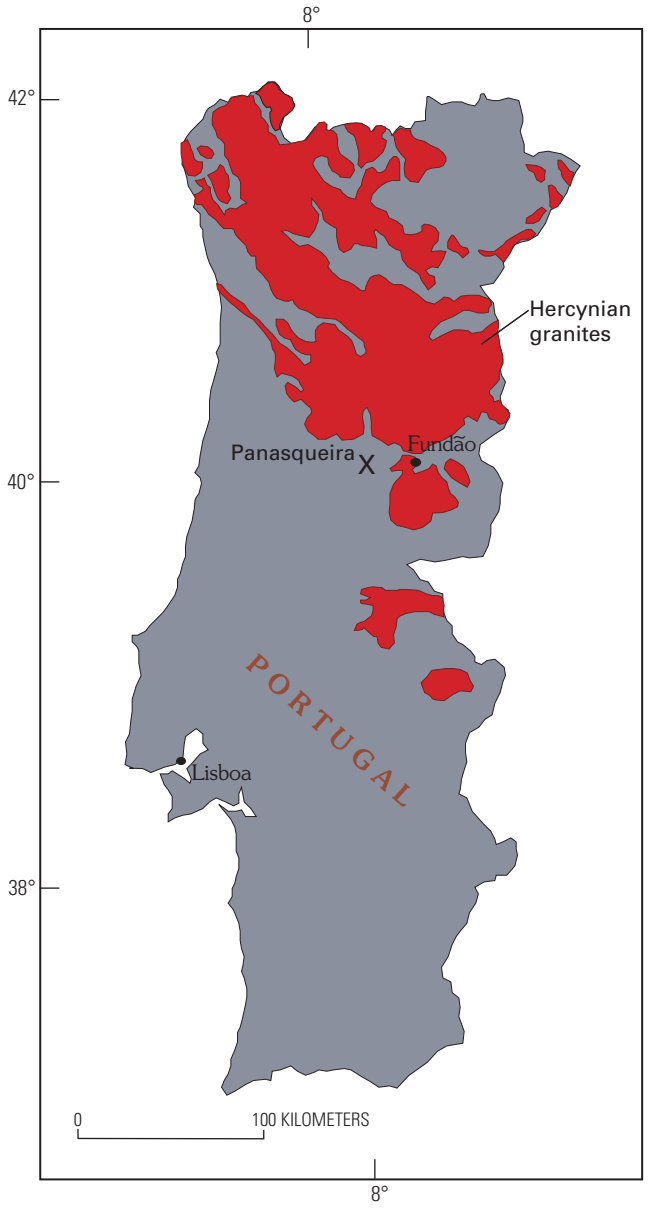

Figure 17. Sketch map of Portugal showing location of Panasqueira. The Panasqueira tin-tungsten deposit is located near Fundão along south edge of Hercynian plutonic and metamorphic belt.

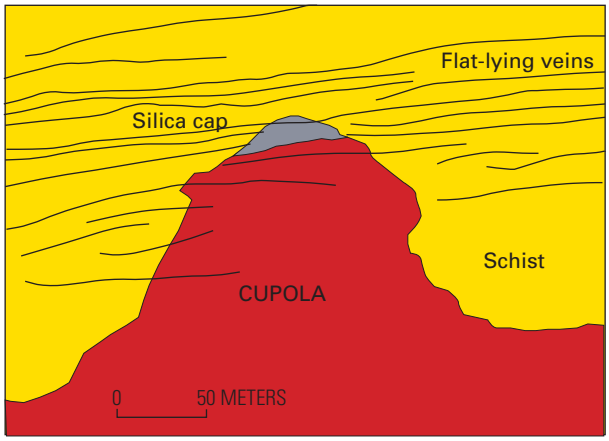

Figure 18. Diagrammatic cross section of the Panasqueira granite cupola that is host to the Sn-W deposit, showing silica cap and near-flat-lying quartz veins.

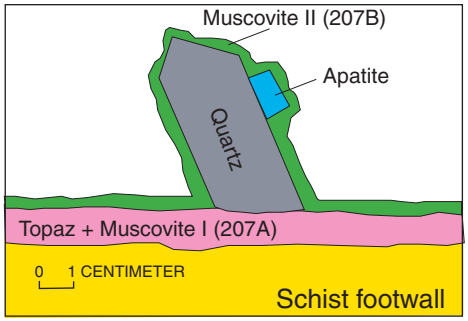

Figure 19. Drawing of sample 207 exhibiting the two substages of the oxide-silicate stage. Drawing shows relationship between older OSS I alteration muscovite (sample 207A) and younger OSS II late-stage muscovite (sample 207B).

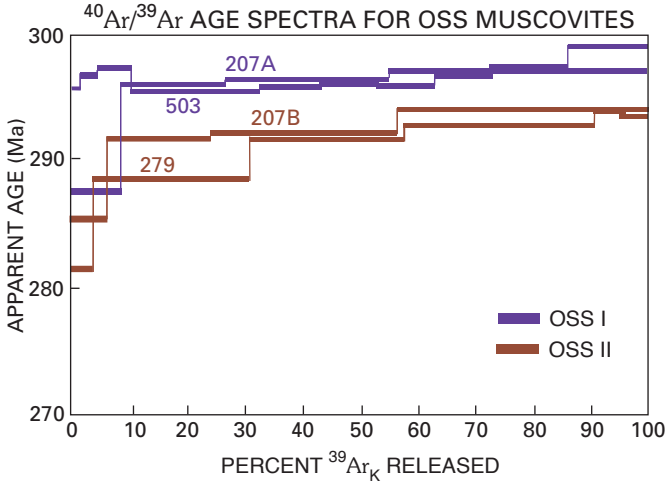

Figure 20. Composite $^{40}Ar/^{39}Ar$ age-spectrum diagrams for muscovite from OSS I and OSS II. Samples 207A and B represent separates from substage I and II respectively and were separated from the sample illustrated in figure 19.

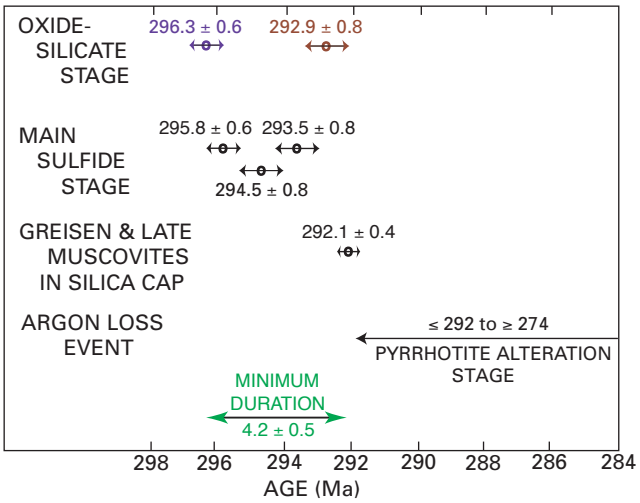

Figure 21. Paragenesis of the Panasqueira deposit, showing detailed results of the $^{40}Ar/^{39}Ar$ geochronology.

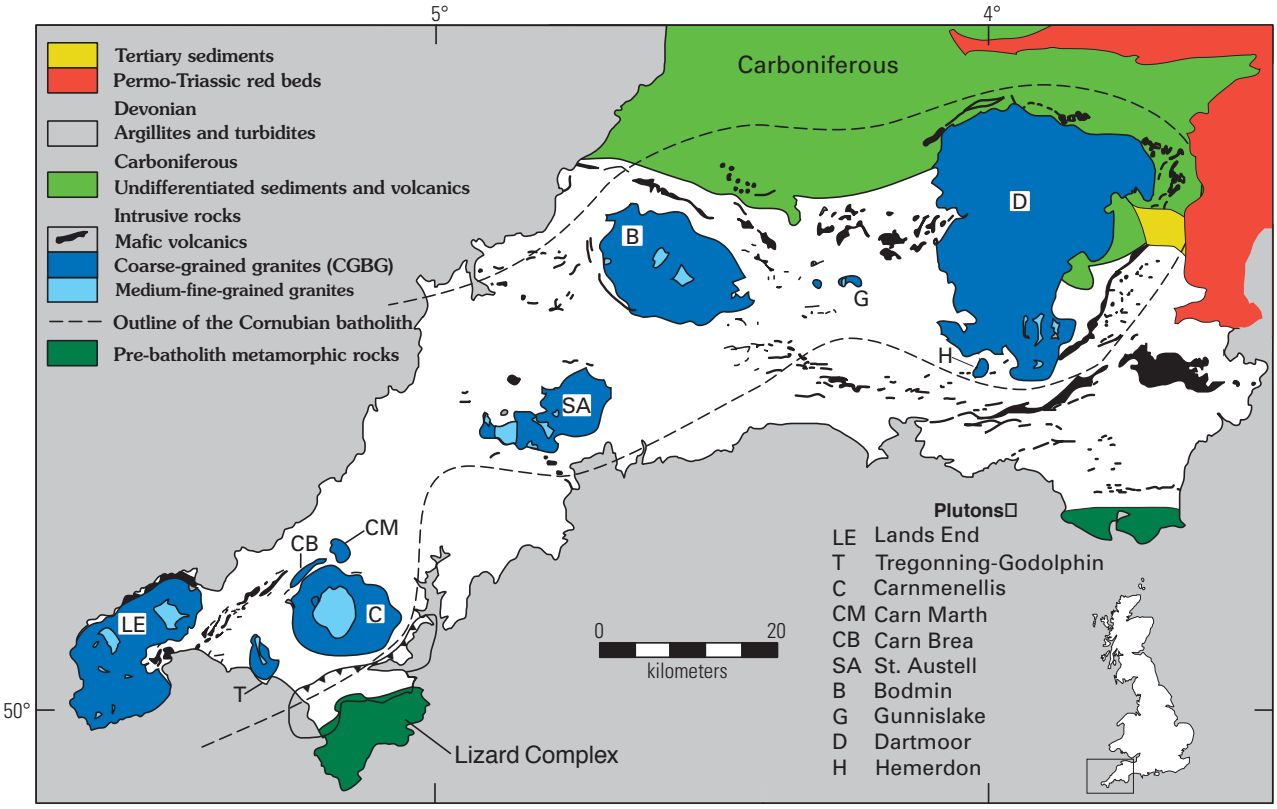

Figure 22. Geologic sketch map of southwest England, showing Cornubian batholith. Generalized geology modified from Chesley and others (1993) and Willis-Richards and Jackson (1989); line with sawteeth, thrust fault; dashed line, extent of geophysical expression of the Cornubian batholith.

The study resolved age differences between the oxide-silicate and main sulfide stages, defined two periods of oxide-silicate activity (fig. 20)—one of which was younger than the main sulfide stage, and showed that geisenization and younger oxide-silicate activity were contemporaneous (fig. 21). Minor argon loss from all dated samples occurred during later thermal activity during the pyrrhotite alteration stage. Beyond these geologic implications, because of the comprehensive crosscutting relationships and fluid-inclusion homogenization temperatures defined by Kelly and Rye (1979), Ar-retention temperature for $2M_1$ muscovite was defined to be between 325° and 270 °C, depending on cooling rate.

Cornubian Batholith and Associated Mineral Deposits, Southwest England

Chesley and others (1993) built on the methods defined by Snee and others (1988) by combining high-precision $^{40}Ar/^{39}Ar$ thermochronology on muscovite, biotite, and hornblende with U-Pb monazite and xenotime and Sm-Nd fluorite geochronology. The metalliferous ore deposits associated with Hercynian-age biotite-muscovite granites of the Cornubian batholith (southwest England) provide a well-defined geologic framework for applying multiple high-precision methods to unravel the details of granite magmatism and the superposed mineralization and cooling history (fig. 22).

The Cornubian batholith was emplaced at the end of the Carboniferous to Permian Hercynian orogeny, which affected much of Europe and central Asia. The batholith has five major plutons and many smaller satellites and is primarily peraluminous in chemical character. Approximately 90 percent of exposed plutonic rock is coarse-grained biotite-muscovite granite. Four later episodes of granite magmatism are grouped under the label "medium-fine-grained granites" in figure 22 and are represented by fine-grained biotite granite, megacrystic lithium-mica granite, fine-grained lithium-mica granite, and fluorite granite. Crosscutting some of the major plutons are vertical to near vertical felsic porphyry dikes, called elvans. Mineralization is associated with multiple, steeply dipping fractures and lodes exhibiting evidence of multiple episodes of mineralizing fluid flow. Four stages of mineralization are observed and are summarized in table 3. Stages 1 through 3 have been directly attributed to intrusion and cooling of the Cornubian batholith. The origin of Stage 4 mineralization is unclear because of its notably low temperature of formation (100°–170°C).

The results of the geochronology study are shown in figure 23. The U-Pb emplacement ages show that granite magmatism across the batholith occurred over a protracted period extending from ≈300 Ma to ≈275 Ma with no major hiatus, and that magmatism within any single pluton occurred over periods of as much as 4.5 m.y. The U-Pb date on monazite (280.4±1.2 Ma) for the Dartmoor granite is statistically identical to the $^{40}Ar/^{39}Ar$ date (280.3±1.0 Ma; calibrated against MMhb-1 hornblende

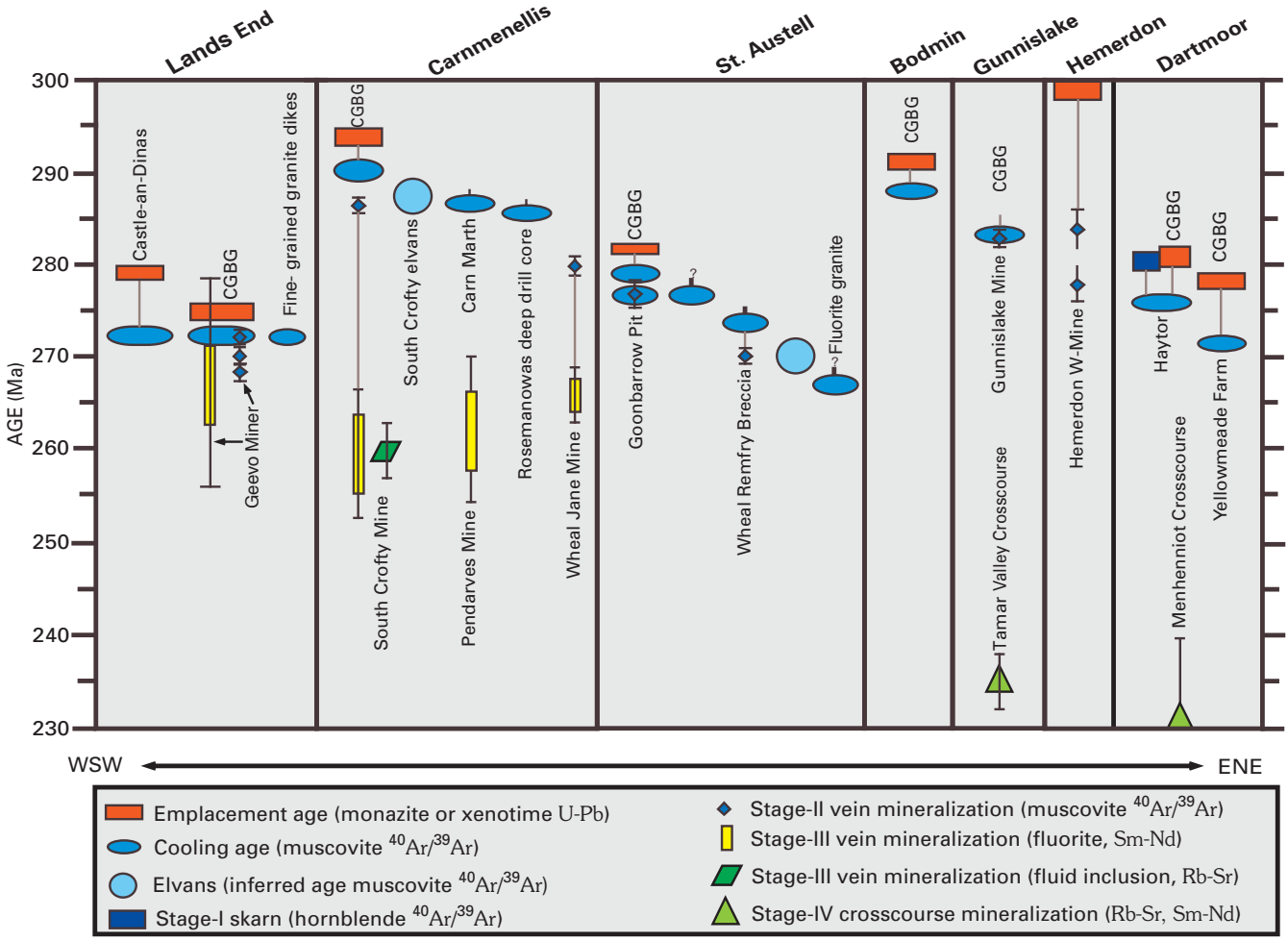

Figure 23. Summary geochronology for Cornubian batholith and associated mineral deposits. All geochronology data are from Chesley and others (1993) and Chesley (1999). Vertical width of symbols (error bars) indicates 1σ error in age; CGBG, coarse-grained biotite granite.

Table 3. Stages of mineralization of the Cornubian batholith, southwest England.

[T_h, fluid-inclusion homogenization temperature; gnt, garnet; px, pyroxene; tourm, tourmaline; amph, amphibole; qz, quartz; fsp, feldspar; musc, muscovite; chl, chlorite; hem, hematite; fluor, fluorite; bar, barite; dol, dolomite; calc, calcite]

	Stage 1	Stage 2		Stage 3	Stage 4
Style	Skarns	Pegmatitic deposits	Sheeted greisen bordered veins. Tourmaline-bearing veins.	Sn-bearing polymetallic fissure veins. Predominantly east-west.	Late polymetalic sulfide veins. "Crosscourse" Predominantly north-south.
Economic metals	Fe, Cu, Sn	Sn, W ±Mo	Sn, W	Sn, Cu, Pb, As, Fe	Pb, Zn, Ag, Fe, Sb, U
Gangue minerals	Gnt, px, tourm, amph	Qz, fsp, musc, tourm	Qz, musc, tourm	Qz, fsp, chl, hem, fluor	Qz, bar, dol, calc, fluor
T_h (°C)	375°–450°	300°–500°	300°–500°	200°–400°	100°–170°

with a date of 520.4 Ma based on Samson and Alexander, 1987) for hornblende from metamorphic skarn at its contact. This concordance confirms proper crosscalibration of the U-Pb and Ar systems in this study. Elvan emplacement was synchronous with granite emplacement and continued to as young as 270 Ma. Cooling rates derived from both the U-Pb and the $^{40}Ar/^{39}Ar$ dates

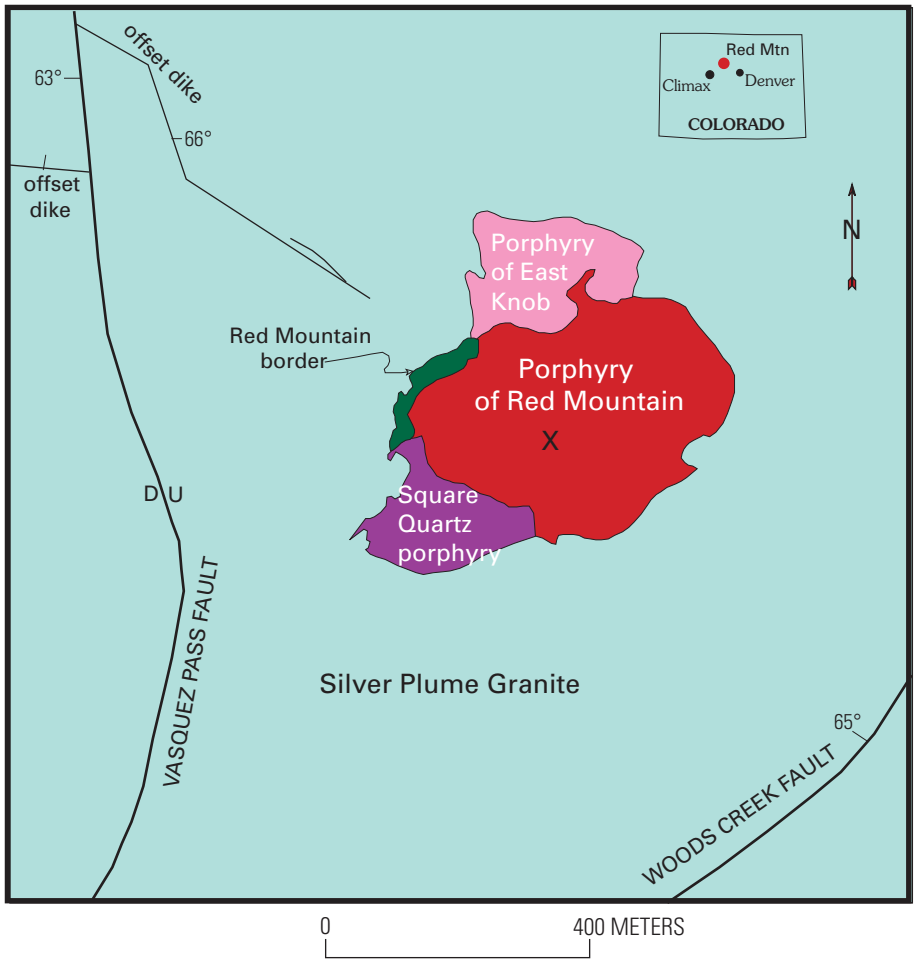

Figure 24. Sketch map of the Red Mountain intrusive center. Generalized surface geology of Red Mountain is modified from Wallace and others (1978), and Geraghty and others (1988). Two faults, the Woods Creek and the Vasquez Pass, cut across the Middle Proterozoic granite of the area. Vasquez Pass fault offsets a dike and indicates down to the east movement of the Red Mountain porphyry system. Only a few stocks of the Red Mountain system are exposed at surface. Numbers show dip of dike and faults; U, upthrown side; D, downdropped side of fault.

are unrelated to emplacement age and show a decrease from southwest to northeast from ≈210 °C/ m.y. to ≈60 °C/ m.y., probably reflecting the effect from the heat added to the crust by the many pulses of magmatism. Stage 1, skarn mineralization, was directly related to intrusion of granites. Between 275 and 265 Ma, chemically evolved granites were emplaced. High-temperature tin and tungsten oxide-silicate mineralization (Stage 2) was broadly synchronous with emplacement of the granite magmas and was as much as 25 m.y. older than the main episode of economic mineralization represented by polymetallic sulfide-fluorite veins (Stage 3). Later formation of polymetallic veins, the crosscourses (Stage 4), is much younger (Chesley, 1999) and commenced after emplacement and cooling of the batholith were completed.

Red Mountain Intrusive System and Associated Urad-Henderson Molybdenum Deposits, Colorado

Geissman and others (1992) acquired paleomagnetic and $^{40}Ar/^{39}Ar$ data from most stocks of the Red Mountain intrusive system and associated Urad-Henderson molybdenum deposits and alteration zones. The Red Mountain intrusive system within the Colorado mineral belt is located in the Front Range of Colorado. The system is of Tertiary age and intrudes Middle Proterozoic (1.4 Ga) Silver Plume Granite (fig. 24) and comprises 15 stocks and 4 igneous breccias (Lovering and Goddard, 1950; Wallace and others, 1978; Carten and others, 1988; Geraghty and others, 1988). Only four of the stocks and breccias are exposed at the surface; the remainder are below the surface and were discovered during the course of exploration and underground mining. The system has been a major molybdenum resource. The purpose of Geissman and others' study was better understanding of the emplacement and cooling history of the system, the relationship between the intrusive events and mineralization, and the postemplacement structural modifications to the complex.

$^{40}Ar/^{39}Ar$ geochronology on potassium feldspar, biotite, and muscovite from the intrusive rocks and alteration zones (figs. 25 and 26) indicates that the thermal activity responsible for the Red Mountain intrusive system started at or before 29.9±0.3 Ma and ended at 26.95±0.09 Ma—more than 3 m.y. of nearly continuous thermal activity. The porphyry of Red Mountain, one of the oldest stocks in the system, was emplaced before 29.9 Ma and

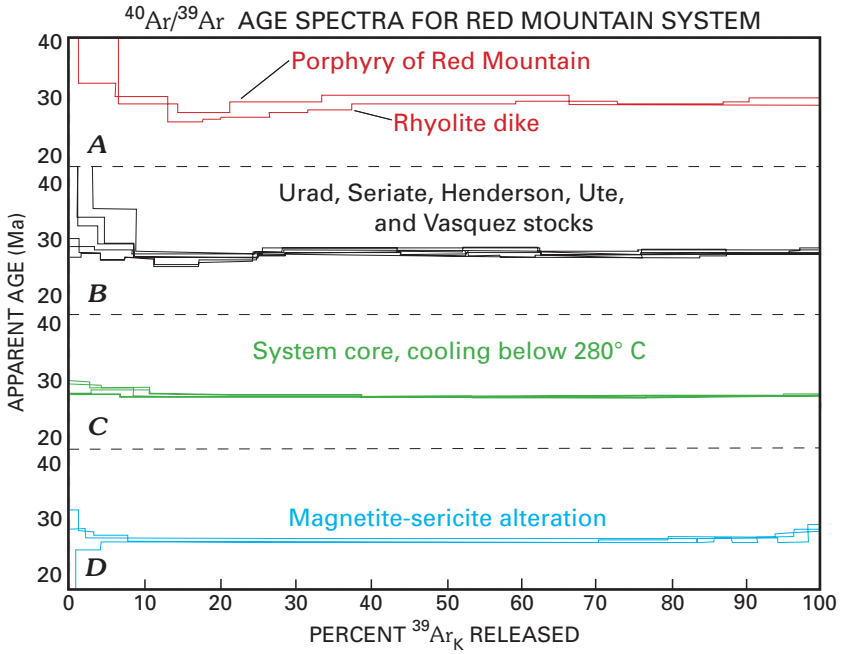

Figure 25. Composite $^{40}Ar/^{39}Ar$ age-spectrum diagram for argon samples from Red Mountain intrusive system and Urad-Henderson mineral deposit. One sigma analytical errors for data for most statistically significant temperature steps are between 0.06 and 0.10 m.y. *A*, Age spectrum for orthoclase from porphyry of Red Mountain and potassium feldspar from a rhyolite dike emplaced into Precambrian host rocks. *B*, Six (five orthoclase and one biotite) age spectra for minerals from the Urad, Seriate, Henderson, Ute, and Vasquez stocks, all of which are only exposed underground. *C*, Six age spectra for biotites from Henderson, Ute, Vasquez, and Seriate stocks within the central part of the Red Mountain intrusive system. *D*, Three age spectra for muscovite from the magnetite-sericite alteration zone around the Seriate stock.

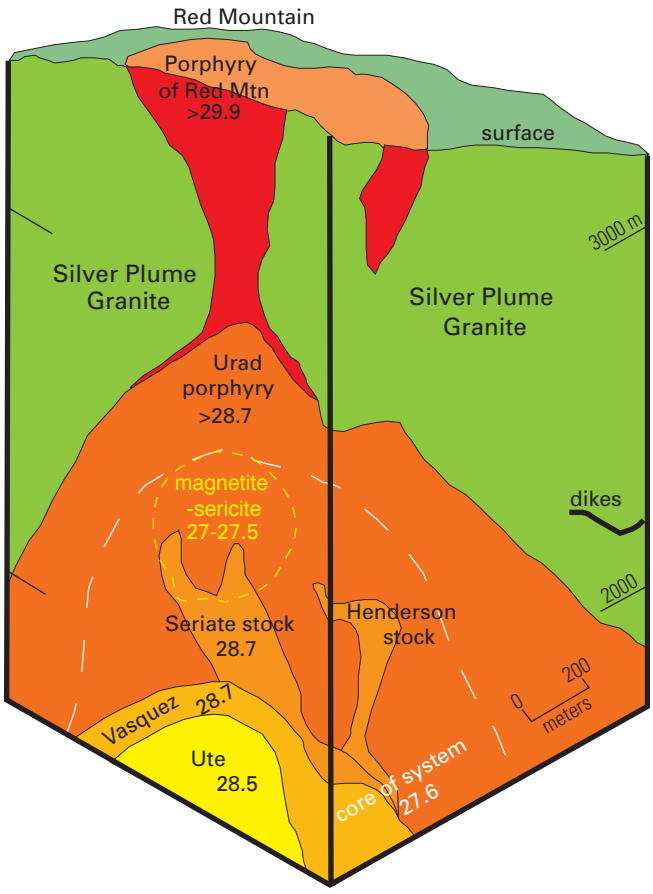

Figure 26. Three-dimensional block diagram of Red Mountain intrusive center, showing relative ages of stocks and cooling after emplacement; all ages are in million years. Dashed white line represents outer edge of part of system that cooled below biotite argon closure temperature at 27.59±0.03 Ma. Circular dashed yellow line marks an area of magnetite-sericite alteration that formed between 27.51±0.03 and 26.95±0.08 Ma at end of system cooling. This area overlaps the system core, but its associated thermal pulse did not reset older phases.

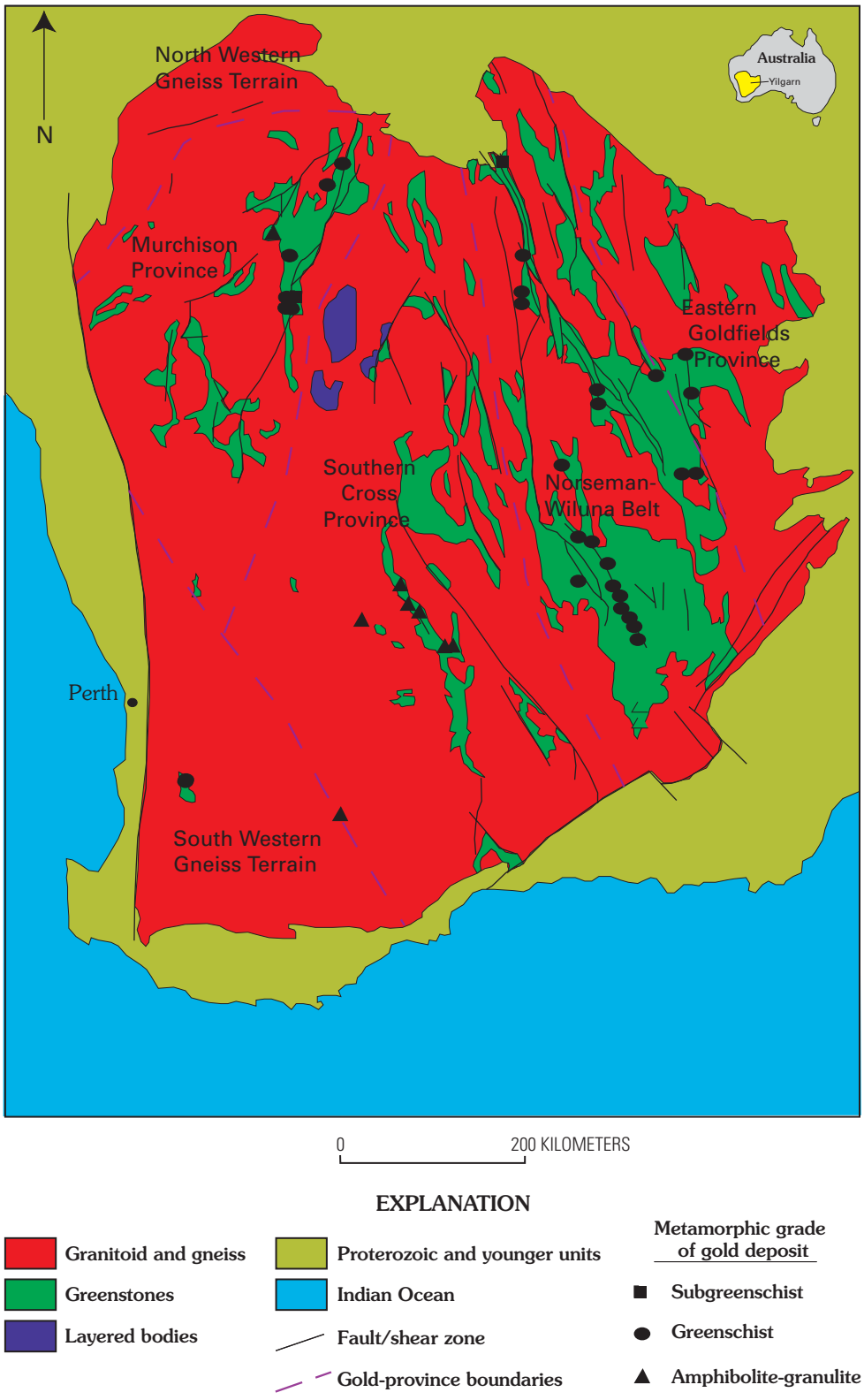

Figure 27. Regional-scale geologic sketch map of Yilgarn-block gold deposits, Western Australia.

possibly before 30.38±0.09 Ma. Nearby lamprophyre dikes were emplaced at 29.8±0.1 Ma; rhyolite dikes intruded at 29.4±0.2 Ma. The Urad and Seriate stocks intruded after 29.8 Ma but before emplacement of the Vasquez stock at 28.71±0.08 Ma. Based on six identical dates from potassium feldspar and biotite from the Urad, Seriate, Henderson, Ute, and Vasquez stocks, the core of the system cooled below the biotite argon closure temperature of about 300 °C at 27.59±0.03 Ma. The last period of thermal activity involved pulses of magnetite-sericite alteration around the Seriate stock between 27.51±0.03 Ma and 26.95±0.08 Ma, and the activity did not thermally overprint unaltered parts of the system.

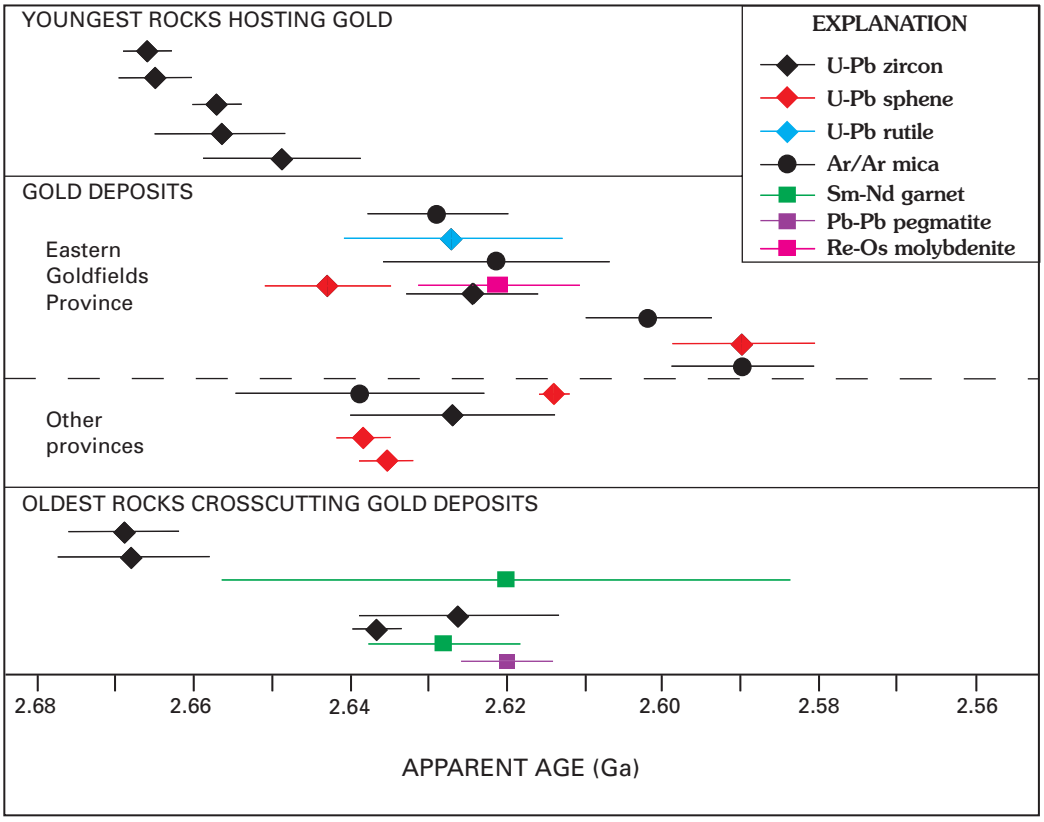

Figure 28. Summary of currently available geochronologic data for gold deposits in Western Australia (modified from Groves and others, 2000).

The combined argon age-spectrum and paleomagnetic data also allow the conclusion that the Red Mountain intrusive system was tilted by subsequent structural activity. The magnitude of tilting was between 15° and 25° and occurred about an approximately north-northeast horizontal axis paralleling the orientation of the Woods Creek fault (fig. 24).

Eastern Goldfields Province, Western Australia

The Eastern Goldfields Province in the Archean-age Yilgarn Craton of Western Australia is one of the world's most important gold provinces and one of the oldest. The gold deposits in the province have been well studied, but high-precision geochronological data on the age of mineralization are lacking, and existing data from several isotopic systems are in many cases contradictory. The purpose of an ongoing study (D.I. Groves, N.J. McNaughton, and L.W. Snee, work in progress) is to use a multi-isotope, multi-mineral approach in several key areas of the province to (1) assess its applicability to problems on Archean gold deposits and (2) provide precise and accurate ages that will allow a reinterpretation of the interrelationship among deformation, metamorphism, and gold mineralization in the Eastern Goldfields.

The distribution of the gold deposits of southwestern Australia is shown on a regional-scale geologic sketch map of the Yilgarn Craton (fig. 27). The exposed geology is part of a craton that was formed in the Archean before about 2.6 Ga. Volcanic and sedimentary precursors of the greenstone metamorphic rocks in this classic granite-greenstone belt were deposited before 2.7 Ga. Four major compressive deformation events affected the craton, and granites intruded during and after deformation. Metamorphism varies across the region from subgreenschist to granulite facies, and the age of metamorphism lies between about 2.685 and 2.63 Ga. Most studies carried out on the gold deposit history indicate that gold was deposited late in the structural evolution of the craton and at peak or post-peak metamorphic conditions.

Geochronologic data shown in figure 28 from numerous sources support a major period of gold mineralization between 2.65 and 2.62 Ga. However, few well-constrained isotopic dates currently exist. The Denver argon geochronology laboratory will focus on providing high-quality $^{40}Ar/^{39}Ar$ geochronology on metamorphic rocks and alteration assemblages in an attempt to constrain the metamorphic cooling history and the age of the gold deposits. We discovered early in the study that the accepted age of the argon geochronology standards will be critical in comparison across isotopic techniques. As pointed out by Renne and others (1998a), age inaccuracies in studies of Archean geochronology are magnified to the extent that 25 m.y. inaccuracies could easily occur. In the case of the Eastern Goldfields, 25 m.y. inaccuracy in argon ages falls significantly outside the analytical precision of the method (approximately 6 m.y., 2σ, at 2.6 Ga) and obviates comparisons with other isotopic methods until the inaccuracy can be resolved.

References Cited

Aldrich, L.T., Davis, G.L., and James, H.L., 1965, Ages of minerals from metamorphic and igneous rocks near Iron Mountain, Michigan: Journal of Petrology, v. 6, pt. 3, p. 445–472.

Alexander, E.C., Jr., Michelson, G.M., and Lanphere, M.A., 1978, MMHb-1—A new $^{40}Ar/^{39}Ar$ dating standard, *in* Zartman, R.E., ed., Short papers of the fourth international conference, geochronology, cosmochronology, isotope geology 1978: U.S. Geological Survey Open-File Report 78-701, p. 6-8.

Arehart, G.B., Foland, K.A., Naeser, C.W., and Kesler, S.E., 1993, $^{40}Ar/^{39}Ar$, K/Ar, and fission track geochronology of sediment-hosted disseminated gold deposits—Implications for depositional processes: Economic Geology, v. 88, p. 622–646.

Armstrong, R.L., Jäger, Emilie, and Eberhardt, Peter, 1966, A comparison of K-Ar and Rb-Sr ages of alpine biotites: Earth and Planetary Science Letters, v. 1, p. 13–19.

Ashley, R.P., and Silberman, M.L., 1976, Direct dating of mineralization at Goldfield, Nevada, by potassium-argon and fission-track methods: Economic Geology, v. 71, p. 904–924.

Baig, M.S., 1990, Structure and geochronology of pre-Himalayan and Himalayan orogenic events in the northwest Himalaya, Pakistan, with special reference to the Besham area: Corvallis, Oreg., Oregon State University Ph. D. dissertation, 397 p.

Baker, Joel, Snee, Lawrence, and Menzies, Martin, 1996, A brief period of flood volcanism in Yemen—Implications for the duration and rate of continental flood volcanism at the Afro-Arabian triple junction: Earth and Planetary Science Letters, v. 138, p. 39–55.

Baksi, A.K., Archibald, D.A., and Farrar, E., 1996, Intercalibration of $^{40}Ar/^{39}Ar$ dating standards: Chemical Geology, v. 129, p. 307–324.

Baldwin, S.L., Harrison, T.M., and Fitz Gerald, J.D., 1990, Diffusion of ^{40}Ar in metamorphic hornblende: Contributions to Mineralogy and Petrology, v. 1990, p. 691–703.

Berger, B.R., Snee, L.W., Hanna, W., and Benham, J.H., 1983, Mineral resource appraisal of the West Pioneers Wilderness Study Area (RARE II), Beaverhead County, Montana: U.S. Geological Survey Miscellaneous Field Studies Map MF–83–1576A, 21 p. and map.

Berger, G.W., 1975, $^{40}Ar/^{39}Ar$ step heating of thermally overprinted biotite, hornblende, and potassium feldspar from Eldora, Colorado: Earth and Planetary Science Letters, v. 26, p. 387–408.

Berger, G.W., and York, Derek, 1981, Geothermometry from $^{40}Ar/^{39}Ar$ dating experiments: Geochimica et Cosmochimica Acta, v. 45, p. 795–811.

Berner, R.A., and Landis, G.P., 1988, Gas bubbles in fossil amber as possible indicators of the major gas composition of ancient air: Science, v. 239, p. 1406–1409.

Bird, M.I., Chivas, A.R., and McDougall, Ian, 1990, An isotopic study of surficial alunite in Australia—2, Potassium-argon geochronology: Chemical Geology, v. 80, p. 133–145.

Brereton, N.R., 1970, Corrections for interfering isotopes in the $^{40}Ar/^{39}Ar$ dating method: Earth and Planetary Science Letters, v. 8, p. 427–433.

Brooks, W.E., and Snee, L.W., 1996, Timing and effects of detachment-related potassium metasomatism on $^{40}Ar/^{39}Ar$ ages from the Windous Butte Formation, Grant Range, Nevada: U.S. Geological Survey Bulletin 2154, 25 p.

Brooks, W.E., Thorman, C.H., and Snee, L.W., 1995, The $^{40}Ar/^{39}Ar$ ages and tectonic setting of the middle Eocene northeast Nevada volcanic field: Journal of Geophysical Research, v. 100, p. 10403–10416.

Carslaw, H.S., and Jaeger, J.C., 1959, Conduction of heat in solids: Oxford, Clarendon Press, 510 p.

Carten, R.B., Geraghty, E.P., Walker, B.M., and Shannon, J.R., 1988, Cyclic development of igneous features and their relationship to high-temperature hydrothermal features in the Henderson porphyry molybdenum deposit, Colorado: Economic Geology, v. 83, p. 266–296.

Cheilletz, Alain, Feraud, Gilbert, Giuliani, Gaston, and Ruffet, GIlles, 1993, Emerald dating through $^{40}Ar/^{39}Ar$ step-heating and laser spot analysis of syngenetic phlogopite: Earth and Planetary Science Letters, v. 120, p. 473–485.

Chesley, J.T., 1999, Integrative geochronology of ore deposits; new insights into the duration and timing of hydrothermal circulation; Society of Economic Geology Reviews in Economic Geology, v. 12, p. 115–141.

Chesley, J.T., Halliday, A.N., Snee, L.W., Mezger, K., Shepherd, T.J., and Scrivener, R.C., 1993, Thermochronology of the Cornubian batholith in southwest England—Implications for pluton emplacement and protracted hydrothermal mineralization: Geochimica et Cosmochimica Acta, v. 57, p. 1817–1835.

Chopin, Christian, and Maluski, Henri, 1980, $^{40}Ar/^{39}Ar$ dating of high-pressure metamorphic micas from the Gran Paradiso area (Western Alps)—Evidence against the blocking temperature concept: Contributions to Mineralogy and Petrology, v. 74, p. 109–122.

Chopin, Christian, and Monie, Patrick, 1984, A unique magnesiochloritoid-bearing high-pressure assemblage from the Monte Rosa, Western Alps—Petrologic and ^{40}Ar-^{39}Ar radiometric study: Contributions to Mineralogy and Petrology, v. 87, p. 388–398.

Christiansen, P.P., and Snee, L.W., 1994, Structure, metamorphism, and geochronology of the Cosmos Hills and Ruby Ridge, Brooks Range schist belt, Alaska: Tectonics, v. 13, p. 193–213.

Clark, A.H., Archibald, D.A., Lee, A.W., Farrar, Edward, and Hodgson, C.J., 1998, Laser probe $^{40}Ar/^{39}Ar$ ages of early and late-stage alteration assemblages, Rosario porphyry copper-molybdenum deposit, Collahuasi district, I Region, Chile: Economic Geology, v. 93, p. 326–337.

Cosca, M.A., Hunziker, J.C., Huon, S., and Massone, H., 1992, Radiometric age constraints on mineral growth, metamorphism, and tectonism of the Gummfluh Klippe, Brianconnais domain of the Prealps, Switzerland: Contributions to Mineralogy and Petrology, v. 112, p. 439–449.

Cosca, M.A., and O'Nions, R.K., 1994, A re-examination of the influence of composition on argon retentivity in metamorphic calcic amphiboles: Chemical Geology, v. 112, p. 39–56.

Dahl, P.S., 1996a, The effects of composition on retentivity of argon and oxygen in hornblende and related amphiboles—A field-tested empirical model: Geochimica et Cosmochimica Acta, v. 60, p. 3687–3700.

Dahl, P.S., 1996b, The crystal-chemical basis for Ar retention in micas—Inferences from interlayer partitioning and implications for geochronology: Contributions to Mineralogy and Petrology, v. 123, p. 22–39.

Dalla-Torre, Michael, Livi, K.J.T., Veblen, D.R., and Frey, Martin, 1996, White K-mica evolution from phengite to muscovite in slates and shale matrix melange, Diablo Range, California: Contributions to Mineralogy and Petrology, v. 123, p. 390–405.

Dalrymple, G.B., Alexander, E.C., Lanphere, M.A., and Kraker, G.P., 1981, Irradiation of samples for $^{40}Ar/^{39}Ar$ dating using the Geological Survey TRIGA reactor: U.S. Geological Survey Professional Paper 1176, 55 p.

Dalrymple, G.B., Izett, G.A., Snee, L.W., and Obradovich, J.D., 1993, $^{40}Ar/^{39}Ar$ age spectra and total fusion ages of tektites from Cretaceous-

Tertiary boundary sedimentary rocks in the Beloc Formation, Haiti: U.S. Geological Survey Bulletin 2065, 20 p.

Dalrymple, G.B., and Lanphere, M.A., 1969, Potassium-argon dating—Principles, techniques, and applications to geochronology: San Francisco, W.H. Freeman, 258 p.

Dalrymple, G.B., and Lanphere, M.A., 1971, $^{40}Ar/^{39}Ar$ technique of K-Ar dating—A comparison with the conventional technique: Earth and Planetary Science Letters, v. 12, p. 300–308.

Dalrymple, G.B., and Lanphere, M.A., 1974, $^{40}Ar/^{39}Ar$ age spectra of some undisturbed terrestrial samples: Geochimica et Cosmochimica Acta, v. 38, p. 715–738.

Dalrymple, G.B., Lanphere, M.A., and Pringle, M.S., 1988, Correlation diagrams in $^{40}Ar/^{39}Ar$ dating—Is there a correct choice?: Geophysical Research Letters, v. 15, p. 589–591.

Davies, J.A., Brown, F., and McCargo, M.R., Jr., 1963, Range of Xe^{133} and Ar^{41} ions of kiloelectron volt energies in aluminum: Canadian Journal of Physics, v. 41, p. 829–843.

Dodson, M.H., 1973, Closure temperature in cooling geochronological and petrological systems: Contributions to Mineralogy and Petrology, v. 40, p. 259–274.

Dong, Hailang, Hall, C.M., Halliday, A.N., and Peacor, D.R., 1997, Laser ^{40}Ar-^{39}Ar dating of microgram-size illite samples and implications for thin section dating: Geochimica et Cosmochimica Acta, v. 61, p. 3803–3808.

Dong, Hailang, Hall, C.M., Peacor, D.R., and Halliday, A.N., 1995, Mechanisms of argon retention in clays revealed by $^{40}Ar/^{39}Ar$ dating: Science, v. 267, p. 355–359.

Dunlap, W.J., 2000, Nature's diffusion experiment—The cooling-rate cooling-age correlation: Geology, v. 28, p. 139–142.

Eberl, D.D., Srodon, J., Kralik, M., Taylor, B.E., and Peterman, Z.E., 1990, Ostwald ripening of clays and metamorphic minerals: Science, v. 248, p. 474–477.

Faure, Gunter, 1986, Principles of isotope geology: New York, Wiley, 589 p.

Feng, Rui, Kerrich, Robert, McBride, Sandra, and Farrar, Edward, 1992, $^{40}Ar/^{39}Ar$ age constraints on the thermal history of the Archaean Abitibi greenstone belt and the Pontiac Subprovince—Implications for terrane collision, differential uplift, and overprinting of gold deposits: Canadian Journal of Earth Sciences, v. 29, p. 1389–1411.

Fitz Gerald, J.D., and Harrison, T.M., 1993, Argon diffusion domains in K-feldspar—I, Microstructures in MH-10: Contributions to Mineralogy and Petrology, v. 113, p. 367–380.

Fleck, R.J., Sutter, J.F., and Elliot, D.H., 1977, Interpretation of discordant $^{40}Ar/^{39}Ar$ age spectra of Mesozoic tholeiites from Antarctica: Geochimica et Cosmochimica Acta, v. 41, p. 15–32.

Foland, K.A., 1994, Argon diffusion in feldspar, *in* Parsons, I., ed., Feldspars and their reactions: Boston, Mass., Kluwer Academic Publishers, p. 415–447.

Foland, K.A., Hubacher, F.A., and Arehart, G.B., 1992, $^{40}Ar/^{39}Ar$ dating of very fine-grained samples—An encapsulated-vial procedure to overcome the problem of ^{39}Ar recoil loss: Chemical Geology, v. 102, p. 269–276.

Foland, K.A., Linder, J.S., Laskowski, T.E., and Grant, N.K., 1984, $^{40}Ar/^{39}Ar$ dating of glauconites—Measured ^{39}Ar recoil loss from well-crystallized specimens: Isotope Geosciences, v. 2, p. 241–264.

Folger, H.W., Snee, L.W., Mehnert, H.H., Hofstra, A.H., and Dahl, A.R., 1996, Significance of K-Ar and $^{40}Ar/^{39}Ar$ dates from mica in Carlin-type gold deposits—Evidence from the Jerritt Canyon District, Nevada, *in* Coyner, A.R., and Fahey, P.L., eds., Geology and ore deposits of the American Cordillera: Geological Society of Nevada Symposium Proceedings, Reno/Sparks, Nevada, April 1995, p. 41–60.

Ford, R.C., and Snee, L.W., 1996, $^{40}Ar/^{39}Ar$ thermochronology of white mica from the Nome District, Alaska—The first ages of lode sources to placer gold deposits in the Seward Peninsula: Economic Geology, v. 91, p. 213–220.

Fortes, P.T.F.O., Cheilletz, Alain, Giuliani, Gaston, and Feraud, Gilbert, 1997, A Brasiliano age (500±5 Ma) for the Mina III gold deposit, Crixas greenstone belt, central Brazil: International Geology Review, v. 39, p. 449–460.

Foster, D.A., Harrison, M.A., Copeland, Peter, and Heizler, M.T., 1990, Effects of excess argon within large diffusion domains on K-feldspar age spectra: Geochimica et Cosmochimica Acta, v. 54, p. 1699–1708.

Gaber, L.J., Foland, K.A., and Corbato, C.E., 1988, On the significance of argon release from biotite and hornblende during $^{40}Ar/^{39}Ar$ vacuum heating: Geochimica et Cosmochimica Acta, v. 52, p. 2457–2465.

Geissman, J.W., Snee, L.W., Graaskamp, G.W., Carten, R.B., and Geraghty, E.P., 1992, Deformation and age of the Red Mountain intrusive system (Urad-Henderson molybdenum deposits), Colorado—Evidence from paleomagnetic and $^{40}Ar/^{39}Ar$ data: Geological Society of America Bulletin, v. 104, p. 1031–1047.

Geraghty, E.P., Carten, R.B., and Walker, B., 1988, Tilting of Urad-Henderson and Climax porphyry molybdenum systems, central Colorado, as related to northern Rio Grande rift tectonics: Geological Society of America Bulletin, v. 100, p. 1780–1786.

Giuliani, Gaston, Zimmermann, J.L., and Montigny, R., 1994, K-Ar and $^{40}Ar/^{39}Ar$ evidence for a Transamazonian age (2030–1970 Ma) for the granites and emerald-bearing K-metasomatites from Campo Formoso and Carnaiba (Bahia, Brazil): Journal of South American Earth Sciences, v. 7, p. 149–165.

Goldfarb, R.J., Miller, L.D., Leach, D.L., and Snee, L.W., 1997, Gold deposits in metamorphic rocks of Alaska: Economic Geology, Monograph 9, p. 151–190.

Goldfarb, R.J., Snee, L.W., Miller, M.L., and Newberry, R.J., 1991, Rapid dewatering of the crust deduced from ages of mesothermal gold deposits: Nature, v. 254, p. 296–298.

Goldfarb, R.J., Snee, L.W., and Pickthorn, W.J., 1993, Orogenesis, high-T thermal events, and gold vein formation within metamorphic rocks of the American Cordillera: Mineralogical Magazine, v. 57, p. 375–394.

Grasty, R.L., and Mitchell, J.G., 1966, Single sample potassium-argon ages using the omegatron: Earth and Planetary Sciences Letters, v. 1, p. 121–122.

Groff, J.A., Heizler, M.T., McIntosh, W.C., and Norman, D.I., 1997, $^{40}Ar/^{39}Ar$ dating and mineral paragenesis for Carlin-type gold deposits along the Getchell Trend, Nevada—Evidence for Cretaceous and Tertiary gold mineralization: Economic Geology, v. 92, p. 601–622.

Groves, D.I., Goldfarb, R.J., Knox-Robinson, C.M., Ojala, J., Gardoll, S., Yun, G.Y., and Holyland, P., 2000, Late kinematic timinig of orogenic gold deposits and significance for computer-based exploration techniques with emphasis on the Yilgarn Block, Western Australia: Ore Geology Reviews, v. 17, p. 1–38.

Haeberlin, Yves, Moritz, Robert, Fontbote, L., and Cosca, Michael, 1999, The Pataz gold province (Peru) within the frame of a mesothermal

gold and antimony belt of the eastern Andean Cordillera, *in* Stanley, C.J., and others, eds., Mineral deposits—Processes to processing, Volume 2: Balkema, p. 1323–1326.

Hall, C.M., Higueras, P.L., Kesler, S.E., Lunar, R., Dong, Hailang, and Halliday, A.N., 1997, Dating of alteration episodes related to mercury mineralization in the Almaden district, Spain: Earth and Planetary Science Letters, v. 148, p. 287–298.

Halliday, A.N., 1978, ^{40}Ar - ^{39}Ar step-heating studies of clay concentrates from Irish orebodies: Geochimica et Cosmochimica Acta, v. 42, p. 1851–1858.

Halliday, A.N., and Mitchell, J.G., 1976, Structural, K-Ar, and ^{40}Ar/^{39}Ar age studies of adularia K-feldspars from the Lizard Complex, England: Earth and Planetary Science Letters, v. 29, p. 227–237.

Hames, W.E., and Bowring, S.A., 1994, An empirical evaluation of argon diffusion geometry in muscovite: Earth and Planetary Science Letters, v. 124, p. 161–167.

Hames, W.E., and Cheney, J.T., 1997, On the loss of ^{40}Ar* from muscovite during polymetamorphism: Geochimica et Cosmochimica Acta, v. 61, p. 3863–3872.

Hames, W.E., and Hodges, K.V., 1993, Laser ^{40}Ar/^{39}Ar evaluation of slow cooling and episodic loss of ^{40}Ar from a sample of polymetamorphic muscovite: Science, v. 261, p. 1721–1723.

Hammerschmidt, Konrad, and Frank, Eric, 1991, Relics of high-pressure metamorphism in the Lepontine Alps (Switzerland)—^{40}Ar/^{39}Ar and microprobe analyses on white K-mica: Schweizerische Mineralogische und Petrographische Mitteilungen, v. 71, p. 261–274.

Hanes, J.A., Archibald, D.A., Hodgson, C.J., and Robert, F., 1992, Dating of Archean auriferous quartz vein deposits in the Abitibi greenstone belt, Canada—^{40}Ar/^{39}Ar evidence for a 70 to 100 m.y. time gap between plutonism-metamorphism and mineralization: Economic Geology, v. 87, p. 1849–1861.

Hanson, G.N., and Gast, P.W., 1967, Kinetic studies in contact metamorphic zones: Geochimica et Cosmochimica Acta, v. 31, p. 1119–1153.

Hanson, G.N., Simmons, K.R., and Bence, A.E., 1975, ^{40}Ar/^{39}Ar spectrum ages for biotite, hornblende, and muscovite in a contact metamorphic zone: Geochimica et Cosomochimica Acta, v. 39, p. 1269–1277.

Harrison, T.M., 1981, Diffusion of ^{40}Ar in hornblende: Contributions to Mineralogy and Petrology, v. 78, p. 324–331.

Harrison, T.M., 1983, Some observations on the interpretation of ^{40}Ar/^{39}Ar age spectra: Isotope Geoscience, v. 1, p. 319–338.

Harrison, T.M., 1990, Some observations on the interpretation of feldspar ^{40}Ar/^{39}Ar results: Chemical Geology, v. 80, p. 219–229.

Harrison, T.M., and Be, K., 1983, ^{40}Ar/^{39}Ar age-spectrum analysis of detrital microclines from the San Joaquin Basin, California—An approach to determining the thermal evolution of sedimentary basins: Earth and Planetary Science Letters, v. 64, p. 244–256.

Harrison, T.M., Duncan, Ian, and McDougall, Ian, 1985, Diffusion of ^{40}Ar in biotite—Temperature, pressure, and compositional effects: Geochimica et Cosmochimica Acta, v. 49, p. 2461–2468.

Harrison, T.M., and Fitz Gerald, J.D., 1986, Exsolution in hornblende and its consequences for ^{40}Ar/^{39}Ar age spectra and closure temperature: Geochimica et Cosmochimica Acta, v. 50, p. 247–253.

Harrison, T.M., Lovera, O.M., and Heizler, M.T., 1991, ^{40}Ar/^{39}Ar results for alkali feldspars containing diffusion domains with differing activation energy: Geochimica et Cosmochimica Acta, v. 55, p. 1435–1448.

Harrison, T.M., and McDougall, Ian, 1982, The thermal significance of potassium feldspar K-Ar ages inferred from ^{40}Ar/^{39}Ar age spectrum results: Geochimica et Cosmochimica Acta, v. 46, p. 1811–1820.

Hart, S.R., 1964, The petrology and isotopic-mineral age relations of a contact zone in the Front Range, Colorado: Journal of Geology, v. 72, p. 493–525.

Heizler, M.T., and Harrison, T.M., 1988, Multiple trapped argon isotope components revealed by ^{40}Ar/^{39}Ar isochron analysis: Geochimica et Cosmochimica Acta, v. 52, p. 1295–1303.

Henry, C.D., Elson, H.B., McIntosh, W.C., Heizler, M.T., and Castor, S. B., 1997, Brief duration of hydrothermal activity at Round Mountain, Nevada, determined by ^{40}Ar/^{39}Ar geochronology: Economic Geology, v. 92, p. 807–826.

Hess, J.C., and Lippolt, H.J., 1986, Kinetics of Ar isotopes during neutron irradiation—^{39}Ar loss from minerals as a source of error in ^{40}Ar/^{39}Ar dating: Chemical Geology, v. 59, p. 223–236.

Hess, J.C., Lippolt, H.J., and Wirth, R., 1987, Interpretation of ^{40}Ar/^{39}Ar spectra of biotites evidence from hydrothermal degassing experiments and TEM studies: Chemical Geology, v. 66, p. 137–149.

Hodges, K. V., Hames, W.E., and Bowring, S.A., 1994, ^{40}Ar/^{39}Ar age gradients in micas from a high-temperature–low-pressure metamorphic terrain—Evidence for very slow cooling and implications for the interpretation of age spectra: Geology, v. 22, p. 55–58.

Hofstra, A.H., Snee, L.W., Rye, R.O., Folger, H.W., Phinisey, J.D., Loranger, R.J., Dahl, A.R., Naeser, C.W., Stein, H.J., and Lewchuk, M., 1999, Age constraints on Jerritt Canyon and other Carlin-type gold deposits in the western United States—Relationship to mid-Tertiary extension and magmatism: Economic Geology, v. 94, p. 769–802.

Huneke, J.C., 1976, Diffusion artifacts in dating by stepwise thermal release of rare gases: Earth and Planetary Science Letters, v. 28, p. 407–417.

Huneke, J.C., and Smith, S.P., 1976, The realities of recoil—^{39}Ar recoil out of small grains and anomalous age patterns in ^{40}Ar-^{39}Ar dating: Proceedings of Lunar Science Conference 7th, p. 1987–2008.

Hunziker, J.C., Frey, Martin, Clauer, Norbert, Dallmeyer, R.D., Friedrichsen, H., Flehmig, W., Hochstrasser, K., Roggwiler, P., and Schwander, H., 1986, The evolution of illite to muscovite—Mineralogical and isotopic data from the Glarus Alps, Switzerland: Contributions to Mineralogy and Petrology, v. 92, p. 157–180.

Ilchik, R.P., 1995, ^{40}Ar/^{39}Ar, K/Ar, and fission track geochronology of sediment-hosted disseminated gold deposits at Post-Betze, Carlin trend, northeastern Nevada—A discussion: Economic Geology, v. 90, p. 208–210.

Izett, G.A., Dalrymple, G.B., and Snee, L.W., 1992, ^{40}Ar/^{39}Ar ages for the Cretaceous-Tertiary boundary tektites from Haiti: Science, v. 252, p. 1539–1542.

Jäger, Emilie, 1962, Rb-Sr determinations on micas and total rocks from the Alps: Journal of Geophysical Research, v. 67, p. 5293–5306.

Jäger, Emilie, 1965, Rb-Sr determinations on minerals and rocks from the Alps: Sciences de la Terre, v. 10, p. 395–406.

Jäger, Emilie, 1967, Die bedeutung der Biotit-Alterswerte (The significance of biotite age values), *in* Jäger, Emilie, Niggli, E., and Wenk, E., eds., Rb-Sr Altersbestimmungen an Glimmern der Zentralalpen (Rb-Sr age determinations on micas from the central Alps): Beitrage zur Geologische Karte der Schweiz, NF, v. 134, p. 28–31.

Jäger, Emile, Niggli, E., and Wenk, E., 1967, Rb-Sr Altersbestimmungen an Glimmern der Zentralalpen (Rb-Sr age determinations on micas from the Central Alps): Beitrage zur Geologische Karte der Schweiz, NF, v. 134, p. 1–67.

Juliani, Caetano, Rye, R.O., Nunes, C.M.D., Snee, L.W., Correa Silva, R.H., Monteiro, L.V.S., Bettencourt, J.S., Neumann, R., and Neto, A.A., in press, Paleoproterozoic high-sulfidation mineralization in the

Tapajós Gold Province, Amazonian Craton—Geology, mineralogy, alunite argon age, and stable isotope constraints: Chemical Geology.

Kaneoka, Ichiro, 1974, Investigation of excess argon in ultramafic rocks from the Kola Peninsula by the $^{40}Ar/^{39}Ar$ method: Earth and Planetary Science Letters, v. 22, p. 145–156.

Kapusta, Y., Steinitz, Gideon, Akkerman, A., Sandler, A., Kotlarsky, P., and Nagler, A., 1997, Monitoring the deficit of ^{39}Ar in irradiated clay fractions and glauconites—Modeling and analytical procedure: Geochimica et Cosmochimica Acta, v. 61, p. 4671–4678.

Kelley, S.P., Arnauld, N.O., and Turner, S.P., 1994, High spatial resolution ^{40}Ar-^{39}Ar investigations using an ultra-violet laser probe extraction technique: Geochimica et Cosmochimica Acta, v. 58, p. 3519–3525.

Kelley, S.P., Bartlett, J.M., and Harris, N.B.W., 1997, Pre-metamorphic Ar-Ar ages from biotite inclusions in garnet: Geochimica et Cosmochimica Acta, v. 61, p. 3873–3878.

Kelley, S.P., and Turner, Grenville, 1991, Laser probe $^{40}Ar/^{39}Ar$ measurements of loss profiles within individual hornblende grains from the Giants Range Granite, northern Minnesota, U.S.A.: Earth and Planetary Science Letters, v. 107, p. 634–648.

Kelly, W.C., and Rye, R.O., 1979, Geologic, fluid inclusion, and stable isotope studies of the tin-tungsten deposits of Panasqueira, Portugal: Economic Geology, v. 74, p. 1721–1822.

Kent, A.J.R., and McCuaig, T.C., 1997, Disturbed $^{40}Ar/^{39}Ar$ systematics in hydrothermal biotite and hornblende at the Scotia gold mine, Western Australia—Evidence for argon loss associated with post-mineralization fluid movement: Geochimica et Cosmochimica Acta, v. 61, p. 4655–4669.

Kent, A.J.R., and McDougall, Ian, 1995, $^{40}Ar/^{39}Ar$ and U-Pb age constraints on the timing of gold mineralization in the Kalgoorlie gold field, western Australia: Economic Geology, v. 90, p. 845–859.

Kent, A.J.R., and McDougall, Ian, 1996, $^{40}Ar/^{39}Ar$ and U-Pb age constraints on the timing of gold mineralization in the Kalgoorlie gold field, western Australia—A reply: Economic Geology, v. 91, p. 795–799.

Keppie, J.D., Dallmeyer, R.D., Krogh, T.E., and Aftalion, M., 1993, Dating mineralization using several isotopic methods—An example from the South Mountain batholith, Nova Scotia, Canada: Chemical Geology, v. 103, p. 251–270.

Kerrich, Robert, 1994, Dating of Archaen auriferous quartz vein deposits in the Abitibi greenstone belt, Canada; $^{40}Ar/^{39}Ar$ evidence for a 70- to 100-m.y.-time gap between plutonism-metamorphism and mineralization—A discussion: Economic Geology, v. 89, p. 679–687.

Kerrich, Robert, and Cassidy, K.F., 1994, Temporal relationships of lode gold mineralization to accretion, magmatism, and deformation—Archean to present; a review: Ore Geology Reviews, v. 9, p. 263–310.

Kerrich, Robert, and Kyser, T.K., 1994, 100 Ma timing paradox of Archean gold, Abitibi greenstone belt (Canada)—New evidence from U-Pb and Pb-Pb evaporation ages of hydrothermal zircons: Geology, v. 22, p. 1131–1134.

Kirschner, D.L., Cosca, M.A., Masson, H., and Hunziker, J.C., 1996, Staircase $^{40}Ar/^{39}Ar$ spectra of fine-grained white mica—Timing and duration of deformation and empirical constraints on argon diffusion: Geology, v. 24, p. 747–750.

Kontak, D.J., Smith, P.K., Reynolds, Peter, and Taylor, K., 1990, Geological and $^{40}Ar/^{39}Ar$ geochronological constraints on the timing of quartz vein formation in the Meguma Group lode-gold deposits, Nova Scotia: Atlantic Geology, v. 26, p. 201–227.

Kontak, D.J., Farrar, Edward, and McBride, S.L., 1994, $^{40}Ar/^{39}Ar$ dating of fluid migration in a Mississippi Valley type-deposit—The Gays River Zn-Pb deposit, Nova Scotia, Canada: Economic Geology, v. 89, p. 1501–1517.

Kunk, M.J., Dalrymple, G.B., and Snee, L.W., 1994, Progress on the preparation of the proposed $^{40}Ar/^{39}Ar$ standard MMhb-2, plans for its calibration, and interlaboratory calibration of argon facilities [abs.], *in* Lanphere, M.A., Dalrymple, G.B., and Turrin, B.D., eds., International Conference on Geochronology, Cosmochronology, and Isotope Geology, 8th, Berkeley, California: U.S. Geological Survey Circular 1107, p. 183.

Lamb, M.A., and Cox, Dennis, 1998, New $^{40}Ar/^{39}Ar$ age data and implications for porphyry copper deposits of Mongolia: Economic Geology, v. 93, p. 524–529.

Landis, G.P., and Snee, L.W., 1991, $^{40}Ar/^{39}Ar$ systematics and argon diffusion in amber—Implications for ancient earth atmospheres: Palaeogeography, Palaeoclimatology, Palaeoecology, v. 97, p. 63–67.

Landis, G.P., Snee, L.W., and Juliani, Caetano, in press, Evaluation of alunite argon ages and fluid inclusion integrity—Step-wise noble gas heating experiments on 1.87-Ga alunite from Tapajos gold province, Brasil: Chemical Geology.

Lanphere, M.A., and Dalrymple, G.B., 1971, A test of the $^{40}Ar/^{39}Ar$ age spectrum technique on some terrestrial materials: Earth and Planetary Science Letters, v. 12, p. 359–372.

Lanphere, M.A., and Dalrymple, G.B., 1976, Identification of excess ^{40}Ar by the $^{40}Ar/^{39}Ar$ age spectrum technique: Earth and Planetary Science Letters, v. 32, p. 141–148.

Lanphere, M.A., and Dalrymple, G.B., 2000, First-principles calibration of ^{38}Ar tracers—Implications for the ages of ^{40}Ar-^{39}Ar fluence monitors: U.S. Geological Survey Professional Paper 1621, 10 p.

Leach, D.L., Hofstra, A.H., Church, S.E., Snee,L.W., Vaughn, R.B., and Zartman, R.E., 1998, Evidence for Proterozoic and Late Cretaceous–early Tertiary ore-forming events in the Coeur d'Alene district, Idaho and Montana: Economic Geology, v. 93, p. 347–359.

Lee, J.K.W., 1993, The argon release mechanisms of hornblende in vacuo: Chemical Geology, v. 106, p. 133–160.

Lee, J.K.W., Onstott, T.C., Cashman, K.V., Cumbest, R.J., and Johnson, D., 1991, Incremental heating of hornblende in vacuo—Implications for $^{40}Ar/^{39}Ar$ geochronology and the interpretation of thermal histories: Geology, v. 19, p. 872–876.

Lippolt, H.J., and Hautmann, Siegfried, 1995, $^{40}Ar/^{39}Ar$ ages of Precambrian manganese ore minerals from Sweden, India, and Morocco: Mineralium Deposita, v. 30, p. 246–256.

Lo, C.H., and Onstott, T. C., 1989, ^{39}Ar recoil artifacts in chloritized biotite: Geochimica et Cosmochimica Acta, v. 53, p. 2697–2711.

Losada-Calderon, A.J., McBride, S.L., and Bloom, M.S., 1994, The geology and $^{40}Ar/^{39}Ar$ geochronology of magmatic activity and related mineralization in the Nevados del Famatina mining district, La Rioja province, Argentina: Journal of South American Earth Sciences, v. 7, p. 9–24.

Love, D.A., Clark, A.H., Hodgson, C.J., Mortensen, J.K., Archibald, D.A., and Farrar, Edward, 1998, The timing of adularia-sericite-type mineralization and alunite-kaolinite-type alteration, Mount Skukum epithermal gold deposit, Yukon Territory, Canada—$^{40}Ar/^{39}Ar$ and U-Pb geochronology: Economic Geology, v. 93, p. 437–462.

Lovera, O.M., 1992, Computer programs to model $^{40}Ar/^{39}Ar$ diffusion data from multidomain samples: Computers and Geosciences, v. 18, p. 789–813.

Lovera, O.M., Harrison, T.M., and Grove, Martin, 1996, Comment on "Multipath Ar transport in K-feldspar deduced from isothermal heating experiments" by Igor Villa: Earth and Planetary Science Letters, v. 140, p. 281–283.

Lovera, O.M., Heizler, M.T., and Harrison, T.M., 1993, Argon diffusion domains in K-feldspar—II, Kinetic properties of MH-10: Contributions to Mineralogy and Petrology, v. 113, p. 381–393.

Lovera, O.M., Richter, F.M., and Harrison, T.M., 1989, The $^{40}Ar/^{39}Ar$ thermochronometry for slowly cooled samples having a distribution of diffusion domain sizes: Journal of Geophysical Research, v. 94, p. 17917–17935.

Lovera, O.M., Richter, F.M., and Harrison, T.M., 1991, Diffusion domains determined by ^{39}Ar release during step heating: Journal of Geophysical Research, v. 96, p. 2057– 2069.

Lovering, T.S., and Goddard, E.N., 1950, Geology and ore deposits of the Front Range, Colorado: U.S. Geological Survey Professional Paper 233, 319 p.

Lund, K.I., Snee, L.W., and Evans, K.V., 1986, Age and genesis of precious metals deposits, Buffalo Hump district, central Idaho—Implications for depth of emplacement of quartz veins: Economic Geology, v. 81, p. 990–996.

Mako, D.A., 1997, Characterization and dating of argillic alteration in the Mercur gold district, Utah—A discussion: Economic Geology, v. 92, p. 633–634.

Marsh, T.M., Einaudi, M.T., and McWilliams, Michael, 1997, $^{40}Ar/^{39}Ar$ geochronology of Cu-Au and Au-Ag mineralization in the Potrerillos district, Chile: Economic Geology, v. 92, p. 784–806.

McDougall, Ian, 1985, K-Ar and $^{40}Ar/^{39}Ar$ dating of the hominid-bearing Pliocene-Pleistocene sequence at Koobi Fora, Lake Turkana, northern Kenya: Geological Society of America Bulletin, v. 96, p. 159–175.

McDougall, Ian, and Harrison, T.M., 1999, Geochronology and thermochronology by the $^{40}Ar/^{39}Ar$ method: New York, Oxford, 269 p.

McIntyre, D.B., 1963, Precision and resolution in geochronometry, *in* Albritton, C.C., ed., The fabric of geology: Reading, Mass., Addison-Wesley, p. 112–134.

Merrihue, Craig, 1965, Trace-element determinations and potassium-argon dating by mass spectroscopy of neutron-irradiated samples [abs.]: Transactions of the American Geophysical Union, v. 46, p. 125.

Merrihue, Craig, and Turner, Grenville, 1966, Potassium-argon dating by activation with fast neutrons: Journal of Geophysical Research, v. 71, p. 2852–2857.

Miggins, D.P., Thompson, R.N., Pillmore, C.L., Snee, L.W., and Stern, C.R., 2002, Extension and uplift of the northern Rio Grande rift—Evidence from $^{40}Ar/^{39}Ar$ geochronology from the Sangre de Cristo Mountains, south central Colorado and northern New Mexico, *in* Menzies, M.A., Baker, Joel, Ebinger, C., and Klemperer, S., eds., Magmatic rifted margins: Geological Society of America Special Paper 362, p. 47–64.

Miller, L.D., Goldfarb, R.J., Gehrels, G.E., and Snee, L.W., 1994, Genetic links among fluid cycling, vein formation, regional deformation, and plutonism in the Juneau gold belt, southeastern Alaska: Geology, v. 22, p. 203–206.

Miller, L.D., Goldfarb, R.J., Snee, L.W., Gent, C.A., and Kirkham, R.A., 1995, Structural geology, age, and mechanisms of gold vein formation at the Kensington and Jualin deposits, Berners Bay district, southeast Alaska: Economic Geology, v. 90, p. 343–368.

Mitchell, J.G., 1968, The argon-40/argon-39 method for potassium-argon age determinations: Geochimica et Cosmochimica Acta, v. 32, p. 781–790.

Morris, H.T., and Tooker, E.W., 1996, Characterization and dating of argillic alteration in the Mercur gold district, Utah—A discussion: Economic Geology, v. 91, p. 477–479.

Napier, R.W., Guise, P.G., and Rex, D.C., 1998, $^{40}Ar/^{39}Ar$ constraints on the timing and history of amphibolite facies gold mineralisation in the Southern Cross area, Western Australia: Australian Journal of Earth Sciences: v. 45, p. 285–296.

Onstott, T.C., Hall, C.M., and York, Derek, 1989, $^{40}Ar/^{39}Ar$ thermochronometry of the Imataca Complex, Venezuela: Precambrian Research, v. 42, p. 255–291.

Onstott, T.C., Miller, M.L., Ewing, R.C., Arnold, G.W., and Walsh, D.S., 1995, Recoil refinements—Implications for the $^{40}Ar/^{39}Ar$ dating technique: Geochimica et Cosmochimica Acta, v. 59, p. 1821–1834.

Onstott, T.C., Mueller, Chris, Vrolijk, P.J., and Pevear, D.R., 1997, Laser $^{40}Ar/^{39}Ar$ microprobe analyses of fine-grained illite: Geochimica et Cosmochimica Acta, v. 61, p. 3851–3861.

Onstott, T.C., and Peacock, M.W., 1987, Argon retentivity of hornblendes—A field experiment in a slowly cooled metamorphic terrane: Geochimica et Cosmochimica Acta, v. 51, p. 2891–2903.

Perkins, Caroline, McDougall, Ian, Claoue-Long, Jonathan, and Heithersay, P.S., 1990, $^{40}Ar/^{39}Ar$ and U-Pb geochronology of the Goonumbla porphyry Cu-Au deposits, NSW, Australia: Economic Geology, v. 85, p. 1808–1824.

Perkins, Caroline, McDougall, Ian, and Walshe, J.L., 1992, Timing of shoshonitic magmatism and gold mineralization, Sheahan–Grants and Glendale, New South Wales: Australian Journal of Earth Sciences, v. 39, p. 99–110.

Perkins, Caroline, and Wyborn, L.A.I., 1998, Age of Cu-Au mineralisation, Cloncurry district, eastern Mt. Isa Inlier, Queensland, as determined by $^{40}Ar/^{39}Ar$ dating: Australian Journal of Earth Sciences, v. 45, p. 233–246.

Phillips, David, 1991, Argon isotope and halogen chemistry of phlogopite from South African kimberlites—A combined step-heating, laser probe, electron microprobe and TEM study: Chemical Geology, v. 87, p. 71–98.

Phillips, David, and Onstott, T.C., 1986, Application of $^{36}Ar/^{40}Ar$ versus $^{39}Ar/^{40}Ar$ correlation diagrams to the $^{40}Ar/^{39}Ar$ spectra of phlogopites from southern African kimberlites: Geophysical Research Letters, v. 13, p. 689–692.

Phinisey, J.D., Hofstra, A.H., Snee, L.W., Roberts, T.T., Dahl, A.R., and Loranger, R.J., 1996, Evidence for multiple episodes of igneous and hydrothermal activity and constraints on the timing of gold mineralization, Jerritt Canyon District, Elko County, Nevada, *in* Coyner, A.R., and Fahey, P.L., eds., Geology and ore deposits of the American Cordillera: Geological Society of Nevada Symposium Proceedings, Reno/Sparks, Nevada, April 1995, p. 15–39.

Pickles, C.S., Kelley, S.P., Reddy, S.M., and Wheeler, J., 1997, Determination of high spatial resolution argon isotope variations in metamorphic biotites: Geochimica et Cosmochimica Acta, v. 18, p. 3809–3833.

Powell, W.G., Hodgson, C.J., Hanes, J.A., Carmichael, D.M., McBride, and Farrar, Edward, 1995, $^{40}Ar/^{39}Ar$ geochronological evidence for multiple postmetamorphic hydrothermal events focused along faults in the southern Abitibi greenstone belt: Canadian Journal of Earth Sciences, v. 32, p. 768–786.

Premo, W.R., Morton, D.M., Snee, L.W., Naeser, N.D., and Fanning, C.M., 1998, Isotopic ages, cooling histories, and magmatic origins for Mesozoic tonalitic plutons from the northern Peninsular Ranges batholith, s. California: Geological Society of America Abstracts with Programs, v. 30, no. 5, p. 59.

Reddy, S.M., Kelley, S.P., and Wheeler, J., 1996, A $^{40}Ar/^{39}Ar$ laser probe study of micas from the Sesia Zone, Italian Alps—Implications for metamorphic and deformation histories: Journal of Metamorphic Petrology, v. 14, p. 493–508.

Renne, P.R., Deino, A.L., Walter, R.C., Turrin, B.D., Swisher, C.C., Becker, T.A., Curtis, G.H., Sharp, W.D., and Jaouni, A.-R., 1994, Intercalibration of astronomical and radioisotopic time: Geology, v. 22, p. 783–786.

Renne, P.R., Karner, D.B., and Ludwig, K.R., 1998a, Absolute ages aren't exactly: Science, v. 282, p. 1840–1841.

Renne, P.R., Swisher, C.C., Deino, A.L., Karner, D.B., Owens, T.L., and DePaolo, D.J., 1998b, Intercalibration of standards, absolute ages and uncertainties in $^{40}Ar/^{39}Ar$ dating: Chemical Geology, v. 145, p. 117–152.

Reynolds, P.H., and Muecke, G.K., 1978, Age studies on slates—Applicability of the $^{40}Ar/^{39}Ar$ stepwise outgassing method: Earth and Planetary Science Letters, v. 40, p. 111–118.

Reynolds, Peter, Ravenhurst, Casey, Zentilli, Marcos, and Lindsay, Darryl, 1998, High-precision $^{40}Ar/^{39}Ar$ dating of two consecutive hydrothermal events in the Chuquicamata porphyry copper system, Chile: Chemical Geology, v. 148, p. 45–60.

Rex, D.C., Guise, P.G., and Wartho, J.-A., 1993, Disturbed $^{40}Ar/^{39}Ar$ spectra from hornblendes—Thermal loss or contamination: Chemical Geology, v. 103, p. 271–281.

Ribeiro-Althoff, A.M., Cheilletz, Alain, Giuliani, Gaston, Feraud, Gilbert, Camacho, G.B., and Zimmermann, J.L., 1997, $^{40}Ar/^{39}Ar$ and K-Ar geochronological evidence for two periods (~2Ga and 650 to 500 Ma) of emerald formation in Brazil: International Geology Review, v. 39, p. 924–937.

Roddick, J.C., 1978, The application of isochron diagrams in $^{40}Ar/^{39}Ar$ dating—A discussion: Earth and Planetary Science Letters, v. 41, p. 233–244.

Roddick, J.C., 1983, High-precision intercalibration of ^{40}Ar-^{39}Ar standards: Geochimica et Cosmochimica Acta, v. 47, p. 887–898.

Roddick, J.C., 1987, Generalized numerical error analysis with applications to geochronology and thermodynamics: Geochimica et Cosmochimica Acta, v. 51, p. 2129–2135.

Roddick, J.C., 1988, The assessment of errors in $^{40}Ar/^{39}Ar$ dating: Geological Survey of Canada Paper 88-2, p. 3–8

Roddick, J.C., Cliff, R.A., and Rex, D.C., 1980, The evolution of excess argon in alpine biotites—A $^{40}Ar/^{39}Ar$ analysis: Earth and Planetary Science Letters, v. 48, p. 185–208.

Roeske, S.M., Dusel-Bacon, Cynthia, Aleinikoff, J.N., Snee, L.W., and Lanphere, M.A., 1995, Metamorphic and structural history of continental crust at a Mesozoic collisional margin, the Ruby terrane, central Alaska: Journal of Metamorphic Petrology, v. 13, p. 25–40.

Rowley, P.D., Snee, L.W., Mehnert, H.H., Anderson, R.E., Axen, G.J., Burke, K.J., Simonds, F.W., Shroba, R.R., and Olmore, S.D., 1992, Structural setting of the Chief Mining District, eastern Chief Range, Lincoln County, Nevada, *in* Thorman, C.H., ed., Application of structural geology to mineral and energy deposits: U.S. Geological Survey Bulletin 2012, p. H1–H17.

Rowley, P.D., Snee, L.W., Anderson, R.E., Nealey, L.D., Unruh, D.M., and Ferris, D.E., 2001, Field trip to the Caliente Caldera Complex, east-striking transverse zones, and nearby mining districts in Nevada-Utah—Implications for petroleum, ground-water, and mineral resources, *in* Erskine, M.C., Faulds, J.E., Bartley, J.M., and Rowley, P.D., eds., The geologic transition, High Plateaus to Great Basin—A symposium and field guide: Utah Geological Association Publica - tion 30, p. 401–418.

Ruffet, Gilles, Feraud, Gilbert, and Amouric, Marc, 1991, Comparison of $^{40}Ar/^{39}Ar$ conventional and laser dating of biotites from the North Tregor batholith: Geochimica et Cosmochimica Acta, v. 55, p. 1675–1688.

Ruffet, Gilles, Feraud, Gilbert, Ballevre, M., and Kienast, J.-R., 1995, Plateau ages and excess argon in phengites—An ^{40}Ar-^{39}Ar laser probe study of Alpine micas (Sesia Zone, Western Alps, northern Alps): Chemical Geology, v. 121, p. 327–343.

Samson, S.D., and Alexander, E.C., 1987, Calibration of interlaboratory $^{40}Ar/^{39}Ar$ dating standard, MMhb-1: Isotope Geoscience, v. 66, p. 27–34.

Scaillet, Stéphane, 1996, Excess ^{40}Ar transport scale and mechanism in high-pressure phengites—A case study from an eclogitized metabasite of the Dora-Maira nappe, western Alps: Geochimica et Cosmochimica Acta, v. 60, p. 1075–1090.

Scaillet, Stéphane, 2000, Numerical error analysis in $^{40}Ar/^{39}Ar$ dating: Chemical Geology, v.162, p. 269–298.

Scaillet, Stéphane, Feraud, Gilbert, Ballevre, M., and Amouric, Marc, 1992, Mg/Fe and [(Mg,Fe)SI-Al_2] compositional control on argon behaviour in high-pressure white micas—A $^{40}Ar/^{39}Ar$ continuous laser-probe study from Dora-Maira nappe of the internal western Alps, Italy: Geochimica et Cosmochimica Acta, v. 56, p. 2851–2872.

Scaillet, Stéphane, Feraud, Gilbert, Lagabrielle, Y., Ballevre, M., and Ruffet, Gilles, 1990, $^{40}Ar/^{39}Ar$ laser-probe dating by step heating and spot fusion of phengites from the Dora-Maira nappe of the western Alps, Italy: Geology, v. 18, p. 741–744.

Scott, R.B., Unruh, D.M., Snee, L.W., Harding, A.E., Nealey, L.D., Blank, H.R., Budahn, J.R., and Mehnert, H.H., 1995, Relation of peralkaline magmatism to heterogeneous extension during the middle Miocene, southeastern Nevada: Journal of Geophysical Research, v. 100, p. 10381–10401.

Setterfield, T.N., Mussett, A.E., and Oglethorpe, R.D.J., 1992, Magmatism and associated hydrothermal activity during the evolution of the Tavua caldera—$^{40}Ar/^{39}Ar$ dating of the volcanic, intrusive, and hydrothermal events: Economic Geology, v. 87, p. 1130–1140.

Shubat, M.A., and Snee, L.W., 1992, High-precision $^{40}Ar/^{39}Ar$ geochronology, volcanic stratigraphy, and mineral deposits of Keg Mountain, west-central Utah, *in* Thorman, C.H., ed., Application of structural geology to mineral and energy deposits: U.S. Geological Survey Bulletin 2012, p. G1–G16.

Sigurgeirsson, T., 1962, Dating of recent basalts with the potassium-argon method (in Icelandic): Reports of Physics Laboratory, University of Iceland, 9 p.

Smith, P.E., Evensen, N.M., and York, Derek, 1993, First successful $^{40}Ar/^{39}Ar$ dating of glauconites—Argon recoil in single grains of cryptocrystalline material: Geology, v. 21, p. 41–44.

Smith, P.E., Schandl, E.S., and York, Derek, 1993, Timing of metasomatic alteration of the Archean Kidd Creek massive sulfide deposit, using $^{40}Ar/^{39}Ar$ laser dating of single crystals of fuchsite: Economic Geology, v. 88, p. 1636–1642.

Snee, L.W., 1982a, Determination of thermal histories in complex plutonic terranes by use of the details of $^{40}Ar/^{39}Ar$ age spectrum diagrams: Eos, v. 63, p. 453.

Snee, L.W., 1982b, Emplacement and cooling of the Pioneer batholith, southwestern Montana: Columbus, Ohio, The Ohio State University Ph. D. dissertation, 320 p.

Snee, L.W., Lund, K.I., Sutter, J.F., Balcer, D.E., and Evans, K.E., 1995, An $^{40}Ar/^{39}Ar$ chronicle of the tectonic development of the Salmon River suture zone, western Idaho, *in* Vallier, T.L., and Brooks, H.C., eds., Geology of the Blue Mountains region of Oregon, Idaho, and Washington; petrology and tectonic evolution of pre-Tertiary rocks of the Blue Mountains region: U.S. Geological Survey Professional Paper 1438, p. 359–414.

Snee, L.W., and Rowley, P.D., 2000, New $^{40}Ar/^{39}Ar$ dates from the Caliente Caldera Complex, Nevada-Utah—At least 10 million years of Tertiary volcanism in one of the world's largest caldera complexes: Geological Society of America Abstracts with Programs, v. 32, no. 7, p. A461.

Snee, L.W., Sutter, J.F., and Kelly, W.C., 1988, Thermochronology of economic mineral deposits—Dating the stages of mineralization at Panasqueira, Portugal, by high-precision $^{40}Ar/^{39}Ar$ age-spectrum techniques on muscovite: Economic Geology, v. 83, p. 335–354.

Staudacher, Th., Jessburger, E.K., Dorflinger, D., and Kiko, J., 1978, A refined ultrahigh-vacuum furnace for rare-gas analysis: Journal of Physics E, Scientific Instruments, v. 11, p. 781–784.

Steiger, R.H., and Jäger, Emilie, 1977, Subcommission on geochronology—Convention on the use of decay constants in geo- and cosmochronology: Earth and Planetary Science Letters, v. 36, p. 359–362.

Steven, T.A., Mehnert, H.H., and Obradovich, J.D., 1967, Age of volcanic activity in the San Juan Mountains, Colorado: U.S. Geological Survey Professional Paper 575–D, p. 47–55.

Stoenner, R.W., Schaeffer, O.A., and Katcoff, S., 1965, Half-lives of Argon-37, Argon-39, and Argon-42, Science, v. 148, p. 1325–1328.

Swisher III, C.C., and 11 others, 1992, Coeval $^{40}Ar/^{39}Ar$ ages of 65.0 million years ago from Chicxulub crater melt rock and Cretaceous-Tertiary boundary tektites: Science, v. 257, p. 954–958.

Till, A.B., and Snee, L.W., 1995, $^{40}Ar/^{39}Ar$ evidence that formation of blueschists in continental crust was synchronous with foreland fold and thrust belt deformation, western Brooks Range, Alaska: Journal of Metamorphic Geology, v. 13, p. 41–60.

Turner, Grenville, 1968, The distribution of potassium and argon in chrondrites, *in* Ahrens, L.H., ed., Origin and distribution of the elements: London, Pergamon, p. 387–398.

Turner, Grenville, 1969, Thermal histories of meteorites by the $^{40}Ar/^{39}Ar$ method, *in* Millman, P.M., ed., Meteoritic research: Dordrecht, Pergamon, p. 407–417.

Turner, Grenville, 1970a, $^{40}Ar/^{39}Ar$ age determinations of lunar rock 12013: Earth and Planetary Science Letters, v. 9, p. 177–180.

Turner, Grenville, 1970b, Argon-40/Argon-39 dating of lunar rock samples: Geochimica et Cosmochimica Acta, supplement 2, Proceedings of the Second Lunar Science Conference, v. 2, p. 1665–1683.

Turner, Grenville, 1971a, Argon-40/argon-39 dating: the optimization of irradiation parameters: Earth and Planetary Science Letters, v. 10, p. 227–234.

Turner, Grenville, 1971b, ^{40}Ar-^{39}Ar ages from the lunar maria: Earth and Planetary Science Letters, v. 11, p. 169–191.

Turner, Grenville, and Cadogan, P.H., 1974, Possible effects of ^{39}Ar recoil in $^{40}Ar/^{39}Ar$ dating: Geochimica et Cosmochimica Acta, Supplement 5, p. 1601–1615.

Vasconcelos, P.M., 1999, K-Ar and $^{40}Ar/^{39}Ar$ geochronology of weathering processes: Annual Reviews of Earth and Planetary Sciences, v. 27, p. 183–229.

Vasconcelos, P.M., Becker, T.A., Renne, P.R., Brimhall, G.H., 1992, Age and duration of weathering—^{40}K-^{40}Ar and $^{40}Ar/^{39}Ar$ analysis of K-Mn oxides: Science, v. 258, p. 451–455.

Vasconcelos, P.M., Brimhall, G.H., Becker, T.A., and Renne, P.R., 1994, $^{40}Ar/^{39}Ar$ analysis of supergene jarosite and alunite—Implications to the paleoweathering history of the western U.S.A. and West Africa: Geochimica et Cosmochimica Acta, v. 58, p. 401–420.

Vasconcelos, P.M., Renne, P.R., Becker, T.A., and Wenk, H.R., 1995, Mechanisms and kinetics of atmospheric, radiogenic, and nucleogenic argon release from cryptomelane during $^{40}Ar/^{39}Ar$ analysis: Geochimica et Cosmochimica Acta, v. 59, p. 2057–2070.

Villa, I.M., 1997, Isotopic closure: Terra Nova, v. 10, p. 42–47.

Wallace, S.R., Mackenzie, W.R., Blair, R.G., and Muncaster, N.K., 1978, Geology of the Urad and Henderson molybdenite deposits, Clear Creek County, Colorado, *with a section on* A comparison of these deposits with those at Climax, Colorado: Economic Geology, v. 73, p. 325–368.

Wänke, Heinrich, and Konig, H., 1959, Eine neue Methode zur Kalium-Argon-Altersbestimmung und ihre Anwendung auf Steinmeteorite (A new method for potassium-argon dating and its application to stoney meteorites): Zeitung Naturforsch, v. 14a, p. 860–866.

Wartho, J.-A., 1995, Apparent argon diffusive loss in $^{40}Ar/^{39}Ar$ age spectra in amphiboles: Earth and Planetary Sciences Letters, v. 134, p. 393–407.

Wartho, J.-A., Dodgson, M.H., Rex, D.C., Guise, P.G., and Knipe, R.J., 1991, Mechanism of Ar release from Himalayan metamorphic hornblende: American Mineralogist, v. 76, p. 1446–1448.

Wendt, Immo, and Carl, Claudia, 1991, The statistical distribution of the mean squared weighted deviation: Chemical Geology, v. 86, p. 275–285.

Willis-Richards, J., and Jackson, N.J., 1989, Evolution of the Cornubian ore field—Part I, Batholith modeling and ore distribution: Economic Geology, v. 84, p. 1078–1100.

Wilson, P.N., and Parry, W.T., 1995, Characterization and dating of argillic alteration in the Mercur gold district, Utah: Economic Geology, v. 90, p. 1197–1216.

Wilson, P.N., and Parry, W.T., 1996, Characterization and dating of argillic alteration in the Mercur gold district, Utah—A reply: Economic Geology, v. 91, p. 479–481.

Wilson, P.N., and Parry, W.T., 1997, Characterization and dating of argillic alteration in the Mercur gold district, Utah—A reply: Economic Geology, v. 92, p. 634–635.

Wijbrans, J.R., and McDougall, Ian, 1986, $^{40}Ar/^{39}Ar$ dating of white micas from an Alpine high pressure metamorphic belt on Naxos (Greece)—The resetting of the argon isotopic system: Contributions to Mineralogy and Petrology, v. 93, p. 187–194.

Wijbrans, J.R., and McDougall, Ian, 1988, Metamorphic evolution of the Attic Cycladic metamorphic belt on Naxos (Cyclades, Greece)—Utilizing $^{40}Ar/^{39}Ar$ age spectrum measurements: Journal of Metamorphic Geology, v. 6, p. 571–594.

Wijbrans, J.R., Schliestedt, M., and York, Derek, 1990, Single grain argon laser probe dating of phengites from blueschist to greenschist transition on Sifnos (Cyclades, Greece): Contributions to Mineralogy and Petrology, v. 104, p. 582–593.

Wintsch, R.P., Kunk, M.J., and Epstein, J.B., 1996, $^{40}Ar/^{39}Ar$ whole-rock data constraints on Acadian diagenesis and Alleghanian cleavage in the Martinsburg Formation, eastern Pennsylvania: American Journal of Science, v. 296, p. 766–788.

Witt, W.K., Swager, C.P., and Nelson, D.R., 1996, $^{40}Ar/^{39}Ar$ and U-Pb age constraints on the timing of gold mineralization in the Kalgoorlie gold field, Western Australia—A discussion: Economic Geology, v. 91, p. 792–811.

Yambrick, R.A., and Snee, L.W., 1989, Early Oligocene calc-alkaline and Middle Miocene bimodal volcanism, Simpson Mountains, west-central Utah: Geological Society of America Abstracts with Programs, v. 21, p. A134.

York, Derek, 1969, Least squares fitting of a straight line with correlated errors: Earth and Planetary Science Letters, v. 5, p. 320–344.

York, Derek, 1984, Cooling histories from $^{40}Ar/^{39}Ar$ age spectra—Implications for Precambrian plate tectonics: Annual Reviews of Earth and Planetary Sciences, v. 12, p. 383–409.

Zweng, P.L., Mortensen, J.K., and Dalrymple, G.B., 1993, Thermochronology of the Camflo gold deposit, Malartic, Quebec—Implications for magmatic underplating and the formation of gold-bearing quartz veins: Economic Geology, v. 88, p. 1700–1721.